ÉCOLE NORMALE SUPÉRIEURE - DÉPARTEMENT DE PHYSIQUE

Laboratoire de Physique Statistique

Habilitation à diriger les recherches

de l'Université Pierre et Marie Curie

Spécialité : PHYSIQUE

par

J-F ALLEMAND

Quelques expériences entre physique, chimie, biologie : formations de boucles dans l'ADN, moteurs moléculaires et ségrégation chromosomique, excitation biphotonique, spectroscopie de corrélation de fluorescence...

Ѕoutenue le 08/12/2006 devant le jury composé de :

M.	François	Gallet	Examinateur
M.	Jean-François	Joanny	Examinateur
M.	Joachim	Rädler	Rapporteur
M.	Christoph	Schmidt	Rapporteur
M.	Dave	Sherratt	Rapporteur

Table des matières

Lamelles de coquilles Saint Jacques aux agrumes

O. Roellinger

Ingrédients pour 4 personnes

16 noix de St-Jacques

garniture : 1 orange 1 pamplemousse 1 citron vert

vinaigrette : 1 c à s de sucre 2 c à s de xérès le jus d'une orange 3 c à s d'huile d'olive 6 c à s d'huile de tournesol

finition : 1 citron jaune fleur de sel moulin de poivre

Matériel:

1 bouteille avec bouchon 1 râpe à zeste

Réalisation

2 heures de préparation

Commencer par la vinaigrette ; colorer à sec dans une casserole le sucre jusqu'à ce qu'il devienne caramel. Arrêter la cuisson avec le xérès et le jus de l'orange (surtout attention au projection). Reporter à ébullition pour bien dissoudre tout le caramel. Débarrasser dans une bouteille et ajouter les huiles. Laisser refroidir.

Prélever la chair des agrumes et tailler en petit dés. Réserver dans une passoire jusqu'au service.

Contrôler bien que le pied des noix soit complètement supprimés et bien les sécher.

Dernière minute

Tailler les noix en fines rondelles et répartir dans les 4 assiettes. Disposer les dés d'agrumes. Secouer énergiquement la bouteille de vinaigrette et saucer généreusement les rondelles. Râper un peu de citron jaune et répartir quelques grains de fleur de sel ainsi que quelques tours de moulin à poivre.

Servir de suite.

http://www.maisons-de-bricourt.com

Première partie

Remerciements et contexte général des travaux

Chapitre 1

Remerciements

Je remercie les professeurs F. Gallet, J.F. Joanny, J. Rädler, C. Schmidt, D. Sherratt, pour avoir accepté de faire partie du jury et d'évaluer mon travail et surtout pour avoir consacré une partie de leur temps pour venir assister à la soutenance et lire ce rapport, qui pour une majorité d'entre eux n'est en partie pas dans leur langue natale.

Les travaux présentés dans ce document sont le résultat du travail de nombreuses personnes avec qui j'ai interagi durant ces dernières années. La qualité de ces travaux leur revient en grande partie. D'autres part d'autres personnes ont eu un importance non négligeable dans mon évolution...je vais essayer de n'oublier personne dans les paragraphes qui suivent.

Tout d'abord un grand merci à David Bensimon et Vincent Croquette avec qui je partage l'encadrement des étudiants, les tâches administratives,...et beaucoup de temps et d'idées ensemble. Grâce à ce partage j'ai pu avancer en relative douceur. Sans quoi le lancement d'une nouvelle instrumentation au moment où je prenais un nouvel enseignement et où mes enfants sont nés m'auraient demandé une énergie qui aurait été sans doute au dessus de mes moyens. Le dynamisme et la compétence que nous avons dans l'équipe sont parfois durs à suivre quand la nuit à été courte à la maison et que l'on a passé la moitié de la journée en enseignement...mais cela est stimulant et reste un exemple que je chercherai à poursuivre.

Les trois permanents que nous sommes dans l'équipe n'arriverions pas à grand chose sans la très très grande qualité des étudiants et post doctorants qui sont passés au laboratoire ces dernières années. J'avais déjà eu la chance de faire ma thèse dans le même groupe avec mes deux amis , Charlie Gosse (CNRS LPN Marcoussis) et Terence Strick (CNRS Institut, Jacques Monod). Par la suite cette qualité ne s'est pas démentie : Berenike (prof à l'université de Munster), Marie Nöelle (Schlumberger) , Nynke (chercheur à l'université de Delft), Gilles, Timothée, Adrien , Keir (NIH), Hiroaki, Elise, Francesco, Pierre... j'espère pour ceux qui sont en cours de thèse qu'ils trouveront le débouché qu'ils méritent comme ceux qui les ont précédés. Une mention spéciale pour deux d'entre eux dont le travail, ou une partie, est présentée dans la suite, Giuseppe (travail sur GalR) et surtout pour Omar (travail sur FtsK, U Santa Barbara) car sans son apport essentiel sur FtsK nous aurions eu du mal à lutter contre la concurrence.

Mon travail, pour sa partie chimique doit beaucoup à Ludovic Jullien, avec lui aussi j'ai pu trouver une collaboration fort enrichissante pour moi. Je remercie aussi tous les membres

de son groupe (Jean Bernard, Ludivine, Thomas, Thomas, André, Nathalie, Chouah, Damien, Odile, Isabelle, Ludivine...), avec là encore une mention spéciale pour Sandrine, et surtout pour Emmanuelle, qui a essuyé les plâtres de mes incompétences initiales expérimentales en fluorescence à deux photons, dont les travaux sont partiellement présentés dans la suite.

L'évolution de ma thématique de recherche doit beaucoup à ma rencontre avec François-Xavier Barre. Cette rencontre fortuite lors d'une conférence m'a amené dans un premier temps à changer de système expérimental sur la thématique du looping...avant de modifier ma thématique de recherche. Merci a Corinne, Sarah qui nous ont fournit en substrats.

Je dois églement beaucoup à Michel Volovitch. Lors de mon séjour dans le laboratoire d'Alain Prochiantz, Michel avec son enthousiasme et ses exceptionnelles qualités pédagogiques m'a appris énormément de biologie et surtout de biologie moléculaire qui m'est maintenant indispensable. Malheureusement le projet que nous avions en commun n'a pas abouti. Il n'y a donc aucune trace dans la littérature scientifique de ce séjour, mais il a été très important pour la suite de mon travail. En dehors de Michel j'ai également beaucoup appris, même si ce n'est peut être pas autant que ce que j'aurai pu(...mais le développement est un sujet complexe), des autres membres du laboratoire, qui ont tous été patients avec le "'petit physicien qui ne connait rien"'. Je leur en suis reconnaissant.

Enseigner au magistère de chimie m'a beaucoup appris. Mais mon expérience d'enseignement au magistère de chimie a également été riche sur le plan humain. Ceci a été en grande partie dû à la grande confiance que m'a faite JN Verpeaux en me laissant beaucoup de responsabilités et avec qui je me suis beaucoup amusé malgré (à moins que cela ne soit grâce à cela?) le nombre important de réunions pas toujours excitantes, des soutenances parfois tristounettes et quelques casse-pieds pour pimenter les choses. Par ailleurs les échanges avec les étudiants, le plaisir que j'ai pu avoir en cours sont dûs à une majorité d'étudiants remarquables.

Merci à Pierre Desbiolles, avec qui j'ai de régulières discussions.

Ma thèse avait été beaucoup lue, pas uniquement pour la science qu'elle contenait mais aussi pour les recettes de cuisine que j'avais incorporé. Je vais recommencer cette expérience dans ce manuscrit, car je crois toujours que gastronomie et recherche ont beaucoup de points communs. Les repas chez Olivier Roellinger à Cancale (bien sur), chez Michel Bras à Laguiole, chez Jean-Paul Abadie à Lorient,ou chez Pascal Barbot ou Guy Savoy à Paris restent des moments inoubliables qui remotivent pour un bon moment quand on a des coups de mou. Je conseille à tous ceux qui le peuvent de profiter des talents de tous ces grands chefs. J'espère qu'ils auront autant de plaisir chez eux que j'en ai eu.

Finalement une fois enlevé le temps pour l'enseignement, celui consacré à la recherche, il me reste tout de même un peu de temps pour une vie privée. Or cette vie privée est fondamentalement ce pourquoi je travaille. Comme la partie professionnelle prend une grande part de mon temps il faut un soutien indispensable de la part des personnes qui partagent ma vie. C'est à ce titre que je remercie Corinne. En plus, avec elle, j'ai commencé juste après ma thèse une expérience de clonage humain dont les résultats définitifs ne seront obtenus que dans vingt ans. C'est indiscutablement l'expérience qui m'a demandé et me demandera

le plus d'énergie...Adrien et Maxime étant des durs à cuire, mais c'est aussi sûrement la plus motivante, et c'est un plaisir de la vivre avec elle!

Chapitre 2

Contexte général

La fin de ma thèse se situe à la fin d'une époque pour les micromanipulations de molécules d'ADN. Cette époque avait débuté avec l'expérience pionnière de Smith, Finzi et Bustamante [1] qui ont pour la première fois mesuré la courbe d'élasticité d'une molécule d'ADN. Du fait des contraintes de leur système expérimental ils ont étudié uniquement le régime entropique de la courbe d'extension (force < 10pN). Ensuite leur collaboration avec J. Marko et E. Siggia a permis de résoudre le modèle théorique décrivant la courbe d'élasticité de l'ADN avec la résolution du modèle du ver [2]. L'étape importante suivante a été l'étude du régime hautes forces, simultanément par les groupes de Bustamante et de Chatenay/Caron à Curie. Ces deux groupes [3, 4] ont mis en évidence une transition structurale dans l'ADN qui permet de passer de la forme B canonique à une forme surétendue , appelée ADN S, pour des forces de l'ordre d'une soixantaine de pN. Dès ce moment, l'utilisation des propriétés élastiques pour sonder les interactions ADN-protéines en temps réel et à l'échelle de la molécule unique a débuté. En effet la structure S de l'ADN, dont la longueur cristallographique est de 1.7 fois celle de l'ADN B, fait fortement penser à la longueur d'un filament d'ADN complexé par RecA. Plusieurs groupes se sont alors intéressés à la polymérisation de RecA sur un ADN sous tension [5, 6, 7].

Notre groupe [8, 9, 10] a complété l'étude de la réponse élastique de l'ADN sous contrainte mécanique en introduisant la technique des pinces magnétiques et étudiant la réponse torsionnelle de l'ADN. Nous avons alors pu mettre en évidence d'autres transitions de phases, dont une totalement nouvelle pour les ADNs que l'on force à avoir un pas hélical plus petit que celui de l'ADN B.

Toutes ces études ont permis de déterminer l'ensemble des propriétés élastiques de la molécule d'ADN dans l'ensemble de la gamme intéressante pour les interactions ADN-protéines. D'autres éléments ont été apportés plus tard par Léger et al. [11] ou encore le groupe de C. Bustamante [12] mais l'essentiel était alors là.

L'utilisation des propriétés élastiques de la molécules comme élément de référence pouvant alors servir à étudier les interactions ADN-protéines mais aussi aux moteurs travaillant sur l'ADN à l'échelle de la molécule unique ouvrant le champ à de nombreuses expériences : protéines structurales[13, 14, 15, 16], protéines impliquées dans la recombinaison homologue ([17, 18, 19, 5, 7, 20, 21], polymérases [22, 23, 24, 25, 26, 27, 28], hélicases [29], encapsidation des virus([30, 31]), enzymes de restrictions ([32, 33, 34, 35], nucléases[36], topoisomérases [37, 38, 39], chromatine[40, 41]....

Mon intérêt personnel sur ce thème s'est tout d'abord porté vers le problème de la formation des boucles dans l'ADN avant de dévier vers celui du transport d'ADN dans les

procaryotes. Ces thèmes sont présentés dans la première partie.

Par ailleurs dans des expériences pionnières les groupes de Yanagida ou Gaub([42, 43, 44]) par exemple ont couplé des techniques de micromanipulations avec une visualisation de molécule unique, ce qui permet d'obtenir des renseignements complémentaires. Ayant déjà des compétences en micromanipulations j'ai voulu développer l'approche des problèmes biophysiques par les techniques de fluorescence. J'ai donc consacré beaucoup de temps à faire de l'instrumentation pour développer cette thématique. Les progrès déjà concrétisés ont donné lieu à la seconde partie du manuscrit.

Compte tenu de la diversité des sujets que j'ai abordé depuis ma thèse me lancer dans une rédaction pédagogique aurait demandé énormément de temps et aurait produit un manuscrit un peu lourd. J'ai fait le choix de présenter une sélection d'articles auxquels j'ai collaboré en essayant de faire ressortir mes motivations scientifiques dans une partie introductive.

Huîtres, encornets et choux tendres

O. Roellinger

Ingrédients

2 douzaines d'huîtres creuses de Cancale bien dentelées. Les meilleures sont celles qui sont élevées sur le sol plutôt qu'en poche : elles prennent ainsi le goût du terroir - 2 petits encornets (demander au poissonnier de les préparer "en blanc" pour obtenir ainsi une chair immaculée et ne pas avoir à vous battre avec l'encre noire) - 1 chou de Pâques (chou nouveau pointu) - 1 dl de coteaux du Layon - Quelques bouquets de mâche - Des feuilles de pimprenelles - 1 dl de bouillon de volaille - 60 g de beurre - 1 feuille de "nori" (algue) séchée

Mélange d'épices : 1 c. à s. de curry de madras, 3 c. à s. de coriandre, 1 pointe de safran en poudre, 2 c. à s. de curcuma, 2 c. à s. de bois d'Inde, 3 cm de cannelle en bâton, un peu d'amchoor (poudre de mangue verte séchée) - Poivre

Préparation de base

Mélange d'épices : mixer le mélange d'épices et le passer à travers une passette fine ou un tamis. Faire réduire le vin blanc, ajouter le bouillon de volaille et 1/3 de c. à c. du mélange. Laisser infuser 20 minutes.

Couper de fines paillettes dans la feuille de nori et les préserver de l'humidité en les enfermant dans une petite boîte hermétique.

Effeuiller le chou et éliminer les grosses côtes (4 feuilles vertes et parfaites seront cuisinées). Dans de l'eau salée, pocher très rapidement les feuilles de chou à découvert, les rafraîchir dans de l'eau glacée, égoutter et réserver sur une assiette.

Ouvrir les huîtres, les décoquiller et les faire attendre dans leur eau, au préalable filtrée.

Couper en lanières de 0,5 cm de large sur 3 cm de long les encornets si vous n'avez pu vous en procurer des petits.

Dernière minute

A l'avance : préparer le mélange d'épices. Il suffit de les chauffer ensemble, à sec, dans une sauteuse, puis de laisser murir ce mélange dans une boîte en bois, pendant 15 jours au moins, avant de l'utiliser.

Un peu plus d'1 heure à l'avance : gratter les moules au couteau, les débarrasser de leur byssus (lien qui leur permet de se fixer aux rochers ou aux bouchots), les laver à grande eau sans les laisser tremper. Eplucher et ciseler l'échalote. Dans une grande casserole (surtout pas en aluminium), faire revenir l'échalote dans le beurre. Ajouter le vin blanc, donner un bouillon et verser les moules en maintenant la cuisson à couvert sur feu vif. Après 2 minutes, secouer le contenu de la casserole, attendre 2 minutes encore, vérifier que toutes les moules sont ouvertes et stopper immédiatement la cuisson. Les moules ne doivent absolument pas cuire après l'ouverture.

Mettre quelques moules entières de coté pour la garniture, décoquiller les autres, réserver.

Filtrer le jus de cuisson. Ajouter la même quantité de crème. Amener vivement à ébullition. Lorsque le jus commence à devenir onctueux, ajouter une cuillerée à café de curry (mélange d'épices) et laisser infuser ce velouté pendant 5 minutes.

http://www.maisons-de-bricourt.com

Deuxième partie

Micromanipulations sur des ADNs isolés

Chapitre 1

Systèmes formant des boucles

1.1 Introduction

La quasi totalité des protéines utilisées en biologie moléculaire se fixent en un seul site. L'exemple type est celui des enzymes de restriction de type II qui reconnaissent une séquence et coupent à l'intérieur de celle-ci ou à son très proche voisinage. Ceci induit l'*a priori* que les protéines se fixant en deux sites sont rares, ce qui n'est pas ce que l'on trouve dans la nature.

Le premier exemple que je vais prendre est celui des enzymes de restriction de type I. Ces enzymes se fixent en une séquence spécifique grâce à une partie du complexe protéique qui reconnait une séquence non méthylée (provenant donc d'ADN étranger) et la méthylant. Deux sous unités, comportant des motifs hélicases, peuvent alors se fixer de chaque côté et, par la consommation d'ATP pomper l'ADN vers la séquence formant ainsi des boucles. Deux autres sous-unités sont impliquées dans la coupure de l'ADN qui peut se faire à plusieurs milliers de paires de bases de la séquence de fixation. S. Halford, spécialiste des enzymes de restrictions, dans une conférence sur ce sujet a affirmé que selon ses estimations il y aurait plus d'enzymes de ce type que celles de typeII (conférence sur les enzymes de restriction à Bristol en 2004). Leur non utilisation en biologie moléculaire comme outil fait que les gens ne les recherchent simplement pas. On peut noter, et le groupe de S. Halford a fait un gros travail la dessus (voir [45] pour une revue par ce groupe sur la formation de boucles), que certaines enzymes de restriction de type II, dont la fonction ne nécessite pas de formation de boucles, peuvent avoir une activité accrue quand deux sites de coupures sont présent et qu'une boucle se forme entre les deux.

La formation de boucles peut servir à la régulation de l'expression de gènes. L'exemple qui va nous intéresser dans la suite est celui du régulateur du galactose GalR [46]. Dans ce système l'ARN polymérase va démarrer la transcription à partir d'un site qui est entouré par deux sites, distants de 113bps, sur lesquels se fixent un tétramère de la protéine GalR. Les tétramères forment ainsi une boucle qui bloque l'ARN polymérase l'empêchant de synthétiser une protéine. Lorsque du galactose est présent dans le milieu, celui-ci inhibe la fixation du tétramère, la boucle ne se forme alors pas et la synthèse protéique peut s'effectuer. Un autre système très proche est celui du lactose.

Les systèmes de recombinaison spécifique en séquence, tels Xer ou Cre , qui servent à insérer ou déléter ou inverser une séquence d'ADN *in vitro* ou *in vivo* [47] sont d'autres exemples importants sur lesquels nous reviendrons dans la suite.

Par ailleurs les chromosomes bactériens sont constitués de boucles topologiques dont

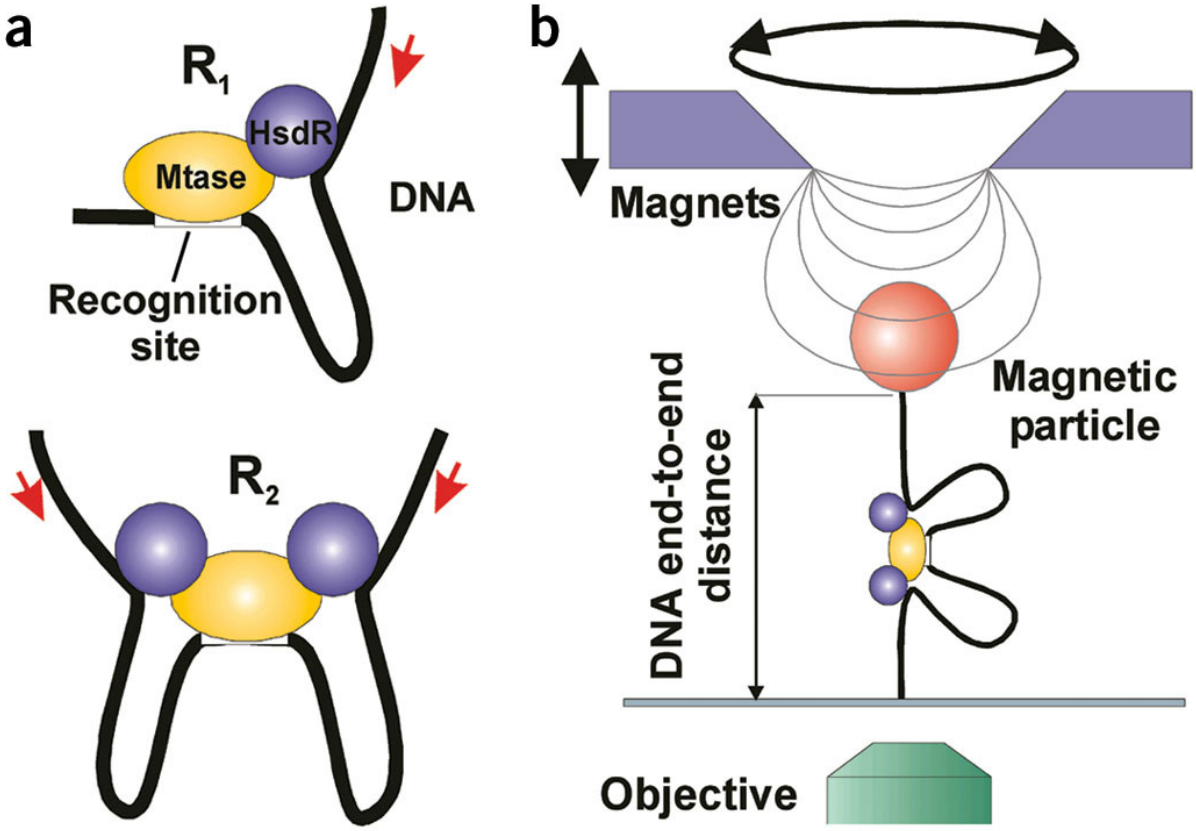

FIG. 1.1 – *TypeI restriction enzyme activity*

la taille est estimée à une grosse dizaine de milliers de paires de bases [48]. Les boucles peuvent ainsi aller de plusieurs dizaines de bases, où le rôle énergétique de la courbure va être prépondérant , à plusieurs dizaines de milliers de paires de bases où l'entropie va être l'ingrédient prépondérant.

1.2 Boucle d'ADN : l'exemple régulateur GalR

En parallèle à mes tentatives, infructueuses, sur un système artificiel , fusion entre un facteur de transcription Engrailed et Gal4, Laura Finzi nous a contacté pour regarder le système du régulateur du Galactose qui forme naturellement une boucle *in vitro*. Son étudiant d'alors, Giuseppe Lia est alors venu au laboratoire pour travailler sur ce système. Il a été le premier utilisateur sérieux du premier microscope, entièrement fait maison, dédié aux micromanipulations que j'ai construit au laboratoire. Le rôle biologique de cette interaction a été décrit dans le paragraphe précédent. Les résultats sont décrits dans l'article suivant.

Supercoiling and denaturation in Gal repressor/heat unstable nucleoid protein (HU)-mediated DNA looping

Giuseppe Lia*†, David Bensimon‡, Vincent Croquette‡, Jean-Francois Allemand‡§, David Dunlap¶, Dale E. A. Lewis‖, Sankar Adhya‖, and Laura Finzi*,**

*Department of Biology, University of Milan, 20133 Milan, Italy; ‡Laboratoire de Physique Statistique and Department de Biologie, and §Departement de Chimie, Ecole Normale Superieure, 75005 Paris, France; ¶San Raffaele Scientific Institute, 20132 Milan, Italy; and ‖Laboratory of Molecular Biology, National Cancer Institute, Bethesda, MD 20892

Contributed by Sankar Adhya, July 31, 2003

The overall topology of DNA profoundly influences the regulation of transcription and is determined by DNA flexibility as well as the binding of proteins that induce DNA torsion, distortion, and/or looping. Gal repressor (GalR) is thought to repress transcription from the two promoters of the *gal* operon of *Escherichia coli* by forming a DNA loop of ≈40 nm of DNA that encompasses the promoters. Associated evidence of a topological regulatory mechanism of the transcription repression is the requirement for a supercoiled DNA template and the histone-like heat unstable nucleoid protein (HU). By using single-molecule manipulations to generate and finely tune tension in DNA molecules, we directly detected GalR/HU-mediated DNA looping and characterized its kinetics, thermodynamics, and supercoiling dependence. The factors required for *gal* DNA looping in single-molecule experiments (HU, GalR and DNA supercoiling) correspond exactly to those necessary for *gal* repression observed both *in vitro* and *in vivo*. Our single-molecule experiments revealed that negatively supercoiled DNA, under slight tension, denatured to facilitate GalR/HU-mediated DNA loop formation. Such topological intermediates may operate similarly in other multiprotein complexes of transcription, replication, and recombination.

The nucleoid structure in the bacterium *Escherichia coli* contains a circular DNA molecule of 4.7 million bp present in highly condensed form. The condensation is mediated by DNA supercoiling and the binding of several small nucleoid-associated proteins, e.g., heat unstable nucleoid protein (HU), integration host factor (IHF), factor for inversion stimulation (FIS), histone-like nucleoid structuring protein (HNS), suppressor of thymidylate synthase mutant phenotype A (StpA), and DNA binding protein from starved cells (Dps). These proteins are known to bend DNA or bind to altered structures of DNA. It is suggested that these proteins are mainly responsible for the compaction of DNA in a way that distinguishes the bacterial nucleoid from eukaryotic chromatin. These proteins are also associated with the machinery of macromolecular biosynthesis, including RNA polymerase and specific gene-regulatory, DNA-binding proteins such as repressors and activators. Indeed, DNA may serve as a scaffold for the organized recruitment and assembly of proteins at specific positions to create nucleoprotein complexes with specific activity and regulatory properties. Such positioning has long been postulated to be the mechanism of repression of the *gal* operon by the gal repressor dimer protein (GalR). GalR represses transcription initiation from the two promoters, *P1* and *P2*, of the *gal* operon by binding to two spatially separated operators, O_E and O_I, which encompass the promoters (1). Repression also requires supercoiled DNA and the presence of the nucleoid-associated protein HU (2). It has been proposed that a DNA loop generated by the interaction of the two operator-bound gal repressors inactivates the promoter (3). Repression of the *gal* operon would, thus, occur when a nucleoprotein complex forms containing supercoiled DNA, two GalR dimers, and HU. However, direct evidence of such looped complex has not been reported previously. Furthermore, an understanding of local conformational changes and their thermodynamic driving forces is required to relate structure to function.

Conventional techniques for studying DNA–protein interactions are restricted to observing the average properties of molecular ensembles. To breach this constraint, we have used magnetic tweezers (4) to unwind and stretch single DNA molecules, containing the regulatory segment of the *gal* operon, to study the molecular mechanism of transcriptional control by the Gal repressor protein. We reasoned that, if DNA looping was to cause transcriptional repression of the *gal* operon, it would be possible to detect transitions between short (looped) and long (unlooped) conformations of single, supercoiled *gal* DNA molecules under moderate tension only in the presence of the GalR and HU proteins (Fig. 1*a*).

Materials and Methods

Sample Preparation and Experimental Set Up. The linear DNA fragments used in the single-molecule experiments are prepared by linearization of plasmid pBR509. pBR509 contains 288 bp of the *gal* operon (from −197 to 91 bp from transcriptional initiation site) between *Eco*RI and *Bam*HI restriction sites of pBR322. pBR509 also contains a sequence of 6,497 bp from the digestion of λ phage with *Bam*HI and *Sph*I. Digestion of pBR509 with *Sal*I and *Eag*I allowed ligation of these two ends with two "tails" labeled with biotin and digoxigenin, respectively. The two different DNA "tails" are synthesized by PCR by using biotin-labeled nucleotides in one and digoxigenin-labeled nucleotides in the other. In so doing, the labels will be on both strands of the DNA tail. The biotinated tail and the digoxigeninated one, ≈1000 bp long, will contain an *Eag*I and a *Sal*I site, respectively. In this way, after digestion of the tails, they can be ligated to the opposite ends of the fragment from pBR509. Single molecules of DNA were attached at one end to the glass surface of a microscope flow-chamber and at the other end to a paramagnetic bead 2.8 μm in diameter. Magnetic tweezers (4) were used to twist and pull single DNA molecules attached to the beads, and the length of the DNA was monitored by 3D, video-rate monitoring of the bead (5). By tracking the 3D position of the tethered bead (5, 6), the extension $l = \langle z \rangle$ of the molecule can be

Abbreviations: HU, heat unstable nucleoid protein; GalR, gal repressor dimer protein; SSB, single-stranded binding protein; ssDNA, single-stranded DNA.

†Present address: Laboratoire de Physique Statistique, Ecole Normale Superieure, 75005 Paris, France.

**To whom correspondence should be addressed at: Dipartimento di Biologia and Centro Interdipartimentale Materiali e Interfacce Nanostrutturate, Università di Milano, Via Celoria 26, 20133 Milan, Italy. E-mail: laura.finzi@unimi.it.

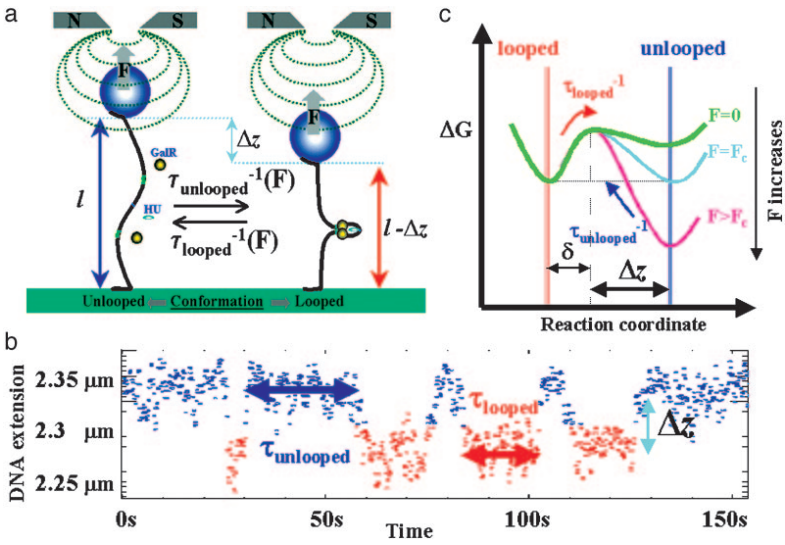

Fig. 1. Experimental set-up. (*a*) A single DNA molecule tethering a magnetic bead to a surface can be twisted and stretched by using small magnets placed above the sample. DNA loop formation by GalR and HU reduces the bead-to-surface distance by an amount Δz at the expense of the work, $F\Delta z$, performed against the stretching force F. The tension on the DNA may be used to tune the transition rates, $(\tau_{unlooped})^{-1}$ and $(\tau_{looped})^{-1}$, between the unlooped and looped state. (*b*) A typical telegraph-like signal. (*c*) A diagram illustrating the variation of ΔG for the reaction involving the DNA conformational change associated with loop opening. The activation energy for loop opening, $E_b - \delta F$, is slightly decreased on pulling, whereas the activation energy for loop formation, $E_f + F\Delta z$, is increased on pulling.

measured, with an error of ≈10 nm with 1-s averaging. The horizontal motion of the bead $\langle \Delta x^2 \rangle$ allows the determination of the stretching force via the equipartition theorem: $F = k_B T / \langle \Delta x^2 \rangle$. F was measured with 10% accuracy. To eliminate microscope drift, differential tracking was performed via a second bead glued to the surface.

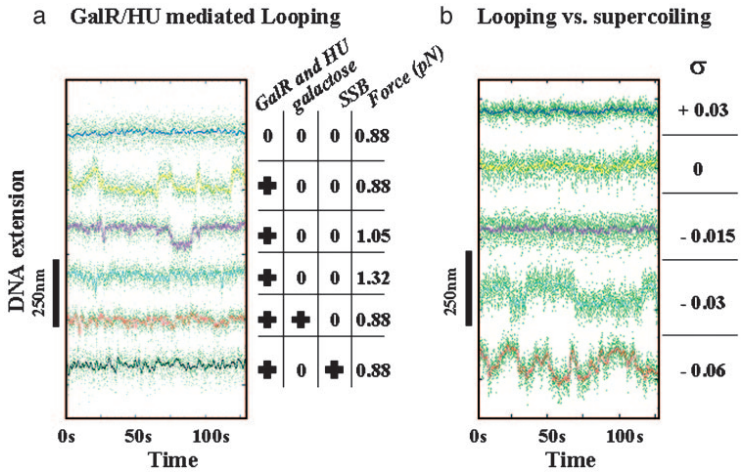

Fig. 2. Traces of DNA length vs. time. The green dots are raw data, whereas the continuous colored lines are the averaged signal. The pertinent conditions are indicated beside each trace. Measurements were conducted at room temperature by using a solution containing 20 mM Tris·HCl (pH 7.8), 1 mM DTT, 50 mM NaCl, and 5 mM $MgCl_2$. The GalR and HU concentrations were 25 nM and 50 nM, respectively. BSA and SSB were used at concentrations of 40 nM. (*a*) Variations in DNA extension at constant supercoiling ($\sigma = -0.03$) and force at $F = 0.88$ pN, unless otherwise stated. DNA with: no proteins (turquoise), GalR and HU (yellow), GalR and HU with a tension of 1.05 pN (purple), GalR and HU with a tension of 1.32 pN (cyan), GalR and HU and galactose (red), and GalR, HU, and SSB (dark green). (*b*) DNA extension at $F = 0.88$ pN, in the presence of GalR and HU as a function of supercoiling. $\sigma = +0.03$ (blue); $\sigma = 0$ (yellow); $\sigma = -0.015$ (purple); $\sigma = -0.03$ (cyan); and $\sigma = -0.06$ (red). σ is the superhelical density in the DNA defined as $(Lk - Lk_0)/Lk_0$, where Lk is the linking number of DNA and is given by the sum of its twist (Tw) and writhe (Wr). In relaxed DNA, $Lk = Lk_0 = Tw$ = (number of bp)/10.4 bp. Similarly, in our single-molecule experimental conditions in which DNA molecules are stretched, the distribution between Tw and Wr is about 3:1 whereas in plasmids (unnicked and under no tension) it is about 1:3. As a result, the torsion within each molecule in our measurements at $\sigma = -0.03$ (i.e., with $Tw \approx 0.022\ Lk_0$) is slightly higher than the torsion present in a plasmid at sigma $= -0.06$ (i.e., with $Tw \approx 0.015\ Lk_0$).

Data Processing. Traces with transitions between longer (unlooped) to shorter (looped) lengths were best fitted to the raw data $l(t)$ (filtered at 2 Hz) by using a sliding Heaviside (step) function: $l_{\text{step}}(t) = s\theta(t - t_1) + l_1$ defined over a time window of size T_{av}. In other words, for every t_0 of the data set, the parameters of the step function (s, t_1, l_1) were fitted such as to minimize the error $(l(t) - l_{\text{step}}(t))^2$ in the time window $t_0 < t < t_0 + T_{\text{av}}$, where only one transition is expected. At the end, the parameters that consistently scored best (χ^2 test) were selected as steps. The time interval between successive looped and unlooped steps was binned to form histograms of τ_{unlooped} (τ_{looped}) corresponding to the time spent in the longer (shorter) state.

Free Energy Calculation: Loop Formation. For an activated process Arrhenius' law yields (7): $\tau_{\text{unlooped}}(F) = \tau_0 \exp((E_f + F\Delta z)/k_BT)$ and $\tau_{\text{looped}}(F) = \tau_0 \exp[(E_b - F\delta)/k_BT]$. τ_{unlooped} and τ_{looped} are the average lifetimes of the unlooped and looped conformations, E_f and E_b are the energy barriers to formation and breakdown of the DNA loop at zero force, k_B is Boltzman's constant, T is the temperature, Δz is the decrease in the DNA's extension due to the formation of a loop, and δ is the minimum separation between the two GalR dimers that leads to loop breakdown (6) [about 1 nm (8)]. Considering both looping and unlooping to be first order reactions, the free energy of looping is therefore: $\Delta G_l = k_BT \ln(\tau_{\text{unlooped}}/\tau_{\text{looped}})$. Notice that at the critical force $F = F_c$ where $\tau_{\text{unlooped}} = \tau_{\text{looped}}$: $\Delta G_l = 0$. The free energy of looping at zero force is thus: $\Delta G_{l,0} = E_f - E_b = -F_c(\Delta z + \delta)$ (see *Supporting Text*, which is published as supporting information on the PNAS web site, www.pnas.org).

Transcription Assays. Supercoiled DNA plasmids (2 nM) were preincubated at 37°C for 5 min in transcription buffer (20 mM Tris acetate/10 mM Mg acetate/50 mM NaCl) supplemented with 1 mM DTT, 1 mM ATP, and 0.8 units recombinant ribonuclease inhibitor (rRNasin) and 20 nM RNA polymerase in a total reaction volume of 50 μl. When required, 80 nM GalR and/or 160 nM HU and/or single-stranded binding protein (SSB) were added before RNA polymerase. To start the transcription reactions, nucleotides were added to a final concentration of 0.1 mM GTP and CTP, 0.01 mM UTP, and 5 μCi [α-^{32}P]UTP (1 Ci = 37 GBq). The reactions were incubated for an additional 10 min before they were terminated by the addition of an equal volume (50 μl) of loading dye (90% formamide/10 mM EDTA/0.1% xylene cyanol/0.1% bromophenol blue). Samples were heated to 90°C for 2–3 min, chilled, then loaded on an 8% sequencing gel and electrophoresed at a constant power of 60 W in TBE (90 mM Tris/64.6 mM boric acid/2.5 mM EDTA, pH 8.3). The RNAI transcripts (108 nt) were used as an internal control to quantify the relative number of *gal* transcripts.

Results and Discussion

DNA molecules that were negatively supercoiled by at least 3% ($\sigma = -0.03$) and stretched with a force (F) of 0.88 pN intermittently switched between two conformations in the presence of both GalR and HU (Figs. 1*b* and 2*a*). We verified that no telegraphic signals were observed in the absence of GalR and/or HU (data not shown), or in the presence of 40 nM D(+)-galactose, an inducer of *gal* transcription (Fig. 2*a*). Similarly, GalR and HU did not generate looping in molecules containing only one operator, O_E or O_I (data not shown). Taken together, these measurements confirm the widely held hypothesis that GalR and HU induce DNA looping in the *gal* operon.

The higher force was expected to shift the thermodynamic equilibrium to favor the unlooped form (Fig. 1*c*). Indeed, the probability of looping decreased when the tension was raised to 1.32 pN (Fig. 2*a*). Interestingly, the length of DNA that separates the GalR binding sites O_E and O_I (113 bp or 38 nm for B-DNA) is less than the 55 ± 5 nm transition (Δz) observed experimentally. This finding is consistent with a recently proposed antiparallel loop (9) in which the DNA exiting the loop complex gradually bends to align in the direction of stretching.

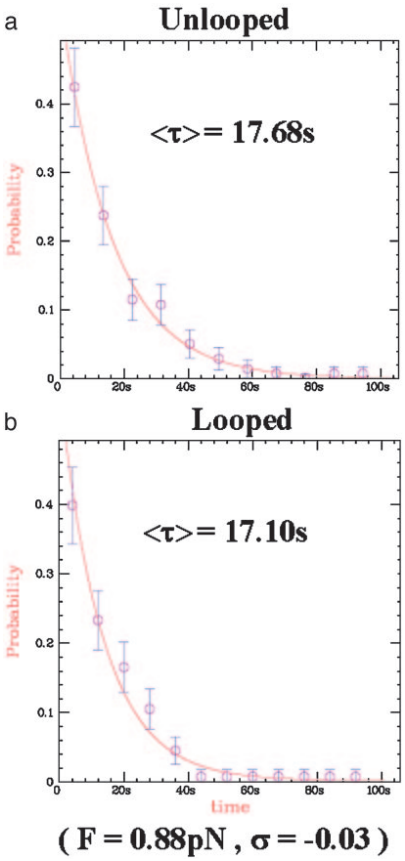

Fig. 3. Mean lifetimes of the looped and the unlooped DNA conformations were calculated from histograms of the lifetimes at $F = 0.88$ pN and 3% negative supercoiling.

Kinetic and Thermodynamic Parameters. By analyzing the lifetimes of the looped and unlooped DNA conformations in traces like those in Fig. 2, we were able to determine the mean lifetimes as a function of force and calculate the free energy changes of the looping reactions. In all cases, the lifetime distributions were well fit by single exponentials (Fig. 3). Thus, in our experiment, loop formation and breakdown can be analyzed as a two-state system. At a force of 0.88 pN, the mean lifetimes for both the looped and unlooped conformations were 17 s. The lifetimes for zero tension were calculated applying the following relations: $\tau_{\text{unlooped}}(F) = \tau_{\text{unlooped}}(0) \exp(F\Delta z/k_BT)$, where $\Delta z \approx 55$ nm and $\tau_{\text{looped}}(F) = \tau_{\text{looped}}(0) \exp(-F\delta/k_BT)$, where $\delta \approx 1$ nm (8) yielding $\tau_{\text{unlooped}}(0) \approx 0.1$ ms and $\tau_{\text{looped}}(0) \approx 21$ s. Thus, the lifetime of the unlooped state dramatically increases with the DNA tension, whereas the life time of the GalR/HU-mediated loop remains

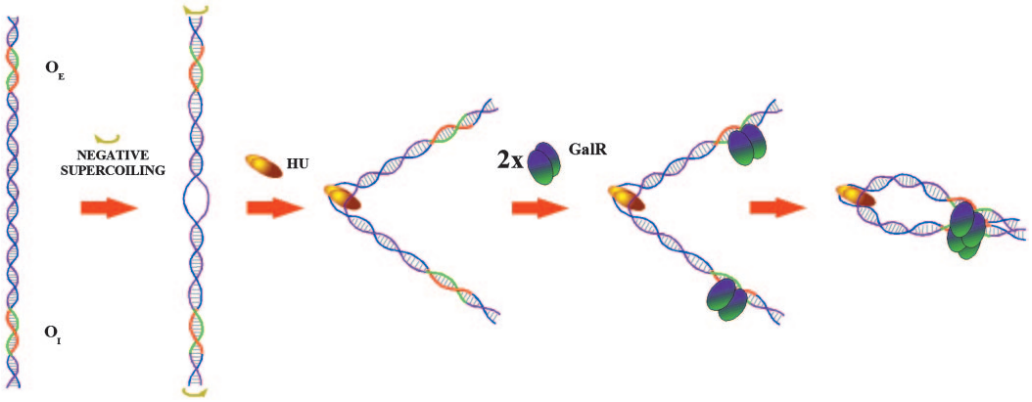

Fig. 4. Suggested model of the mechanism of GalR/HU-induced DNA loop formation. Negative supercoiling favors the opening of a bubble of a few base pairs in the DNA. HU binds preferentially to it, subsequently bending the ssDNA and stabilizing the interaction between two GalR dimers and loop closure.

essentially unchanged. From these lifetimes, we estimated the free energy change involved in the GalR/HU-mediated loop: $\Delta G_{l,0} = k_B T \ln \tau_{unlooped}(0)/\tau_{looped}(0) \approx -12\ k_B T$ or -7.1 kcal/mol (see *Materials and Methods*, *Supporting Text*, and refs. 8 and 10). This is a surprisingly large free energy change, commensurate with the $12\,k_B T$ liberated by the hydrolysis of one ATP molecule.

A comparison of this value with that estimated from data reported for the lac repressor protein (LacI) (11), underscores the thermodynamic role, played by the HU protein. In the case of LacI-induced DNA loops, Matthews and colleagues (11) used filter binding of supercoiled plasmids or linear DNA fragments (12) to estimate the unlooping equilibrium constant to be 890 in the presence of supercoiling and 510 times larger in the absence of supercoiling (11). From the relation $\Delta G = -k_B T \ln K_{eq}$, the free energy for LacI-mediated DNA looping in their supercoiled DNA can be determined to be $-6.8\ k_B T$ (4 kcal/mol). In single-molecule experiments (13), a similar value of $-7\ k_B T$ can be calculated from the ratio of mean lifetimes for looped and unlooped states (K_{eq}) of linear DNA in the presence of LacI by using the 510 factor found by Matthews and colleagues (12) to account for supercoiling. Considering that (*i*) LacI has a higher affinity for its operator site, O_1, than GalR has for O_E and O_I, (*ii*) LacI is a stable bidentate tetramer, whereas GalR dimers interact weakly, and (*iii*) the 305-bp *lac* DNA loop is more flexible than the 113-bp *gal* DNA loop, HU seems to dramatically stabilize looping in the *gal* system.

The Role of HU and DNA Supercoiling. To further clarify the roles of HU and DNA supercoiling, we studied DNA loop formation and breakdown in DNA molecules with different values of supercoiling (Fig. 2*b*) under a condition when the free energy for loop formation is 0 ($F \approx 0.9$ pN). Transitions were not observed in either positively supercoiled DNA ($\sigma = +0.03$), relaxed DNA ($\sigma = 0$), or in DNA unwound by 1.5% ($\sigma = -0.015$). However, loop formation and breakdown were observed for DNA unwound by 3% or more ($\sigma = -0.03$ or -0.06), which exceeds the 1.5% required to denature AT-rich regions in DNA under tension (14–16). Considering that the HU binding site at the apex of the *gal* DNA loop is AT rich and palindromic (9, 17), and that HU preferentially binds to altered DNA structures such as denatured or cruciform DNA (18–22), we reasoned that HU may facilitate GalR-mediated looping by tightly binding the

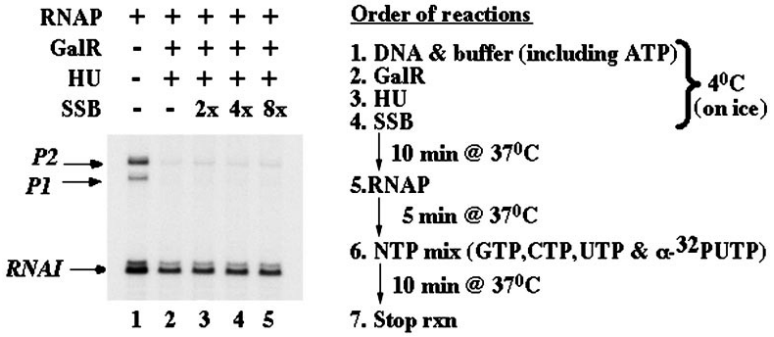

Fig. 5. *In vitro* transcription assay. Radiolabeled RNA products of an *in vitro* transcription assay were separated by gel electrophoresis (*Left*). A scheme of the procedure is on the *Right*. SSB added to lanes 3–5 did not interfere with repression of transcription from promoters *P1* and *P2* due to looping induced by GalR/HU (lane 2). No repression is observed without GalR/HU (lane 1).

single-stranded DNA (ssDNA) in the unwound segment induced by negative supercoiling. Such a conformation would lower the energy required for looping, because ssDNA is more flexible than double-stranded DNA. The model just hypothesized is described in Fig. 4.

To test this hypothesis, we investigated whether or not SSB interfered with GalR/HU-mediated looping. SSB (23) and HU (24) proteins both have dissociation constants in the nanomolar range for binding to single-stranded DNA. Addition of SSB to our assay eliminated all transitions between looped and unlooped conformations (Fig. 2*a*), whereas BSA, used as a control, had no effect (data not shown). This result suggested that HU binding to ssDNA might be required for repression of the *gal* operon. SSB was also used in an *in vitro* transcription assay using supercoiled plasmids ≈3 kb long. In this case, SSB added before RNA polymerase did not alter simultaneous repression of *P1* and *P2* by HU and GalR (Fig. 5).

Energetic considerations nicely explain the difference between the *in vitro* transcription and the looping experiments. With 0.9 pN of tension in the DNA, the ΔG of loop formation is 0 and that of SSB binding to DNA is approximately $-9\ k_BT$ (25). Thus, SSB is an effective competitor of GalR/HU-mediated looping. On the other hand, in the transcription assay in which the DNA is not stretched, the free energy change associated with loop formation becomes approximately $-12\ k_BT$. At the same time, SSB binding becomes less favorable given the higher temperature of this assay (26) and cannot compete effectively with the looping reaction. Stretching the DNA deftly shifted the free energy landscape to favor competition by SSB, and it remains to be shown that *gal* DNA is under similar tension *in vivo*.

Conclusion

Our work shows that manipulation of single molecules permits the analysis of macromolecular machinery of increasing complexity. Kinetic control achieved through tensioning single DNA molecules permitted the characterization of a loop that is remarkably stabilized thermodynamically by the HU protein. Such a high negative free energy change ensures rapid repression when galactose is unavailable. SSB interfered with the formation of the loop in gently stretched molecules, which might be relevant to conditions *in vivo*, in which genomic DNA is supercoiled, topologically constrained by proteins, and locally tensioned by DNA processing enzymes (27). Transcriptional control via such a loop would be inherently sensitive to the local environmental and energetic context. The multifactorial and characteristic kinetic and thermodynamic properties of *gal* DNA looping distinguish a dynamic system for reducing the expression of the products of *gal* operon (28). Besides induction (loop breakdown) of the operon by D(+)-galactose, which acts by inactivating GalR, the loop must break down for expression in response to anabolic needs resulting from changes in DNA superhelicity or HU concentration (29–31).

This work was supported by grants from Ministero dell'Istruzione, dell'Università e della Ricerca (MIUR) and the Human Frontier Science Program (HFSP) (to L.F.); grants from MIUR (to D.D.); an Erasmus fellowship (to G.L.); grants from Association pour la Recherche sur le Cancer (ARC) (to V.C.), Centre National de la Recherche Scientifique (CNRS), Ecole Normale Supérieure (ENS), Université Paris VI, and Université Paris VII and CEE MolSwitch (to D.B.); support from the French Ministere de la Recherche (to J.-F.A.); and grants from the National Institutes of Health Intramural Research Program (to S.A. and D.E.A.L.).

1. Irani, M. H., Orosz, L. & Adhya, S. (1983) *Cell* **32,** 783–788.
2. Aki, T., Choy, H. E. & Adhya, S. (1996) *Genes Cells* **1,** 179–188.
3. Choy, H. E., Park, S. W., Parrack, P. & Adhya, S. (1995) *Proc. Natl. Acad. Sci. USA* **92,** 7327–7331.
4. Strick, T. R., Allemand, J. F., Bensimon, D. & Croquette, V. (1996) *Science* **271,** 1835–1837.
5. Grosse, C. & Croquette, V. (2002) *Biophys. J.* **82,** 3314–3329.
6. Strick, T. R., Allemand, J. F., Croquette V. & Bensimon, D. (1998) *J. Stat. Phys.* **93,** 647–672.
7. Rief, M., Fernandez, J. & Gaub, H. (1998) *Phys. Rev. Lett.* **81,** 4764–4767.
8. Marko, J. F. & Siggia, E. D. (1997) *Biophys. J.* **73,** 2173–2178.
9. Geanacopoulos, M., Vasmetzis, G., Zhurkin, V. B. & Adhya, S. (2001) *Nat. Struct. Biol.* **8,** 432–436.
10. Liphardt, J., Onoa, B., Smith, S. B., Tinoco, I., Jr., & Bustamante, C. (2001) *Science* **292,** 733–737.
11. Whitson, P. A., Hsieh, W.-T., Wells, R. & Matthews, K. S. (1987) *J. Biol. Chem.* **262,** 4943–4946.
12. Hsieh, W.-T., Whitson, P., Matthews, K. S. & Wells, R. D. (1987) *J. Biol. Chem.* **262,** 14583–14591.
13. Finzi, L. & Gelles, J. (1995) *Science* **267,** 378–380.
14. Strick, T. R., Croquette, V. & Bensimon, D. (1998) *Proc. Natl. Acad. Sci. USA* **95,** 10578–10583.
15. Allemand, J.-F., Bensimon, D., Lavery, R. & Croquette, V. (1998) *Proc. Natl. Acad. Sci. USA* **95,** 14152–14157.
16. Hwa, T., Marinari, E., Sneppen, K. & Tang, L. (2003) *Proc. Natl. Acad. Sci. USA* **100,** 4411–4416.
17. Aki, T. & Adhya, S. (1997) *EMBO J.* **16,** 3666–3674.
18. Bonnefoy, E., Takahashi, M. & Rouvière-Yaniv, J. (1994) *J. Mol. Biol.* **242,** 116–129.
19. Castaing, B., Zelwer, C., Laval, J. & Boiteux, S. (1995) *J. Biol. Chem.* **270,** 10291–10296.
20. Kobryn, K., Lavoie, D. & Chaconas, G. (1999) *J. Mol. Biol.* **289,** 777–784.
21. Grove, A., Galeone, A., Mayol, L. & Geiduschek, E. P. (1996) *J. Mol. Biol.* **260,** 196–206.
22. Grove, A. & Lim, L. (2001) *J. Mol. Biol.* **311,** 491–502.
23. LeCaptain, D. J., Michel, M. A. & Van Orden, A. (2001) *Analyst* **126,** 1279–1284.
24. Kamashev, D. & Rouvière-Yaniv, R. (2000) *EMBO J.* **19,** 6527–6535.
25. Bujalowski, W. & Lohman T. M. (1987) *J. Mol. Biol.* **195,** 897–907.
26. Overman, L. B., Bujalowski, W. & Lohman, T. (1988) *Biochemistry* **27,** 456–471.
27. Forde, N. R., Izhaky, D., Woodcock, G. R., Wuite, G. J. & Bustamante, C. (2002) *Proc. Natl. Acad. Sci. USA* **99,** 11682–11687.
28. Adhya, S. (1987) in *Escherichia coli and Salmonella typhimirium*, ed. Neidhardt, F. (Am. Soc. Microbiol., Washington, DC) pp. 1503–1512.
29. Claret, L. & Rouvière-Yaniv, J. (1997) *J. Mol. Biol.* **273,** 93–104.
30. Wei, Y., Lee, J. M., Richmond, C., Blattner, F. R., Rafalski, J. A. & LaRossa, R. A. (2001) *J. Bacteriol.* **183,** 545–556.
31. Azam, T. A. & Ishihama, A. (1999) *J. Biol. Chem.* **274,** 33105–33113.

Chapitre 2

FtsK

2.1 Contexte

Lorsque les expériences sur GalR ont démarré au laboratoire c'est donc Giuseppe Lia qui a effectué les expériences au quotidien. Je me suis dit alors que j'allais chercher un autre système expérimental compte tenu de mes échecs sur le système artificiel Engrailed/Gal4.

Le système expérimental qui m'intéressait le plus *a priori* était celui de la Cre recombinase. En effet la Cre recombinase reconnaît deux sites très spécifiques les sites LoxP. Suivant l'orientation de ceux-ci, la Cre recombinase coupe littéralement la séquence d'ADN présente entre les deux sites ou inverse l'orientation de l'ADN entre les sites. Cette enzyme est utilisée *in vivo* pour supprimer certains gènes ou en déclencher d'autres. Cela veut dire l'interaction ADN protéine est suffisamment forte et spécifique pour interagir entre deux sites distants de plusieurs milliers de bases... alors même que la probabilité de la simple rencontre des deux sites est *a priori* faible. Ce système est parfait pour des expériences *in vitro* car tous les ingrédients sont connus et disponibles commercialement. J'ai pu effectuer des quelques expériences préliminaires avec ce système mais je n'ai pu observer de recombinaison qu'en l'absence de force. Il faut dire pour être sur d'observer une délétion j'avais mis des sites LoxP distants de 1.5kbases ce qui compte tenu du rôle de la force sur la formation de boucle est une distance trop grande pour espérer voir quelque chose avec une force raisonnable permettant son observation en temps réel. Un des problèmes intrinsèques à ce système pour nos expériences est qu'il induit une vraie réaction qui détruit le substrat si le réaction produit une délétion de l'ADN. Si l'orientation des sites LoxP est telle que l'on a une simple inversion de la séquence entre les sites dans ce cas on a une réaction reproductible mais on ne sait pas vraiment si la réaction a eu lieu. J'ai donc cherché à trouver des mutants qui se fixent sur l'ADN, forment la boucle, appelée synapse mais ne coupent pas.

Pour cela je suis allé à la conférence bi-annuelle sur la recombinaison de sites spécifiques qui était organisée en 2002 à Oxford par le prof. D. Sherratt. Lors de cette conférence j'ai rencontré F.X. Barre qui travaillait sur le système de recombinaison XerC/D d'*E. coli*. J'avais noté ce système comme potentiellement intéressant mais deux points majeurs m'avaient gênés. Premièrement le système n'existe pas commercialement ce qui me posait un problème pratique mais de plus dans ce système les deux recombinases ont besoin d'un troisième partenaire FtsK pour fonctionner....Rajouter un composant étant toujours rajouter une source de problèmes expérimentaux j'étais donc assez réticent. Cependant F.X. Barre m'a convaincu qu'il maîtrisait suffisamment FtsK pour que cette protéine ne soit pas un soucis et que je pouvais donc regarder le système Xer plutot que Cre (ce qui pour moi revenait effective-

ment au même a priori en terme de boucles). Par ailleurs comme durant son post doc chez D. Sherratt il avait montré que FtsK était un moteur cela pouvait déjà être intéressant en soi...ce fut je crois une excellente idée. Seule complication D. Sherratt partait quelques mois après chez N. Cozzarelli et C. Bustamante pour travailler sur le même sujet...voila de quoi pimenter notre recherche...

2.2 FtsK et son rôle chez *E. coli*

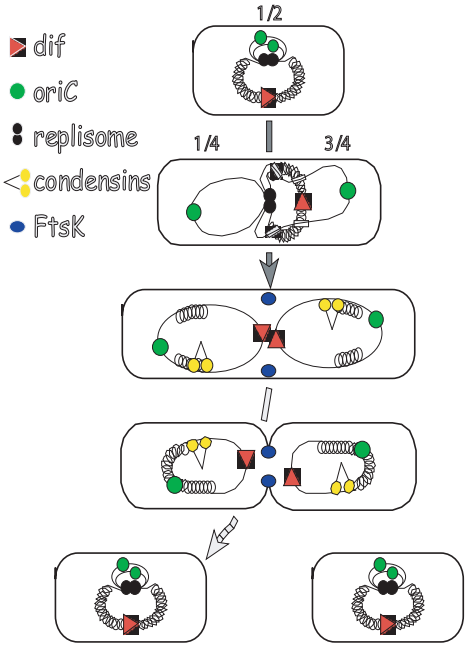

FIG. 2.1 – *Schéma simplifié de la division celullaire chez E. coli. Le génome de la bactérie est circulaire et contient 4.1Mbps. OriC est la séquence où démarre la réplication. Toute la machinerie de la répication est notée réplisome. Les condensines servent à compacter l'ADN qui sinon ne tiendrait pas dans la bactérie. La non coordination des processus cellulaires fait que la fermeture du septum peut se faire alors que les chromosomes ne sont pas encore correctement positionnés et de l'ADN peut se trouver ainsi piégé. Les séquences dif sont à l'opposé sur le chromosome de OriC. Cette région est celle qui a la plus forte probabilité d'être piégée lors de la fermeture du septum. Le moteur FstK se positionne au niveau du septum et pompe l'ADN chromosomique dans le bon compartiment. Figure venant de [49].*

Le chromosome d'*E. coli* est circulaire et sa séquence possède environ 4Mbases. Pour ce qui nous intéresse dans ce qui suit, son organisation est caractérisée par une origine de réplication, nommée oriC, qui se situe en un point du chromosome qui est symétriquement opposé au site *dif* qui est reconnu par les recombinases Xer C et XerD. Les sites de terminaisons de la réplication se situant au voisinage du site *dif* (voir [50] pour une revue des points évoqués ci-dessous).

La division cellulaire bactérienne ne fait pas intervenir de coordination temporelle comme chez les eucaryotes. Réplication, migration des chromosomes ont lieu en même temps. De

plus à la différence de ce qui existe chez les eucaryotes il n'y a pas de fuseau mitotique avec des moteurs bien identifiés pour amener le chromosome bactérien dans la bonne cellule, mère ou fille. Ceci pose le problème de la ségrégation des chromosomes. Il n'y aucune raison pour qu'au moment ou le septum se ferme pour donner les cellules filles la totalité de l'ADN soit au bon endroit. Il faut donc envisager l'existence d'un moteur pour pomper l'ADN au bon endroit. Chez *Bacilus Subtilis* un moteur était déjà identifé comme étant

nécessaire à l'enpaquetage de l'ADN lors de la sporulation : SpoIIIE [51]. Des analyses de séquences montrent une grande similarité entre les deux protéines. FtsK était donc un parfait candidat pour remplir ce rôle d'autant plus qu'il a été montré que FtsK se localise au niveau du septum (lieu où se contracte la paroi cellulaire lors de la division cellulaire) au moment de la division. Par ailleurs FtsK est connu pour avoir un second rôle majeur au cours du

cycle bactérien. Lors du cycle cellulaire des recombinaisons homologues ont lieu(échange de brins d'ADN entre deux molécules présentant des séquences homologues). Suivant le nombre d'échanges de brins la formation de dimères de chromosomes est possible. Cela se produit dans un peu plus de 10% des divisions cellulaires. Evidemment la présence de ce dimère de 8Mbases au lieu de deux monomères de 4Mbases est mauvais pour la survie de la bactérie et celle-ci a développé un moyen de résoudre ces dimères. Sans cette résolution la croissance des bactéries produit des filaments d'ou le nom de la protéine FtsK. Les recombinases XerC et D qui reconnaissent les sites *dif*, présents en double exemplaire sur le chromosome de dimères, permettent de faire l'échange de brins supplémentaire qui permet de séparer les deux monomères. Or cette réaction a besoin d'un troisième partenaire : la réaction n'est complète que si FtsK contacte XerD. La conclusion de ces observations est que

FtsK est positionnée au niveau du septum lors de la division bactérienne. Elle doit pomper l'ADN qui resterait bloqué dans la mauvaise cellule pour éviter qu'il ne soit coupé lors de la fermeture du septum et de plus FtsK doit pomper de manière à amener les sites *dif* au voisinage l'un de l'autre pour que la recombinaison catalysée par les recombinases XerC et D permette de résoudre les dimères potentiels.

Le laboratoire de D. Sherratt, durant le séjour post doctoral de FX Barre avait pu montrer un vitro l'activité ATPase de la partie C terminale de FtsK et sa capacité à induire un couple de torsion dans l'ADN montrant ainsi une activité de translocation [52].

Notre première tâche a donc été de voir ce que produisait l'addition de FtsK dans notre expérience de micromanipulation de molécules d'ADN. Il faut être conscient qu'*a priori* une expérience de micromanipulation d'ADN ne permet pas de détecter l'activité d'une simple translocase. En effet une fois sa fixation effectuée une translation de celle-ci ne doit pas induire de changement de longueur de la molécule sous traction. Seule la production de supertours ou la formation de boucles permettrait d'observer une translocase. Il se trouve que la protéine FtsK tronquée avec laquelle nous avons travaillé produit les deux effets. Les ré-

sultats principaux que nous avons obtenus se trouvent dans les deux articles suivants.

En plus de ces résultats sur les aspects purement moteurs de FtsK nous avons également étudié l'effet de séquences reconnues par FtsK et qui influent sur sa direction de translocation [53].

The EMBO Journal (2004) 23, 2430–2439 | © 2004 European Molecular Biology Organization | All Rights Reserved 0261-4189/04
www.embojournal.org

THE EMBO JOURNAL

Fast, DNA-sequence independent translocation by FtsK in a single-molecule experiment

Omar A Saleh[1], Corine Pérals[2], François-Xavier Barre[2,*] and Jean-François Allemand[1,3,*]

[1]Laboratoire de Physique Statistique et Département de Biologie, Ecole Normale Supérieure, Paris, France, [2]Laboratoire de Microbiologie et de Génétique Moléculaire, Toulouse, France and [3]Laboratoire Pasteur, Département de Chimie, Ecole Normale Supérieure, Paris, France

Escherichia coli **FtsK is an essential cell division protein, which is thought to pump chromosomal DNA through the closing septum in an oriented manner by following DNA sequence polarity. Here, we perform single-molecule measurements of translocation by $FtsK_{50C}$, a derivative that functions as a DNA translocase *in vitro*. $FtsK_{50C}$ translocation follows Michaelis–Menten kinetics, with a maximum speed of ~6.7 kbp/s. We present results on the effect of applied force on the speed, distance translocated, and the mean times during and between protein activity. Surprisingly, we observe that $FtsK_{50C}$ can spontaneously reverse its translocation direction on a fragment of *E. coli* chromosomal DNA, indicating that DNA sequence is not the sole determinant of translocation direction. We conclude that *in vivo* polarization of FtsK translocation could require the presence of cofactors; alternatively, we propose a model in which tension in the DNA directs FtsK translocation.**

The EMBO Journal (2004) **23,** 2430–2439. doi:10.1038/sj.emboj.7600242; Published online 27 May 2004
Subject Categories: genome stability & dynamics; microbiology & pathogens
Keywords: chromosome segregation; DNA translocation; FtsK; magnetic tweezers; molecular motor

Introduction

Active transportation of DNA from one cellular compartment to another is central to many biological processes, such as viral DNA packaging, conjugation, sporulation, and cell division. In bacteria, a new class of proteins was recently identified that mediate the transport of double-stranded DNA through cell membranes and cell walls: the FtsK/SpoIIIE/TraSA family (Bath *et al*, 2000; Possoz *et al*, 2001; Aussel *et al*, 2002). These proteins belong to the AAA+ (ATPase Associated with various Activities) superfamily. As such, they are thought to form hexameric motors, which are responsible for the active translocation process. They are involved in a wide range of functions: TraSA is encoded by the plasmid pSAM2 of *Streptomyces ambofaciens*, and is responsible for the transfer of the plasmid from donor cells into acceptor cells during conjugation (Possoz *et al*, 2001). SpoIIIE is responsible for the transport of a chromosome into the small polar prespore compartment during sporulation in *Bacillus subtilis* (Bath *et al*, 2000). FtsK is an essential *Escherichia coli* cell division protein (Begg *et al*, 1995). Its N-terminal membrane domain is localized to the division septum (Wang and Lutkenhaus, 1998; Yu *et al*, 1998a), and is necessary for its formation (Draper *et al*, 1998; Chen and Beckwith, 2001). Its C-terminal motor domain ($FtsK_C$) is implicated in chromosome segregation (Liu *et al*, 1998; Yu *et al*, 1998b). Indeed, $FtsK_C$ has two essential roles in chromosome dimer resolution (see Aussel *et al*, 2002; Capiaux *et al*, 2002; Corre and Louarn, 2002, and references therein for review). Chromosome dimers, formed by homologous recombination in organisms with circular chromosomes, are a threat to normal repartitioning of genetic information at cell division. In *E. coli*, chromosome dimers are resolved into monomers by the addition of a crossover at a specific 28 bp site, *dif*, by two tyrosine recombinases, XerC and XerD. Chromosome dimer resolution first requires colocalization of the *dif* sites; this is accomplished by translocation of the chromosomes by $FtsK_C$ (Capiaux *et al*, 2002; Corre and Louarn, 2002). Secondly, the recombination reaction itself is activated by $FtsK_C$ (Aussel *et al*, 2002), probably through a direct interaction with XerC/D (Yates *et al*, 2003; Massey *et al*, 2004). In addition, DNA translocation by FtsK could participate in segregation of normal chromosomes (Yu *et al*, 1998b; Donachie, 2002; Lau *et al*, 2003).

Coupled to these processes, there must be a mechanism of translocation polarity; that is, an orienting mechanism that ensures the DNA is transported in the correct direction. In *B. subtilis*, it has been argued that preferential assembly of SpoIIIE in one daughter cell establishes polarity in chromosome partitioning during sporulation (Sharp and Pogliano, 2002). In normal vegetative growth in *E. coli*, in contrast to sporulating *B. subtilis*, there is no obvious morphological nor protein expression difference between the two daughter cells that could explain asymmetric assembly of FtsK. Instead, it has been postulated that FtsK translocation polarity is defined by chromosomal sequence polarity, that is, a high skew of oligomeric sequences along the two replichores that inverts at *dif* (Salzberg *et al*, 1998; Lobry and Louarn, 2003). Chromosome dimer resolution is effective only when *dif* is located within a narrow zone of the chromosome (Cornet *et al*, 1996), functionally defined as the junction between DNA segments of opposite sequence polarity (Corre *et al*, 2000; Perals *et al*, 2000). Sequence polarity can be perturbed by the introduction, close to *dif*, of exogenous DNA, such as the genome of phage lambda (Corre *et al*, 2000). This change inactivates chromosome dimer resolution, and augments the

*Corresponding authors. François-Xavier Barre, Laboratoire de Microbiologie et de Génétique Moléculaire, 118 Route de Narbonne, 31062 Toulouse, France. Tel.: +33 5 61 33 59 86; Fax: +33 5 61 33 58 86; E-mail: barre@ibcg.biotoul.fr or Jean-François Allemand, Laboratoire de Physique Statistique, Ecole Normale Supérieure, 24, Rue Lhomond, 75005 Paris, France. Tel.: +33 1 44 32 34 96; Fax: +33 1 44 32 34 33; E-mail: allemand@lps.ens.fr

Received: 23 February 2004; accepted: 27 April 2004; published online: 27 May 2004

probability of endogenous recombination in an FtsK-dependent manner (Corre and Louarn, 2002). This has led to the idea that polarization of the chromosome sequence could direct FtsK's translocation so as to juxtapose the chromosomal *dif* sites; this mechanism could also assist in clearing the septum of any residual DNA.

In vitro evidence for DNA translocation by the ATPase-motor domains of SpoIIIE and FtsK has been obtained, but all the assays employed were indirect, precluding detailed analysis of the translocation reaction (Bath *et al*, 2000; Aussel *et al*, 2002; Ip *et al*, 2003). Here, we directly monitor the DNA translocase activity of $FtsK_{50C}$, an active, oligomeric C-terminal truncation of FtsK (Aussel *et al*, 2002), at the single-molecule level using magnetic tweezers (Strick *et al*, 1996). We measure, in various conditions of applied force and ATP concentration, the velocity, length, and duration of individual translocation events. Using these data, we deduce basic mechanochemical parameters of the protein's translocation reaction.

Surprisingly, we find that $FtsK_{50C}$ can spontaneously reverse its translocation direction, and thus travel both ways on the same segment of DNA. We test translocation on both lambda genomic DNA and an *E. coli* chromosomal fragment that has been shown to be polarized *in vivo* (Perals *et al*, 2000). No bias in translocation is observed on either of these substrates, suggesting that DNA sequence polarity does not directly affect $FtsK_{50C}$ activity. We conclude that *in vivo* polarization of FtsK translocation could require additional cofactors, such as domains of the full protein not included in the truncation used here. Alternatively, we propose a mechanism in which force, rather than DNA sequence, directs the protein's *in vivo* motion.

Results

$FtsK_{50C}$ causes transient decreases of DNA extension

Magnetic beads (4.5 μm) are tethered to a glass capillary by a section of DNA (see Figure 1A), as described in Materials and methods. We use a portion of lambda DNA in all experiments presented, with one exception (noted below) in which we use

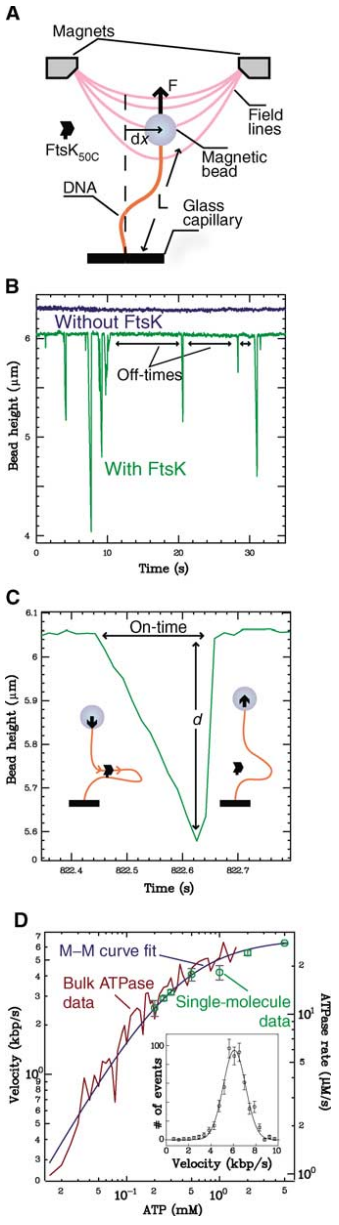

Figure 1 (**A**) Schematic representation of the measurement apparatus. A magnetic bead is tethered to a glass capillary by a single, nicked DNA molecule. Magnets above the capillary create a field gradient that pulls on the bead with a force *F*, which is determined by measuring the bead's lateral fluctuations d*x*. By optically tracking the bead, we measure the extension *L* of the DNA with time. (**B**) Typical measurement of DNA extension, both with and without $FtsK_{50C}$ in the solution. The plotted data were measured at $F = 10.7$ pN and with 5 mM ATP; the data sets have been offset for clarity. We attribute the transient decreases in DNA extension to the creation of loops of DNA by single complexes of $FtsK_{50C}$. (**C**) A typical individual event extracted from the data shown in (B). All events begin with a constant-velocity decrease in DNA extension; we attribute the slope of the descent to the translocation velocity of the complex. The velocity, distance travelled *d*, and on-time are easily measured because of the well-defined event shape. As sketched, loop formation requires the complex to bind the DNA in two locations; see Figure 6 and Discussion for details. (**D**) $FtsK_{50C}$ activity versus ATP concentration for both bulk (rate of ATP consumption; red curve) and single molecule (translocation velocity; green points) assays. Both data sets are well fit by the Michaelis–Menten equation $V_{max}[ATP]/([ATP] + K_m)$, with, respectively, $V_{max} = 30 \pm 2$ ATP/s and 6.7 ± 0.1 kbp/s, and $K_m = 270 \pm 40$ and 330 ± 20 μM. The fit to the single-molecule data (blue curve) is shown; it is highly coincident with the bulk data fit, which is omitted for clarity. Single-molecule data are taken at $F \sim 5$ pN, and each point is the average of typically 100 events; plotted bars indicate standard error. Inset: Histogram of measured translocation velocities (open circles) with best-fit Gaussian curve (solid line); data taken at 5 mM ATP and $F = 6$ pN.

a fragment of *E. coli* chromosomal DNA. We search for beads that are tethered by a single, nicked DNA molecule; while we are able to identify and utilize unnicked DNA molecules, we concentrate here on nicked molecules so as to avoid the topological complications of supercoiling. Once a suitable bead is found, we flush the capillary with ATP-laden buffer, add purified $FtsK_{50C}$ monomers to a final concentration of 5–10 nM, and begin tracking the DNA extension with time. After a short time, many transient decreases in DNA extension are observed, as shown in Figure 1B. Preliminary data on unnicked molecules (OA Saleh, S Bigot, FX Barre and JF Allemand, in preparation) are in general very similar to nicked-molecule data; thus, nicks appear not to affect the protein activity. The typical waiting time between events ($\sim$5 s) is greater than the typical event timespan ($\sim$0.2 s), indicating that the measured activity is due to the action of a single protein complex. Note that the structure of $FtsK_{50C}$ in solution is unknown, and apparently multimeric (Aussel *et al*, 2002); throughout the text, we refer to the active protein unit as a complex. The events continue to occur for a long time without need of additional proteins or ATP. We detect no events in the absence of either ATP or $FtsK_{50C}$, and we find that existing activity stops upon addition of EDTA to a final concentration of 20 mM. From these observations, we conclude that the events are caused by the ATP-dependent DNA translocation activity of $FtsK_{50C}$.

Translocation velocity represents protein activity

Each event begins with a linear decrease in bead height (Figure 1C), from which we can extract both the translocation velocity and the total distance travelled by the protein. Very rarely, we observe events containing pauses that interrupt the constant-velocity decrease. The pauses have no correlation with position along the DNA, and only occur in situations where many protein complexes appear to be active. We attribute pausing to protein–protein interactions, and do not characterize them here; see Supplementary data for more information. Within a single measurement (i.e., on one DNA molecule, and at constant force and ATP concentration), the translocation velocity measured from all events is normally distributed (inset, Figure 1D). Infrequently, an event is observed with almost precisely double the mean translocation velocity of other events in the data set (see Supplementary data). Such events presumably arise from two-motor activity (see Discussion), and are removed from all the analysis presented. The width of the distribution is accounted for by measurement noise and variations due to the stochastic stepping motion of the motor protein (Svoboda *et al*, 1994); thus, within the experimental noise, we observe no protein-to-protein or sequence-based velocity variation.

To confirm that $FtsK_{50C}$'s ATPase activity causes its translocation, we compare, at various ATP concentrations, the single-molecule velocity with the bulk ATPase activity measured in an excess of DNA (insuring each functional protein is active). As shown in Figure 1D, the assays agree quite well: each independently indicates that $FtsK_{50C}$ follows simple Michaelis–Menten kinetics with $K_m \sim 0.3$ mM ATP and respective maximum velocities of $\sim$6.7 kbp/s and $\sim$30 ATP/$FtsK_{50C}$ monomer/s. Note that the latter is only a relative measure since it ignores the presence of nonfunctional (misfolded) proteins. These results, in the light of previous data showing that ATPase activity is highly stimulated in the presence of DNA (Aussel *et al*, 2002), are consistent with a mechanism in which ATP consumption is restricted to DNA-bound $FtsK_{50C}$, and leads directly to DNA translocation.

Reversal of the translocation direction

After the initial translocation, the recovery back to the original bead height occurs in one of two ways, as shown in Figure 2A. The first type of recovery is an abrupt jump that occurs at speeds $>$20 μm/s, which is too fast to be resolved in our system. This is consistent with the protein completely unbinding, and the bead rising at a rate determined by the applied force and hydrodynamic Stokes drag (e.g. a 2 pN force will move a 4.5 μm diameter bead through water at a terminal velocity of $\sim$50 μm/s). The second type of recovery is a slower, constant-velocity increase, with a slope (at low forces) nearly equivalent to that of the decrease. We believe that slow recoveries are caused by a single complex that, after decreasing the bead height, reverses its translocation direction and causes the bead to rise (see Discussion and Figure 2A sketches). Both types of recoveries occur at all forces; at a given force, events with slow and fast recoveries are randomly interspersed. However, it is clear that the frequency of occurrence of direction reversals depends on the applied force: the proportion of slow recoveries decreases from $\sim$50% at low forces to nearly zero at high forces (inset, Figure 2A). Rarely, we observe events with more complicated mixed recoveries, wherein the bead height first increases slowly, then abruptly, or *vice versa* (see Supplementary data).

Direction reversal has potential implications for the *in vivo* mechanism of FtsK translocation polarity, as it shows that, on the section of lambda DNA utilized, the protein can travel in both directions on the same DNA sequence. To further explore this effect, we perform measurements on a fragment of *E. coli* chromosomal DNA with a proven *in vivo* polarity effect (Perals *et al*, 2000). As shown in Figure 2B, we still observe direction reversal events on the *E. coli* DNA, with no difference in either the shape of individual events, or the frequency of occurrence of slow recoveries. Furthermore, full-length direction reversal events occur (wherein the bead is brought from full height down to the capillary surface, then back up again, all at constant speed; see Figure 2B), indicating that no subsection of the *E. coli* DNA fragment has a definitive effect on the translocation direction of the complex.

Force dependence of the translocation velocity

In our assay, the applied force F depends only on the distance of the magnets to the capillary; we can easily adjust this distance to study the dependence of translocation velocity on force. During initial translocation, the protein lowers the bead, and must perform work against the applied force. In contrast, during direction-reversed translocation, the bead rises, so the protein works with the (upward) force. Thus, we can use initial translocation to measure the velocity with forces hindering the protein's motion, and reversed translocation to measure the velocity with forces assisting the motion (following previous practice, we define a hindering force as positive). In Figure 3, we show the force–velocity relationships measured in the presence of 1 and 5 mM ATP. At both concentrations, there is a clear plateau of constant velocity for small forces, along with a transition to increasingly higher velocities at large assisting forces; this transition occurs, respectively, at -4 and -11 pN

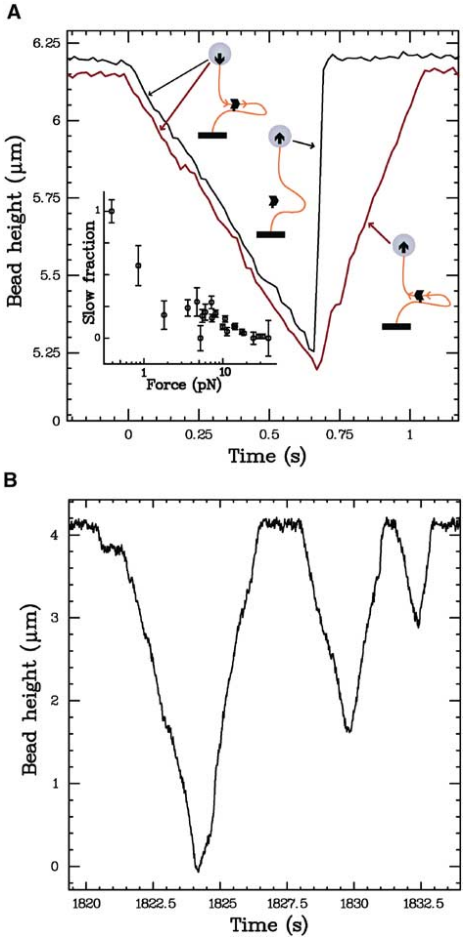

Figure 2 (**A**) Illustration of different types of recoveries. After decreasing, the DNA extension can recover its full length either abruptly (black curve) or slowly (red curve). As sketched, we attribute the former to protein unbinding, and the latter to a reversal of the translocation direction. The fraction of events exhibiting a slow recovery is force dependent, as plotted in the inset. The distance travelled before a reversal of direction is random, and consistent with the distribution of distances travelled before unbinding (see Figure 4). The events plotted were measured at 18 pN and 5 mM ATP, and are offset for clarity. The inset includes data taken at ATP concentrations from 0.5 to 5 mM; we observe no variation in the slow fraction with ATP. (**B**) Translocation of a fragment of *E. coli* chromosomal DNA that has been shown to have *in vivo* polar activity (Perals *et al*, 2000); data taken at 5 mM ATP and $F=1$ pN. All the three plotted events have slow, direction-reversal recoveries. In particular, in the first event, $FtsK_{50C}$ translocates the entire length of the DNA in both directions, indicating that no portion of the DNA sequence has a strong effect in biasing the translocation direction.

for 1 and 5 mM ATP. At 5 mM ATP, the velocity begins to clearly decrease for $F>15$ pN; no such transition is seen in the 1 mM data up to $F=29$ pN.

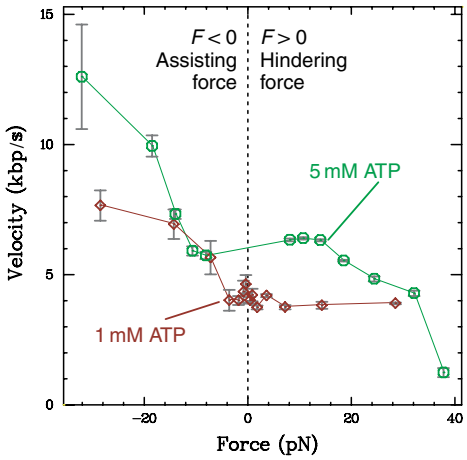

Figure 3 Force–velocity relations for $FtsK_{50C}$ measured at 1 and 5 mM ATP. At both ATP concentrations, there is a plateau of constant velocity for small forces. The velocity measured at 5 mM ATP begins to decrease above a hindering force of 15 pN, while no decrease is seen in the 1 mM data up to 29 pN. The hindering-force data indicate that the $FtsK_{50C}$ reaction pathway has force-independent biochemical step(s) in series with force-dependent mechanical step(s) (see Discussion). Plotted bars indicate standard error; large error estimates indicate regimes where the event frequency and size are small (see Figure 4).

Mean event length and on-time decrease with force

We are unable to measure the velocity above ~35 pN because of a strong decrease in the size of each event, and in the frequency of event occurrence. The length and duration (i.e., on-time) of each event correspond, respectively, to the distance travelled by the protein, and the time spent bound to the DNA, before unbinding or reversing direction (see Figure 1C). Within a measurement at a given force and ATP concentration, both distance and on-time vary from event to event. We find that the distribution of each is always exponential (see inset, Figure 4B), indicating a constant unbinding probability with time (and thus distance, given the nearly constant velocity within a given measurement; see inset, Figure 1D); we can then fit an exponential curve to each distribution and extract the mean distance and on-time for the given conditions. In this way, we measure, at constant 5 mM ATP, the variation of mean distance and on-time with applied force. As shown in Figure 4A, the mean on-time decreases strongly, and exponentially, with force. Fitting the data to $t_0\exp(-F/F_0)$ gives a decay constant $F_0=11.3\pm0.9$ pN and a mean on-time at zero force of $t_0=1.6\pm0.3$ s. The mean distance travelled also decreases strongly with force, as shown in Figure 4B. At low forces, the translocation velocity is fairly constant (Figure 3), so we expect the mean distance to vary in the same manner as the mean on-time. This is indeed the case: an exponential fit to the low-force points gives a decay constant $F_0=11.6\pm3.2$ pN, nearly equivalent to the decay constant of the mean on-time. Above 20 pN, the mean distance drops off more quickly due to the decrease in velocity at high forces.

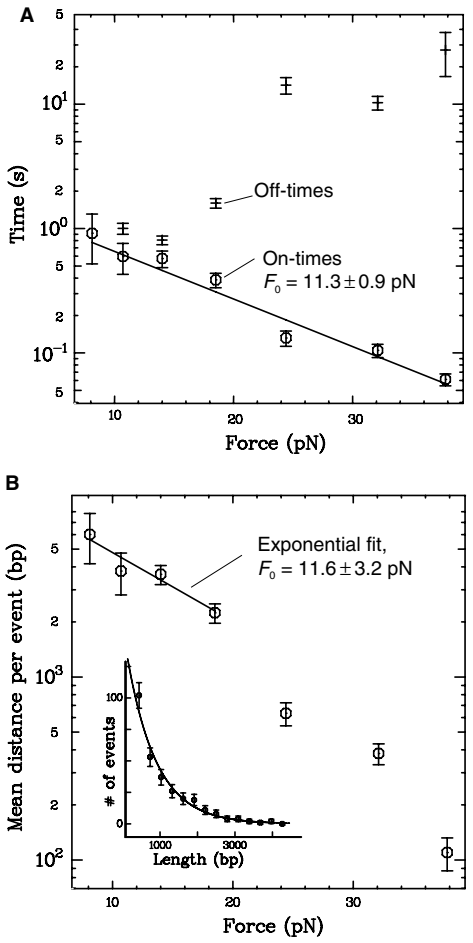

Figure 4 (**A**) Force dependence of the on- and off-times at 5 mM ATP. As with the distance travelled (see inset, B), the distribution of on-times from many events within a measurement is exponential (data not shown), indicating a constant unbinding probability with time. We extract a mean on-time from each distribution through fitting an exponential function. Here, we plot the variation with force of the mean on-time (circles), and fit it with an exponential function $t_0 \exp(-F/F_0)$. The mean on-time decreases with force with a decay constant $F_0 = 11.3 \pm 0.9$ pN and an on-time at zero force of $t_0 = 1.6 \pm 0.3$ s. This exponential force dependence can be simply explained if we assume that binding of the protein causes a distortion that decreases the DNA length by at least 0.36 ± 0.03 nm (see Discussion). (**B**) Dependence of the mean distance travelled per event on force at 5 mM ATP. The mean distance travelled at a given force should follow directly from the on-times (A) and the velocity (Figure 3). Indeed, at low forces, where the velocity is constant, we observe an exponential decay constant, $F_0 = 11.6 \pm 3.2$ pN, nearly identical to that of the on-times. For higher forces, the decrease in velocity causes the measured mean distance to drop off even more quickly. Inset: A typical distribution of distances, and exponential fit; data taken from ~300 events at $F = 24$ pN and 5 mM ATP.

Force dependence of the off-times

Along with the distances and on-times, we extract from each measurement distributions of the off-times, that is, the time duration between events (see Figure 1B). The off-time distributions from a given measurement clearly do not follow a single exponential curve, but rather a curve that is the sum of (at least) two exponentials with, respectively, fast and slow time constants (see Supplementary data). The presence of fast and slow rebinding rates is presumably due to the varying timescales of processes that contribute to protein–DNA binding (see Discussion). We find strong variations in the mean off-time for different measurements, which we attribute to variations in the amount and active percentage of the added protein. However, since a single addition of protein to the capillary results in long-lasting activity, we can vary the force and confidently measure the response of the off-times at constant protein concentration. As shown in Figure 4A, we find that the mean values of the off-time increase with force, indicating that binding rate of the protein to the DNA is decreased by the application of higher forces.

Noise analysis reveals $FtsK_{50C}$ step size

The completion of an enzymatic cycle results in a single forward step of a motor protein. If the step size is larger than the measurement noise, and the average time to complete an enzymatic cycle is larger than the time resolution of the measurement, it would be possible to observe individual steps directly. This is not the case here: we observe no discrete steps in the traces of bead position versus time. However, it is still possible to estimate the step size by considering the fluctuations in the measurement. In the absence of protein activity, the resolution of our measurement is limited by the bead's Brownian fluctuations, which, at low frequency f, create a frequency-independent 'white' noise. During protein activity (i.e., during the linear decrease in bead height), we find that the measurement noise increases at low frequencies as $1/f^2$, and thus cannot be attributed only to Brownian fluctuations (see Figure 5). Such a low-frequency increase in noise has been observed in previous single-molecule measurements (Svoboda *et al*, 1994), and has been shown to be proportional to the enzymatic step size (Svoboda *et al*, 1994; Charvin *et al*, 2002); it is caused by the random distribution of the times between individual steps (Svoboda *et al*, 1994).

To estimate the step size, we select the active segment of a suitable event and compute, at each time point, the difference between the bead's measured position and its mean position (as predicted by the mean velocity). We then find the power spectrum of that difference, average the spectra over many events from a single measurement, and fit this average with the theoretically predicted curve (Charvin *et al*, 2002); an example is shown in Figure 5. By performing this analysis, we estimate that the step size of $FtsK_{50C}$ is 12 ± 2 bp. In our application of the model, we assume that the entire enzymatic cycle has only one rate-determining step. Relaxation of this assumption (i.e., if the rates of two or more substeps of the cycle are comparable) would decrease the randomness of the distribution of times between steps (Svoboda *et al*, 1994); in turn, the estimated step size would necessarily increase to account for the measured level of noise. Thus, our estimate of 12 ± 2 bp is technically a lower bound. We see no significant variation in the step size with ATP concentrations of 1 or

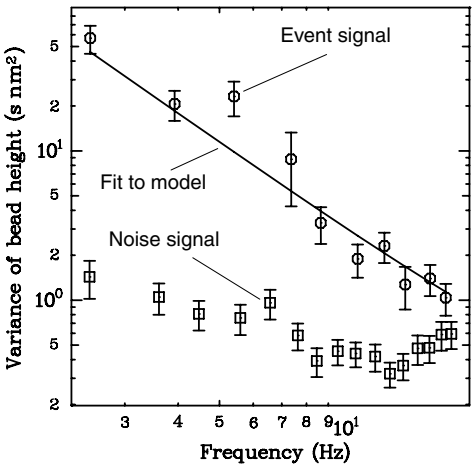

Figure 5 Power spectrum analysis of the variance in bead height during (circles) and in the absence of (squares) protein activity. Each set of points is the average of 26 segments of a data trace acquired at 5 mM ATP and $F = 19$ pN. The spectrum of noise during protein activity shows a clear $1/f^2$ increase over the spectrum of the measurement noise alone. Note that the latter spectrum is calculated from quiescent segments between the bursts of activity that give rise to the former spectrum, and is thus a nearly simultaneous measure of the background noise. This increase is due to stochastic variations of the motion of the protein, and is proportional to the protein's step size δ. The line is a fit to the predicted increase (Charvin *et al*, 2002): $y = \delta\langle v\rangle/2\pi^2 f^2 + b$, where $\langle v\rangle$ is the mean velocity and b accounts for the (white) measurement noise. From many such fits, we find that, if the $FtsK_{50C}$ enzymatic cycle has a single rate-determining step, it advances 12 ± 2 bp per cycle.

5 mM or forces between 5 and 19 pN. If we assume the active motor is a hexamer (Aussel *et al*, 2002), and that 100% of the added protein in the bulk ATPase measurement were active, we can use the maximum velocities of translocation (~6.7 kbp/s) and ATP hydrolysis (~30 ATP/monomer/s) to estimate that the $FtsK_{50C}$ motor moves ~37 bp per hydrolyzed ATP. Given the step size, this leads to the impossible result that less than one ATP is hydrolyzed per enzymatic cycle. It is important to note that this does not invalidate our result for the lower bound of the step size: a much more likely explanation is that a significant fraction of the protein in the ATPase assay was inactive; this would not affect the single-molecule measurement.

Discussion

$FtsK_{50C}$ forms loops of DNA

We attribute the observed transient decreases in DNA extension (Figure 1B) to the extrusion of loops of DNA by translocating protein complexes: a protein solely moving along a DNA molecule will cause no change in extension in our assay, and since each molecule is nicked we rule out shortening due to an accumulation of supercoils. Formation of DNA loops has been postulated before to explain the topological modification of DNA substrates by $FtsK_{50C}$ complexes (Aussel *et al*, 2002; Ip *et al*, 2003). A recurrent tentative hypothesis was that loop extrusion was due to the activity of two connected motors, with each translocating, but in opposite directions (Ip *et al*, 2003). Since FtsK is an AAA+ protein, it is probable that each motor is a hexamer encircling the DNA; thus two connected motors would form a double ring. We cannot rule out that each complex contains more than two motors; on the contrary, the characteristics of direction-reversal events are best explained by an $FtsK_{50C}$ complex containing three or more motors (see below). The formation of such higher order complexes is compatible with previously published electron microscopy and gel filtration data on $FtsK_{50C}$ (Aussel *et al*, 2002).

A single motor is active during loop extrusion

The range of measured timespans indicates that each event is due to only a single complex of $FtsK_{50C}$. As mentioned, each complex might be composed of several functional hexameric motors, two of which could bind to the DNA and form a loop. However, we argue that only one motor is translocating during the observed events: at low forces, the processivity increases to the extent that we see full-length, constant-velocity events (in which the bead starts at full height and is brought smoothly to the capillary surface). If loops were extruded by two motors simultaneously, a full-length, constant-speed event would only occur if each motor bound exactly to the middle of the DNA and worked in opposite directions until each hit a surface (the bead or the capillary). Such a precise starting position should be rare, yet we observe this type of event frequently at low force. Further evidence disfavoring multiple active motors is the appearance of direction-reversal events, in which the velocities of descent and ascent are nearly equivalent (Figure 2A). This process is difficult to explain if two motors are acting, since both motors would have to switch directions simultaneously. For these reasons, we conclude that during each measured event, only one motor is translocating.

Localizing the protein to a DNA extremity

Although only one motor is active, loop formation requires the $FtsK_{50C}$ complex to contact the DNA in two locations. In what manner could the complex form a second, nontranslocating contact? The protein could possibly have a second (immobile) type of DNA-binding domain, but this is unlikely for an aforementioned reason: full-length, constant-velocity events require that the protein begins translocation at one of the extremities of the DNA, and random DNA binding would not efficiently localize the protein to an extremity. Instead, we suggest that the second binding location is also a motor bound to the DNA, but stalled at the bead or capillary surface, as diagrammed in Figure 6. In this scenario, a diffusing complex first binds to the DNA through one motor, which translocates (without loop formation or a change in bead height) and transports the complex to a surface, where the motor stalls but remains bound to the DNA. Other motors in the complex are then free to bind; translocation of these motors causes loop formation and reduces the bead height. The complex is localized to the extremity of the DNA, as required to explain the measured full-length events. The rare events with twice the normal velocity (see Supplementary data) occur when a second motor binds before the first has stalled, resulting in a change in bead height at twice the single-motor rate. Finally, this model explains the multiple

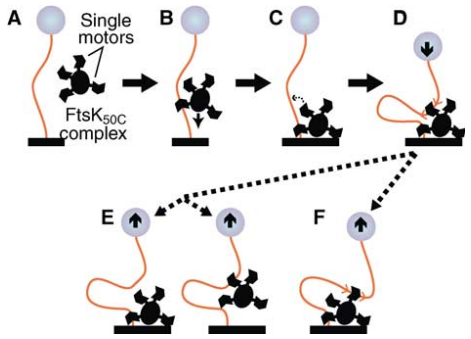

Figure 6 Diagram of proposed steps in loop formation by $FtsK_{50C}$ complexes. (**A**) Free complexes, containing several identical (probably hexameric) motors, diffuse into the vicinity of the DNA. (**B**) The complexes bind the DNA through a single motor, which translocates and carries the complex toward an extremity of the DNA without changing the bead height. (**C**) Upon reaching the surface, the motor stalls but does not unbind, allowing other motors in the complex to bind and translocate. (**D**) Translocation of the second motor extrudes a loop of DNA, and decreases the bead height at the single-motor velocity. The decrease can be halted by (**E**) unbinding of either motor, leading to a fast recovery of the bead height, or (**F**) reversal of the translocation direction, and a slow recovery of bead height. We believe that direction reversal proceeds through unbinding of the translocating motor, followed by binding and translocation by an oppositely directed motor from the same complex (see Discussion).

timescales in the off-time distributions (see Supplementary data): short off-times occur when only one of the two motors unbinds, leaving the complex in close proximity to the DNA and thus enabling fast rebinding, while long off-times occur when both motors unbind, and rebinding is limited by free diffusion of the protein complexes.

Brief motor unbinding accompanies direction reversal

As shown in the inset to Figure 2A, direction reversal is less likely at higher forces. This can be explained by assuming that direction reversal first involves unbinding of the translocating motor, followed immediately by binding of an oppositely directed motor: the observed decrease in binding rate with force (i.e., the increase in off-time, see Figure 4A) would then explain the decrease in the probability of direction reversal with force (inset, Figure 2A). The oppositely directed motor could, in principle, be an inverted configuration of the first motor, but we consider it more likely that it is a different (but nearby) motor within the same complex.

Considerations on the mechanochemistry of the $FtsK_{50C}$ motor

The force–velocity relationships of $FtsK_{50C}$ (Figure 3) show a clear plateau for small forces of either orientation, along with a decrease in velocity (at saturating 5 mM ATP) for large hindering forces. This behavior is qualitatively similar to both theoretical predictions (Keller and Bustamante, 2000) and previous results obtained on RNA polymerase (Wang *et al*, 1998; Neuman *et al*, 2003). The behavior is indicative of two types of sequential steps in the reaction that causes forward movement of the protein: a force-dependent mechanical step (involving motion along the DNA), and one or more force-independent biochemical steps (involving no motion along the DNA, but rather, for example, ATP binding or a change in the protein's internal conformation). The mechanical step requires the protein to change the height of the bead by a distance δ and perform a work against the force of $F\delta$; thus, the kinetic barrier of that step will increase at high hindering forces, decreasing the rate. If, at zero force, the mechanical step is much faster than the biochemical step, the zero-force velocity v_0 will depend only on the step size and the biochemical step rate. As the force increases, the mechanical step rate slows until it becomes comparable to the biochemical step rate. For small F, the biochemical step determines the rate (and the velocity equals v_0, independent of the force), while for large F the mechanical step determines the rate (and the velocity decreases with force). This description qualitatively matches our data at 5 mM ATP. Furthermore, it is consistent with the 1 mM ATP data, where no velocity decrease is seen up to $F = 29$ pN. The decrease to 1 mM ATP slows the ATP-binding process, thus slowing the rate of the biochemical steps. To make the mechanical step rate comparable to this lowered biochemical rate (i.e., to see a velocity decrease) will thus require a larger force than was needed at 5 mM ATP; we apparently do not reach this regime at the maximum force of 29 pN utilized in the 1 mM data.

For assisting forces, our data notably deviate from the above model and the measurements on RNA polymerase (Neuman *et al*, 2003); in both, there is a continuation of the constant-velocity plateau. Instead, we observe a clear increase in velocity for large assisting forces (Figure 3). The velocity increase is not likely due to a change in the enzymatic turnover rate (since it is unlikely that assisting force would quicken the limiting biochemical processes), but rather due to an increase in the mechanical step size. Supporting this, we note that the velocity is still dependent on ATP in this regime; thus, the biochemical processes are still rate-determining. However, since our data are sparse at large negative forces due to the rarity of direction reversals (inset, Figure 2A) and the decrease in event size (Figure 4A), we cannot rule out the existence of a completely separate mechanism of forward motion.

Force dependence of binding statistics indicates a distortion of the DNA

The mean value of the on-time decreases exponentially with force (see Figure 4A) until, at high hindering force, protein activity is limited by this parameter. The exponential dependence can be accounted for by assuming that the DNA length when bound by $FtsK_{50C}$ is shorter than when free. We model this effect as a two-state system (Evans and Ritchie, 1997; Rief *et al*, 1998), where the bound and unbound states are separated by a transition state with a higher free energy. Any DNA length change l between the bound and transition states would require unbinding to perform a work $-Fl$ against the applied force. This would affect the mean on-time (the inverse of the mean unbinding rate) by a factor $\exp(-Fl/kT)$, consistent with our observations of an exponential dependence on force. Based on the fitted exponential decay constant of 11.3 ± 0.9 pN, we estimate that unbinding of $FtsK_{50C}$ causes the DNA length to increase by $l \geqslant 0.36 \pm 0.03$ nm (the estimate is a lower bound since the measurement is not sensitive to any further change in DNA length between the transition and unbound state; see

Supplementary data). This length change is much smaller than the minimal 80 bp binding site required to stimulate $FtsK_{50C}$'s ATPase activity (Massey *et al*, 2004). Therefore, it is consistent only with a small bend in the DNA induced at the protein's binding site.

Implications of direction reversal for models of FtsK polarity

It has been suggested that some chromosomal oligomeric sequences, with a high skew that inverts at *dif*, could direct the FtsK translocation process (Perals *et al*, 2000; Corre and Louarn, 2002), just like Chi sequences alter the enzymatic properties of RecBCD complexes (Spies *et al*, 2003). In this regard, direction reversal is surprising because it indicates that $FtsK_{50C}$ can move in both directions on the same segment of DNA. Furthermore, we observe full-length direction-reversal translocation events on a lambda DNA fragment of approximately half the size of the phage genome; introduction of a complete phage lambda genome has been shown to perturb chromosome polarity *in vivo* (Corre *et al*, 2000). To confirm this finding, we perform experiments on a fragment of the *E. coli* genome that was shown to be polarized (Perals *et al*, 2000). Full-length translocation events after direction reversal are again observed (Figure 2B). We conclude that the oligomeric DNA motifs that polarize the *E. coli* and lambda genomes do not constitute absolute blocks to DNA translocation by $FtsK_{50C}$. We cannot rule out the possibilities that their action is probabilistic, or that it requires the presence of the N-terminal or linker domains of FtsK. However, our data raise the possibility that DNA sequence information plays only an indirect role on polarity of translocation by FtsK. For example, an additional protein could bind to specific DNA sequences and block FtsK translocation, just like Tus binding to Ter sites can stop replication forks (Kamada *et al*, 1996), or, rather than acting on FtsK, the DNA sequence could direct progressive, oriented condensation of the nucleoids, thereby imposing that the *dif* region is the last chromosomal section to be moved by FtsK.

A force-rectified translocation model could impose directionality

Based on the observed sensitivity of the travelled distance to force (Figure 4B), we propose an alternate mechanism that could account for *in vivo* FtsK directionality. The parameters of the exponential curve fit of mean on-time versus force (Figure 4A), along with the maximum speed, indicate that at zero force the $FtsK_{50C}$ complex will travel, on average, ~11 kbp per binding event. Since DNA translocation most likely involves the binding of two identical motor units (Figure 6), the zero-force mean distance for each motor is then twice that of the complex, or ~22 kbp. This is much less than the total length of the *E. coli* chromosome (4.5 Mbp). However, the chromosome is compacted in the cell and it is highly probable that to clear the septum, FtsK works on DNA loops of sizes similar to the zero-force mean distance.

We propose that a septum-bound FtsK motor, upon binding a chromosomal loop, can translocate in either direction. However, if pumping in the wrong direction, it will pull against the large fraction of condensed DNA and work against other proteins in the nascent daughter cell that maintain the chromosome position, such as MukB and active next-generation DNA replisomes (Sherratt, 2003). The counteracting activities of FtsK and these other proteins will create a tension in the DNA analogous to the force we apply to the bead in our assay. Just as we observe (Figure 4B), this tension will decrease the distance FtsK can travel before unbinding. FtsK motors that pump in the wrong direction will thus quickly fall off, allowing other, perhaps correctly oriented, motors to bind. Although the lack of structural data on FtsK precludes affirmation, the formation of higher order complexes by $FtsK_{50C}$ and the resulting *in vitro* direction-reversal activity might indicate that higher order complexes are also formed *in vivo* by FtsK, which would facilitate this process. Motors pumping in the correct direction will not create tension in the DNA, and will translocate a correspondingly greater distance. In this way, FtsK would clear any misplaced chromosomal loops that pass through the septum. Interestingly, this model could be applied to sporulation in *B. subtilis*, assuming that condensation of DNA in the prespore generates sufficient tension.

This force-rectified translocation model applies to segregation of normal daughter chromosomes and to resolution of chromosome dimers. For normal chromosome segregation, FtsK would simply accelerate the clearing process; both genetic and cellular biology data indicate that FtsK is not absolutely required for cohesion and mid-cell positioning of the large terminus region of the *E. coli* chromosome (Capiaux *et al*, 2002; Corre and Louarn, 2002). In the presence of chromosome dimers, misplaced loops could still occur; FtsK would clear these loops from the septum until there remained only the two chromosome-connecting strands that contain the *dif* sites required for XerC/D recombination.

$FtsK_{50C}$'s high velocity enables fast processing of misaligned DNA

$FtsK_{50C}$'s maximum velocity of ~6.7 kbp/s makes it the fastest DNA-based motor protein yet measured. Speeds similar to our measurements have been estimated for the total transfer rate of the *B. subtilis* genome into a nascent spore by SpoIIIE (Errington *et al*, 2001). As mentioned above, we do not expect FtsK to mobilize such a large fraction of the *E. coli* genome, but rather a tangle of DNA loops. Unravelling such a tangle could require loops to be successively processed several times, as has been reported *in vitro* for replicative catenanes (Ip *et al*, 2003); thus $FtsK_{50C}$'s high speed could be needed to complete multiple processing of misaligned loops quickly.

Materials and methods

Protein, substrate DNA, and slide preparation

$FtsK_{50C}$ is purified as described in Aussel *et al* (2002). λ DNA (bp 25 882–45 679) is amplified by long-range PCR. *E. coli* chromosomal DNA (bp 8877–22 422 after the XerC-binding site of *dif*) is purified from plasmid pFC94 (Perals *et al*, 2000). DNA substrates are ligated to biotin- and digoxigenin-modified DNA fragments, which are prepared by PCR using cognate modified nucleotides. The resulting constructs are incubated with 4.5 μm diameter paramagnetic streptavidin beads and added to 1-mm square cross-section glass capillaries, which had been washed with 0.1 M NaOH, coated with SigmaCote, and sequentially incubated with solutions of anti-digoxigenin and bovine serum albumin (BSA). We insure that the beads we use are bound to the capillary by a single, nicked DNA molecule, and not a single unnicked, molecule or multiple molecules, as described in Strick *et al* (1996, 1998).

Measurement of applied force and bead height

The image of each bead is captured by a CCD camera at 60 Hz and processed, using custom-written software, to give the 3D bead position. Before protein addition, we calibrate the apparatus for each bead by measuring the applied force as a function of magnet/capillary separation distance. The applied force is measured by monitoring the mean squared transverse fluctuations $\langle dx^2 \rangle$ of the bead (see Figure 1A), and applying the equipartition theorem: $\frac{1}{2}kT = \frac{1}{2}\langle dx^2 \rangle F/L$, where L is the measured bead height (Strick *et al*, 1996). Microscope drift is removed by simultaneously tracking a reference bead stuck to the capillary surface, and subtracting its height from that of the experimental bead.

Addition of protein to the capillary

Experiments are performed in a buffer containing 10 mM $MgCl_2$, 10 mM Tris pH 7.9, 50 mM NaCl, 1 mM DTT, 0.01% Triton X-100, and ATP. In all, 5–10 µl of 200 nM $FtsK_{50C}$ monomers is added to 200 µl of buffer in the capillary, and gently mixed.

Long data acquisitions

Activity resulting from a single addition of protein can last for hours. To control for possible degradation of the protein or ATP in that time, we measure the activity at a reference force multiple times throughout the experiment. We never observe a decrease in velocity in those reference measurements. In some long measurements, we do observe an increase in the mean off-time; we attribute this to a decrease in the active protein concentration through degradation or nonspecific adsorption to the capillary. Data sets containing such a decrease are not used to construct the off-time plot in Figure 4A.

Data analysis

Measured traces of bead height correspond directly to DNA extension; no filtering has been applied to any of the plots shown. Translocation velocities, lengths, and on- and off-times are extracted by analyzing each data set with custom-written software that applies a filter (Chung and Kennedy, 1991) in order to identify events automatically, while still measuring each parameter from the unfiltered data. Data quoted in units of base pairs have been corrected for the difference between measured DNA extension and the true contour length by applying the worm-like chain model for DNA elasticity (Bouchiat *et al*, 1999). To calculate the fraction of slow recoveries (inset, Figure 2A), the number of slow recovery segments of a certain minimum size (typically 0.5 µm; less at higher forces) are counted, and divided by the total number of events of that size; the threshold is needed due to the difficulty in characterizing very short recoveries. For the fluctuation analysis, within a data set, only long (>0.75 µm) events are analyzed. A straight line is fit to, and subtracted from, each event to acquire the difference at each time point. The mean variance from the fit line is computed for each event; typically, the mean variance across all events forms a compact distribution. Outliers from this distribution (more than 2 standard deviations larger than the mean) sometimes occur, and are considered to contain anomalous noise; thus, the corresponding events are discarded. Power spectra are then calculated from the suitable events using standard algorithms.

Bulk ATPase assay

Reactions are performed with 100 nM of $FtsK_{50C}$ (monomer), 5 nM of 3 kb supercoiled plasmid DNA, 1 nM [α^{32}P]ATP and cold ATP in 10 µl of 10 mM Tris–HCl, pH 7.9, 10 mM $MgCl_2$, 50 mM NaCl, and 1 mM DTT. Reactions are incubated for 3 min before being stopped with EDTA and excess ATP. The ratio of ATP to ADP is analyzed by thin layer chromatography. We check that our measurements correspond to initial rates and that DNA is in a 10-fold excess in the reaction (data not shown).

Supplementary data

Supplementary data are available at *The EMBO Journal* Online.

Acknowledgements

We thank D Bensimon, V Croquette, J-M Louarn, and F Cornet for constant support and helpful discussions. We thank V Croquette for sharing analysis software, and J-Y Bouet, G Charvin, K Neuman, and T Lionnet for critical reading of the manuscript. Research was funded by the CNRS and the Ecole Normale Supérieure. Research in Paris was supported by grants from the French Research Ministry ACI Jeune Chercheur program and from the EU MolSwitch program. Research in Toulouse was supported by grants from the CNRS ATIP program and from the French Research Ministry Fundamental Microbiology ACI program.

References

Aussel L, Barre FX, Aroyo M, Stasiak A, Stasiak AZ, Sherratt D (2002) FtsK is a DNA motor protein that activates chromosome dimer resolution by switching the catalytic state of the XerC and XerD recombinases. *Cell* **108:** 195–205

Bath J, Wu LJ, Errington J, Wang JC (2000) Role of *Bacillus subtilis* SpoIIIE in DNA transport across the mother cell-prespore division septum. *Science* **290:** 995–997

Begg KJ, Dewar SJ, Donachie WD (1995) A new *Escherichia coli* cell division gene, *ftsK*. *J Bacteriol* **177:** 6211–6222

Bouchiat C, Wang MD, Allemand JF, Strick T, Block SM, Croquette V (1999) Estimating the persistence length of a worm-like chain molecule from force–extension measurements. *Biophys J* **76:** 409–413

Capiaux H, Lesterlin C, Perals K, Louarn JM, Cornet F (2002) A dual role for the FtsK protein in *Escherichia coli* chromosome segregation. *EMBO Rep* **3:** 532–536

Charvin G, Bensimon D, Croquette V (2002) On the relation between noise spectra and the distribution of time between steps for single molecular motors. *Single Molecules* **3:** 43–48

Chen JC, Beckwith J (2001) FtsQ, FtsL and FtsI require FtsK, but not FtsN, for co-localization with FtsZ during *Escherichia coli* cell division. *Mol Microbiol* **42:** 395–413

Chung SH, Kennedy RA (1991) Forward-backward nonlinear filtering technique for extracting small biological signals from noise. *J Neurosci Methods* **40:** 71–86

Cornet F, Louarn J, Patte J, Louarn JM (1996) Restriction of the activity of the recombination site *dif* to a small zone of the *Escherichia coli* chromosome. *Genes Dev* **10:** 1152–1161

Corre J, Louarn JM (2002) Evidence from terminal recombination gradients that FtsK uses replichore polarity to control chromosome terminus positioning at division in *Escherichia coli*. *J Bacteriol* **184:** 3801–3807

Corre J, Patte J, Louarn JM (2000) Prophage lambda induces terminal recombination in *Escherichia coli* by inhibiting chromosome dimer resolution. An orientation-dependent *cis*-effect lending support to bipolarization of the terminus. *Genetics* **154:** 39–48

Donachie WD (2002) FtsK: Maxwell's demon? *Mol Cell* **9:** 206–207

Draper GC, McLennan N, Begg K, Masters M, Donachie WD (1998) Only the N-terminal domain of FtsK functions in cell division. *J Bacteriol* **180:** 4621–4627

Errington J, Bath J, Wu LJ (2001) DNA transport in bacteria. *Nat Rev Mol Cell Biol* **2:** 538–544

Evans E, Ritchie K (1997) Dynamic strength of molecular adhesion bonds. *Biophys J* **72:** 1541–1555

Ip SCY, Bregu M, Barre F-X, Sherratt DJ (2003) Decatenation of DNA circles by FtsK-dependent Xer site-specific recombination. *EMBO J* **22:** 6399–6407

Kamada K, Horiuchi T, Ohsumi K, Shimamoto N, Morikawa K (1996) Structure of a replication-terminator protein complexed with DNA. *Nature* **383:** 598–603

Keller D, Bustamante C (2000) The mechanochemistry of molecular motors. *Biophys J* **78:** 541–556

Lau IF, Filipe SR, Soballe B, Okstad OA, Barre FX, Sherratt DJ (2003) Spatial and temporal organization of replicating *Escherichia coli* chromosomes. *Mol Microbiol* **49:** 731–743

Liu GW, Draper GC, Donachie WD (1998) FtsK is a bifunctional protein involved in cell division and chromosome localization in *Escherichia coli*. *Mol Microbiol* **29:** 893–903

Lobry JR, Louarn JM (2003) Polarisation of prokaryotic chromosomes. *Curr Opin Microbiol* **6:** 101–108

Massey TH, Aussel L, Barre F-X, Sherratt DJ (2004) Asymmetric activation of Xer site-specific recombination by FtsK. *EMBO Rep* **5:** 399–404

Neuman KC, Abbondanzieri EA, Landick R, Gelles J, Block SM (2003) Ubiquitous transcriptional pausing is independent of RNA polymerase backtracking. *Cell* **115:** 437–447

Perals K, Cornet F, Merlet Y, Delon I, Louarn JM (2000) Functional polarization of the *Escherichia coli* chromosome terminus: the *dif* site acts in chromosome dimer resolution only when located between long stretches of opposite polarity. *Mol Microbiol* **36:** 33–43

Possoz C, Ribard C, Gagnat J, Pernodet JL, Guerineau M (2001) The integrative element pSAM2 from *Streptomyces*: kinetics and mode of conjugal transfer. *Mol Microbiol* **42:** 159–166

Rief M, Fernandez JM, Gaub HE (1998) Elastically coupled two-level systems as a model for biopolymer extensibility. *Phys Rev Lett* **81:** 4764–4767

Salzberg SL, Salzberg AJ, Kerlavage AR, Tomb JF (1998) Skewed oligomers and origins of replication. *Gene* **217:** 57–67

Sharp MD, Pogliano K (2002) Rote of cell-specific SpoIIIE assembly in polarity of DNA transfer. *Science* **295:** 137–139

Sherratt DJ (2003) Bacterial chromosome dynamics. *Science* **301:** 780–785

Spies M, Bianco PR, Dillingham MS, Handa N, Baskin RJ, Kowalczykowski SC (2003) A molecular throttle: the recombination hotspot *chi* controls DNA translocation by the RecBCD helicase. *Cell* **114:** 647–654

Strick TR, Allemand JF, Bensimon D, Bensimon A, Croquette V (1996) The elasticity of a single supercoiled DNA molecule. *Science* **271:** 1835–1837

Strick TR, Allemand JF, Bensimon D, Croquette V (1998) Behavior of supercoiled DNA. *Biophys J* **74:** 2016–2028

Svoboda K, Mitra PP, Block SM (1994) Fluctuation analysis of motor protein movement and single enzyme-kinetics. *Proc Natl Acad Sci USA* **91:** 11782–11786

Wang LL, Lutkenhaus J (1998) FtsK is an essential cell division protein that is localized to the septum and induced as part of the SOS response. *Mol Microbiol* **29:** 731–740

Wang MD, Schnitzer MJ, Yin H, Landick R, Gelles J, Block SM (1998) Force and velocity measured for single molecules of RNA polymerase. *Science* **282:** 902–907

Yates J, Aroyo M, Sherratt DJ, Barre FX (2003) Species specificity in the activation of Xer recombination at *dif* by FtsK. *Mol Microbiol* **49:** 241–249

Yu XC, Tran AH, Sun Q, Margolin W (1998a) Localization of cell division protein FtsK to the *Escherichia coli* septum and identification of a potential N-terminal targeting domain. *J Bacteriol* **180:** 1296–1304

Yu XC, Weihe EK, Margolin W (1998b) Role of the C terminus of FtsK in *Escherichia coli* chromosome segregation. *J Bacteriol* **180:** 6424–6428

ARTICLES

nature structural & molecular biology

Analysis of DNA supercoil induction by FtsK indicates translocation without groove-tracking

Omar A Saleh[1], Sarah Bigot[2], François-Xavier Barre[2,3] & Jean-François Allemand[1,4]

FtsK is a bacterial protein that translocates DNA in order to transport chromosomes within the cell. During translocation, DNA's double-helical structure might cause a relative rotation between FtsK and the DNA. We used a single-molecule technique to quantify this rotation by observing the supercoils induced into the DNA during translocation of an FtsK complex. We find that FtsK induces ~0.07 supercoils per DNA helical pitch traveled. This rate indicates that FtsK does not track along DNA's groove, but it is consistent with our previous estimate of FtsK's step size. We show that this rate of supercoil induction is markedly near to the ideal value that would minimize *in vivo* disturbance to the chromosomal supercoil density, suggesting an origin for the unusual rotational behavior of FtsK.

Proteins that translocate DNA must contend with DNA's double-helical structure, and thus might rotate relative to the DNA while moving linearly. If rotation by a translocating protein is not allowed, the DNA will be forced to rotate, creating an excess of positive rotation (that is, supercoils) in advance of the protein, and an identical number of negative supercoils in its wake[1]. Previous studies have measured the supercoils induced by a variety of DNA translocases, and concluded in each case that the protein tracks DNA's groove while translocating[2–7].

FtsK is a bacterial protein with a DNA translocation activity used to transport chromosomal DNA during the late stages of cell division[8–10]. *In vivo*, FtsK is bound to the cell membrane at the closing division septum, so DNA transported by FtsK will be forced to absorb all relative rotation. Thus, if FtsK were to induce many supercoils (for example, by tracking DNA's groove while translocating at ~7 kbp s^{-1}; ref. 11), the topology of the translocated chromosome would be greatly disturbed, requiring a huge corrective effort by the cell's topoisomerases[12].

DNA translocation by FtsK can be studied *in vitro* using a truncated form of the protein, $FtsK_{50C}$, that omits the membrane-bound N-terminal domain of the protein while retaining the ATPase and DNA translocase activities of the C-terminal domain[9]. $FtsK_{50C}$ translocation *in vitro* can extrude loops of DNA, as was inferred first from bulk experiments[9,13] and confirmed by single-molecule measurements[11]. Loop extrusion requires that the protein bind the DNA in two places. We previously concluded that one of these contacts is an active, translocating motor, whereas the other is a static binding contact[11]; this was recently confirmed by another study[14]. During *in vivo* loop extrusion, the two contacts between FtsK and DNA fix the protein complex relative to the DNA, and topologically separate the DNA inside the loop (in the protein's wake) from that outside the loop (in advance of the protein), thus preventing the mixing and mutual annihilation of negative and positive supercoils in each domain[9,13]. We exploited these properties to study $FtsK_{50C}$ induced supercoiling at the single-molecule level.

RESULTS

Single-molecule assay of DNA topology

We carried out the measurements by tracking in real time the extension of a single DNA molecule that tethers a magnetic bead to the interior of a square glass capillary[15] (**Fig. 1a**; see Methods). Two magnets placed above the capillary pull on the bead, stretching the molecule with a constant force. We can add supercoils of either polarity to the DNA molecule by rotating these magnets. At the relevant stretching forces (0.2–0.5 pN), the initially added supercoils only twist the DNA and do not substantially change the DNA's extension[16] (**Fig. 1b**). After a critical number of turns (N_c) are added (corresponding to a supercoil density, σ_c) the molecule buckles; additional turns do not change the twist, but are absorbed as plectonemes, writhed structures that decrease the DNA's extension in linear proportion to the number of turns added (**Fig. 1b**). For low stretching forces, buckling occurs symmetrically; that is, there are transitions at $\pm N_c$. Symmetry is lost when the DNA is stretched above ~0.5 pN because negatively supercoiled DNA denatures in that regime[16]. To avoid this, we used forces <0.5 pN in all experiments described here.

We prepared a DNA–bead complex, we rotated the magnets to create negative plectonemes, and then, in the presence of ATP, introduced $FtsK_{50C}$ and recorded the subsequent translocation events (see Methods). In typical traces of DNA extension versus time with $FtsK_{50C}$, there were many clear changes from the baseline extension owing to protein activity (**Fig. 2a**). We acquired 92 individual events; every event contains a marked increase in the measured DNA exten-

[1]Laboratoire de Physique Statistique et Département de Biologie, Ecole Normale Supérieure, UMR8550 associé au CNRS et aux Universités Paris VI et VII, Paris, France. [2]Laboratoire de Microbiologie et de Génétique Moléculaire, CNRS UMR5100, Toulouse, France. [3]Centre de Génétique Moléculaire, CNRS UPR2167, Gif-sur-Yvette, France. [4]Laboratoire Pasteur, Département de Chimie, Ecole Normale Supérieure, Paris, France. Correspondence should be addressed to O.A.S. (oasaleh@lps.ens.fr).

Published online 10 April 2005; doi:10.1038/nsmb926

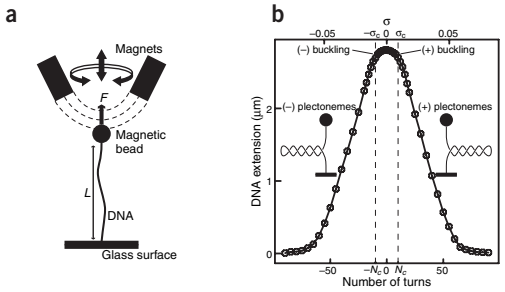

Figure 1 Stretching and supercoiling a single DNA molecule. (**a**) Experimental setup. A single DNA molecule is connected to a magnetic bead (1-μm diameter) and the interior of a square glass capillary. Magnets placed above the capillary stretch the molecule with a constant force F; the resulting DNA extension, L, is measured in real-time by optically tracking the bead's position. Rotating the magnets introduces a controllable number of supercoils into the DNA molecule. (**b**) Extension of a supercoiled DNA molecule stretched with 0.3 pN. The molecule has its maximum extension when relaxed (0 added turns). Small numbers of added turns twist the DNA without substantially changing the extension. The molecule buckles after $N_c \equiv 10$ turns have been added; given the measured 4.3 μm contour length, this corresponds to $\sigma_c \equiv 0.008$. Turns added beyond buckling form plectonemes that cause a linear decrease in extension with rotation with a typical slope $m_p \equiv 70$ nm turn^{-1}.

sion (region ii, **Fig. 2b**) before a decrease (regions iii and iv, **Fig. 2b**). In our previous measurements using rotation-insensitive nicked DNA molecules, no such increase was ever observed[11].

FtsK$_{50C}$ translocation induces supercoils

The shape of the events can be understood by considering the two mechanisms at work: loop extrusion by translocation and supercoil induction (schematics in **Fig. 2b**). Loop extrusion removes DNA from the region in advance of the protein (the 'tether'), placing it into the trailing loop, and can only decrease the DNA extension. However, supercoil induction can increase the extension: if protein translocation induces positive supercoils into the tether, these will annihilate the existing negative plectonemes. DNA length previously sequestered within the plectonemes will be released, increasing the tether's extension[7]. The measured increase thus indicates that FtsK$_{50C}$ adds positive supercoils into the tether, and that plectoneme removal dominates over loop extrusion. The maximum height of the increase, Δ_{max} (**Fig. 2b**), occurs upon removal of the last plectoneme (at the negative buckling threshold of the tether), after which loop extrusion is the sole remaining effect and the extension decreases. This picture is supported by the observation that Δ_{max} increases with the initial number of negative plectonemes (**Fig. 2c**), indicating that the increase in extension is caused by continuous supercoil induction by translocation, and not by one-time supercoil induction upon protein binding.

The consistency of supercoil induction

After the tether passes through the negative buckling threshold, if FtsK$_{50C}$ continues to add positive supercoils, it will eventually cause the tether to pass through the positive threshold. Experimentally, this would be visible as a sudden increase in the rate of descent when positive plectonemes begin to form. Indeed, we observed events with such an increase in rate (region iv, bottom trace in **Fig. 2b**), but rarely: only 5 of the 92 events show a clear acceleration. In the remainder of the events, the DNA extension decreased linearly until the end of the event (region iii, top trace in **Fig. 2b**) with speeds of 3–4 kbp s^{-1}, consistent with previous measurements on nicked DNA at the same ATP concentrations[11]. Thus, we find that FtsK$_{50C}$ does not consistently add supercoils beyond the negative buckling threshold. In contrast, every translocation event clearly shows an initial increase in DNA extension; thus FtsK does consistently add supercoils to a negatively coiled tether.

We attribute FtsK$_{50C}$'s sporadic inability to induce the positive buckling threshold to discrete slipping by the protein when it works to add positive supercoils to a positively twisted DNA molecule. This conclusion is based on a small number of translocation events on positively coiled DNA in which we observe features apparently caused by discrete

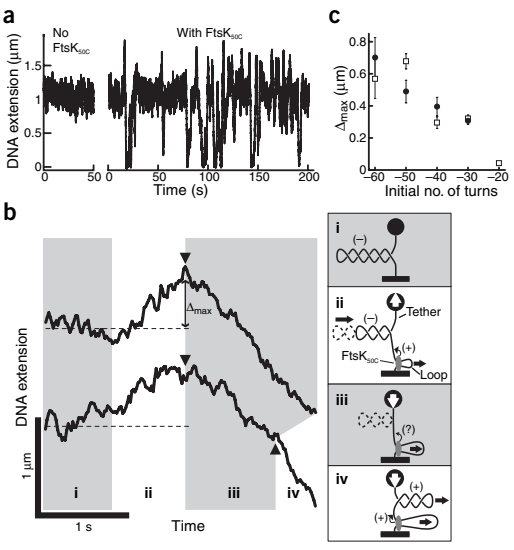

Figure 2 FtsK$_{50C}$ translocation events on supercoiled DNA. (**a**) A typical measurement of DNA extension versus time, both with and without FtsK$_{50C}$ in the solution, with $F = 0.4$ pN, 0.3 mM ATP, and –60 turns added. The protein's activity causes many clear increases and decreases of the extension from its baseline value. (**b**) A magnified view of two FtsK$_{50C}$ translocation events from the trace in **a**. Both events show a clear initial increase in extension over the baseline value (dotted lines) and passage through the negative buckling threshold, whereas only the bottom event shows passage through the positive buckling threshold. The interpreted mechanism for each region, i–iv, of the events is shown in the corresponding sketch, and depends on simultaneous extrusion of a loop (pictured) and protein-based addition to the tether of positive supercoils (indicated by the small arrow); this is described in detail in the main text. Note that loop extrusion is carried out by a single FtsK$_{50C}$ motor within a larger complex, as was found previously[11,14], and that the trailing loop will always be negatively supercoiled (this is omitted from the sketches for clarity). We sketch the FtsK$_{50C}$ complex at one extremity of the DNA. It is also possible that it extrudes loops from the middle of the DNA tether[14]; this does not change the interpretation of the data presented here. (**c**) The height of the maximum increase in DNA extension over baseline, Δ_{max}, clearly increases with the number of initial negative turns. Each data point corresponds to 4–15 events, and is reported as the mean value with s.e. Data were taken with 0.3 mM ATP and $F \equiv 0.4$ pN; the two sets of symbols correspond to data taken on two DNA molecules.

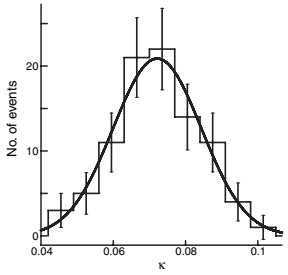

Figure 3 A histogram of κ values computed from each of 92 events. The distribution (plotted with statistical error bars) has mean 0.072 and s.d. 0.011, and is well-fit by a Gaussian curve, as shown, emphasizing its symmetric, normal shape. The variance of the distribution is close to that expected from experimental noise alone. Thus we observed no variation in protein behavior from event to event: within the uncertainty of the experiment, all $FtsK_{50C}$ complexes induced supercoils at an identical rate of $\kappa \cong 0.07$.

slipping (**Supplementary Fig. 1** online). A change in protein behavior in this regime is not unexpected: as the tether becomes progressively shorter and more positively supercoiled, the protein must do an increasing amount of work to effect changes to the DNA topology. This required work might eventually surpass the limited amount of energy available to the protein per enzymatic cycle (from ATP hydrolysis); at this point, the protein's activity must somehow change. Based on our observations, we believe $FtsK_{50C}$ responds by transiently unbinding from the DNA (in other words, discrete slipping), allowing relaxation of the torsional stress, which consequently decreases the energetic load on further translocation-induced topological changes. Owing to the small number of events in which slipping has been directly observed, we consider this model speculative; further work will be required to verify it. However, because FtsK's natural substrate, the *Escherichia coli* chromosome, is negatively supercoiled, the measured characteristics of $FtsK_{50C}$ translocation on negatively supercoiled DNA are the most accurate representation of the protein's natural behavior, and we will now quantitatively analyze those results.

Quantifying supercoil induction

We quantify $FtsK_{50C}$ supercoil induction through the dimensionless variable κ: the number of supercoils induced by the protein per DNA helical pitch traveled; note that $\kappa = 1$ for a groove-tracking protein. We determine κ for $FtsK_{50C}$ by relating Δ_{max} to the number of turns added by the protein: after translocating a distance d, the protein will induce $N_{FtsK} = \kappa d / p$ turns, where p is the length of DNA's helical pitch. Each induced turn increases the extension by m_p, the slope of the linear region of the extension/rotation curve (**Fig. 1b**). Simultaneously, loop extrusion decreases the extension by $d = pN_{FtsK} / \kappa$; the increase Δ is the sum of the two effects: $\Delta = m_p N_{FtsK} - d = N_{FtsK}(m_p - (p / \kappa))$. The maximum, Δ_{max}, occurs when no plectonemes remain, corresponding to $N_{FtsK} = |N_o| - N_c$, where N_o is the initial number of turns. Using this, we can relate κ to known parameters:

$$\kappa = p(|N_o| - N_c) / [m_p(|N_o| - N_c) - \Delta_{max}]. \quad (1)$$

To apply equation (1), we use $p = 10.4$ bp $= 3.54$ nm. We extract N_c (typically ~10 turns) and m_p (~70 nm turn^{-1}) from each DNA molecule's extension/rotation curve (**Fig. 1b**), and we measure Δ_{max} by fitting a piecewise linear curve to each translocation event (**Supplementary Methods** online).

In a histogram of κ as calculated from equation (1) for each of the 92 events (**Fig. 3**), the κ values form a nearly symmetric distribution with a mean of 0.072 and a relative s.d. (16%) that closely corresponds to our estimate of the experimental error in determining each individual value (~13%). Thus, within the error, all $FtsK_{50C}$ complexes behave identically in this experiment. Furthermore, the consistency of the κ values across all events indicates that $FtsK_{50C}$ undergoes no random slipping processes as it travels on negatively twisted DNA. Thus we conclude that $\kappa = 0.07 \pm 0.01$ represents $FtsK_{50C}$'s true supercoil induction rate. The quoted error originates from a systematic additive uncertainty of $\sigma_c \cong 0.01$ in the derivation of equation (1) (data not shown).

DISCUSSION

$\kappa = 0.07$ corresponds to one positive supercoil induced ahead of the motor (and one negative supercoil behind) per ~150 bp translocated. Because a groove-tracking protein would induce one turn per pitch (~10.5 bp) traveled, we conclude that $FtsK_{50C}$ does not translocate DNA by tracking the major or minor groove. Instead, this value is consistent with a mechanism in which $FtsK_{50C}$ moves along DNA by skipping over the grooves with a step size slightly longer than DNA's helical pitch (**Fig. 4**).

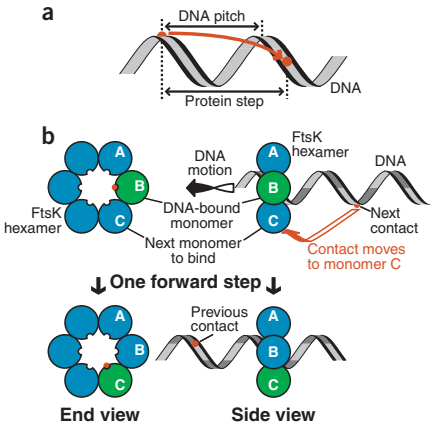

Figure 4 Possible $FtsK_{50C}$ translocation mechanism. (**a**) A protein that moves along DNA with a step slightly larger than DNA's pitch will rotate slightly while moving forward. (**b**) Model for DNA translocation by a fixed $FtsK_{50C}$ complex. A hexameric, ring-like complex of monomers is threaded by a double-stranded DNA molecule. By analogy to other hexameric translocases[19,20], DNA binding and release might occur successively by neighboring monomers, as shown. Initially monomer B is bound to the DNA; passage through an enzymatic cycle advances the complex by one forward step, resulting in monomer C bound to the DNA, and a slight rotation of the DNA. In our experiment, the DNA is torsionally constrained, so this added rotation creates supercoiling. Our data ($\kappa = 0.07 \pm 0.01$) fixes the ratio of rotation to distance traveled, independent of the translocation model. In the pictured model, $\kappa \cong 0.07$ results in an estimate of ~13 bp for $FtsK_{50C}$'s step size, in agreement with previous data that estimated the step to be 12 ± 2 bp (ref. 11). Other translocation mechanisms, involving different sequences of monomer binding, also give step estimates consistent with the previous data, and thus cannot be ruled out.

This mechanism would link $FtsK_{50C}$'s κ to the amount of rotation for each step; in turn, the rotation per step depends on the deviation of the step size from the pitch (a similar link between step size and rotation has been observed for myosin moving along actin[17,18]). We can use this model to relate κ to the protein's step size, but we must account for the protein's structure: $FtsK_{50C}$ is thought to oligomerize to form a DNA-threaded hexameric ring[9]. Translocation probably proceeds by coordinated DNA binding and release that occurs successively by neighboring monomers (**Fig. 4b**), as has been proposed for other hexameric DNA translocases[19,20]. Assuming binding activity proceeds around the ring in a right-handed sense, we find that $\kappa = 0.07$ implies a step size of 13.1 bp, in marked agreement with our previous measurement of 12 ± 2 bp (ref. 11). Owing to the imprecision in the previous measurement, we cannot rule out other mechanisms that give similar κ-based step size estimates, such as if next-nearest neighbors are sequentially active, or if binding activity proceeds by nearest neighbors in a left-handed sense.

What is the benefit for the cell of a particular value of κ for FtsK? Given FtsK's role in transporting chromosomes[8–10], a low value of κ would be advantageous because it would minimize disturbance to the chromosomal supercoil density, σ_o. Extending this argument, we hypothesize that translocation by FtsK, ideally, would not change the supercoil density of the DNA being transported. This ideal case does not correspond to $\kappa = 0$ because the chromosome is intrinsically supercoiled and the protein acts as a topological barrier. Instead, the ideal case occurs if $\kappa = -\sigma_o$. Under this constraint, FtsK will remove supercoils in front, and add them behind, at a rate that maintains a constant supercoil density by compensating for the protein's motion (**Supplementary Methods**). The supercoil density σ_o of the *E. coli* chromosome is approximately –0.06 to –0.075 (refs. 21,22). Thus, our measurement of $\kappa = 0.07 \pm 0.01$ for $FtsK_{50C}$ is markedly consistent with the ideal value predicted to cause no disturbance to the chromosomal topology ($\kappa = -\sigma_o$, within the uncertainty of each parameter). We carried out a bulk experiment that supports this idea and found that the topology of a plasmid with, initially, $\sigma \cong -0.06$ does not change after $FtsK_{50C}$ translocation (**Supplementary Fig. 2** online).

If FtsK's κ is indeed tuned to the chromosomal supercoil density, this implies that a prime consideration in the evolution of FtsK's translocation mechanism was the global topology of the bacterial chromosome. By extension, other translocases involved in the transport of double-stranded DNA, such as SpoIIIE from *Bacillus subtilis*[23], could also be expected to match their supercoil induction rate to the supercoil density of the DNA being transported. This idea could be tested by measuring the value of κ for such DNA translocases in various species, and in particular from thermophilic bacteria that have different values of σ_o.

METHODS

Sample preparation and experimental conditions. $FtsK_{50C}$ was purified as described[9]. The DNA substrate used was a 13.5-kb section of *E. coli* chromosomal DNA purified from plasmid pFC94 (ref. 24), identical to that used previously[11]. Each end of the DNA was ligated to a fragment containing either biotin- or digoxigenin-modified nucleotides; upon incubation, these modified extremities bind, respectively, streptavidin-coated magnetic beads (Dynal) and a glass capillary presenting anti-digoxigenin (Roche). We used magnetic beads either 1 or 2.8 μm in diameter; no difference was seen in data taken with different sized beads. Glass capillaries (1-mm square cross section) were prepared as described[11]. Experiments were done at 23 °C in a buffer containing 10 mM $MgCl_2$, 10 mM Tris, pH 7.9, 50 mM NaCl, 1 mM DTT, 0.01% (v/v) Triton X-100 and ATP. After a suitable bead–DNA complex was found (see below), 2–4 μl of 200 nM $FtsK_{50C}$ monomers were added to the ~200 μl of buffer in the capillary and gently mixed; the protein injection was repeated as necessary.

Single molecule assay. Tethered bead–DNA complexes were viewed in an inverted microscope; bead tracking and resulting measurement of the force were done as described[11]. We insured that each bead used was tethered by a single, un-nicked DNA molecule by measuring the extension/rotation curve (**Fig. 1b**): a nicked molecule shows no variation in extension with rotation, whereas a tether containing multiple DNA molecules exhibits distinctive features easily differentiated from those of a single DNA molecule[16]. We characterized suitable complexes by first insuring that the extension/rotation curve was symmetric; this typically occurs below ~0.5 pN. The extension/rotation curve was used to find N_c and m_p. Second, we measured the DNA extension as a function of force, which we used to find the contour length and persistence length of the molecule by fitting it with the worm-like chain model for DNA extensibility[25].

Data analysis. Measured traces of bead height correspond directly to DNA extension; no filtering was been applied to any of the plots shown. Before analysis, units involving DNA extension (m_p and the measured DNA extension versus time) were adjusted by the factor of relative extension predicted by the worm-like chain model (typically ~0.75, arising from $F \cong 0.4$ pN, and a persistence length of ~40 nm). Thus, all units were dealt with in terms of DNA contour length, as required by our definition of κ. While the worm-like chain model technically does not apply to twisted DNA, it offers a good approximation; this is justified by the fact that the DNA extension varies only slightly when twist is added before buckling (**Fig. 1b**).

Events were analyzed only if preceded by a section of constant baseline extension. κ was extracted from each event by application of equation (1), using values for p, N_o, N_c and m_p as already described. The final parameter, Δ_{max}, was found by fitting a piecewise linear curve to the translocation events (**Supplementary Methods**). We estimated the error in the determination of Δ_{max} using a bootstrap analysis[26]. The typical error in each calculation of κ, found by standard propagation of the error in each variable in equation (1), is 13%. Note that, owing to the structure of equation (1) and the typical value of Δ_{max}, κ is relatively insensitive to small changes in the value of Δ_{max}; thus although the relative error in determining the value of Δ_{max} can be quite large in some cases, the resulting uncertainty in κ is still fairly small.

Note: Supplementary information is available on the Nature Structural & Molecular Biology website.

ACKNOWLEDGMENTS

We thank D. Bensimon and V. Croquette for helpful discussions, and K. Neuman for critical reading of the manuscript. This work was supported by the DRAB 2004 program. Research in Paris was also supported by grants from the ACI Jeune Chercheur program and from the European Union MolSwitch program. Research in Toulouse was also supported by grants from the Centre National de la Recherche Scientifique ATIP program and from the French Research Ministry Fundamental Microbiology ACI program.

COMPETING INTERESTS STATEMENT

The authors declare that they have no competing financial interests.

Received 2 February; accepted 17 March 2005
Published online at http://www.nature.com/nsmb/

1. Liu, L.F. & Wang, J.C. Supercoiling of the DNA template during transcription. *Proc. Natl. Acad. Sci. USA* **84**, 7024–7027 (1987).
2. Yang, L., Jessee, C.B., Lau, K., Zhang, H. & Liu, L.F. Template supercoiling during ATP-dependent DNA helix tracking—studies with simian virus-40 large tumor antigen. *Proc. Natl. Acad. Sci. USA* **86**, 6121–6125 (1989).
3. Tsao, Y.P., Wu, H.Y. & Liu, L.F. Transcription-driven supercoiling of DNA—direct biochemical evidence from *in vitro* studies. *Cell* **56**, 111–118 (1989).
4. Koo, H.S., Claassen, L., Grossman, L. & Liu, L.F. ATP-dependent partitioning of the DNA template into supercoiled domains by *Escherichia coli* UvrAB. *Proc. Natl. Acad. Sci. USA* **88**, 1212–1216 (1991).
5. Janscak, P. & Bickle, T.A. DNA supercoiling during ATP-dependent DNA translocation by the type I restriction enzyme EcoAI. *J. Mol. Biol.* **295**, 1089–1099 (2000).
6. Harada, Y. *et al.* Direct observation of DNA rotation during transcription by *Escherichia coli* RNA polymerase. *Nature* **409**, 113–115 (2001).
7. Seidel, R. *et al.* Real-time observation of DNA translocation by the type I restriction modification enzyme EcoR124I. *Nat. Struct. Mol. Biol.* **11**, 838–843 (2004).
8. Lesterlin, C., Barre, F.-X. & Cornet, F. Genetic recombination and the cell cycle: what we have learned from chromosome dimers. *Mol. Microbiol.* **54**, 1151–1160 (2004).
9. Aussel, L. *et al.* FtsK is a DNA motor protein that activates chromosome dimer resolution by switching the catalytic state of the XerC and XerD recombinases. *Cell* **108**, 195–205 (2002).
10. Lau, I.F. *et al.* Spatial and temporal organization of replicating *Escherichia coli* chromosomes. *Mol. Microbiol.* **49**, 731–743 (2003).

11. Saleh, O.A., Perals, C., Barre, F.-X. & Allemand, J.-F. Fast, DNA-sequence independent translocation by FtsK in a single-molecule experiment. *EMBO J.* **23**, 2430–2439 (2004).
12. Champoux, J.J. DNA topoisomerases: structure, function, and mechanism. *Annu. Rev. Biochem.* **70**, 369–413 (2001).
13. Ip, S.C.Y., Bregu, M., Barre, F.-X. & Sherratt, D.J. Decatenation of DNA circles by FtsK-dependent Xer site-specific recombination. *EMBO J.* **22**, 6399–6407 (2003).
14. Pease, P.J. *et al.* Sequence-directed DNA translocation by purified FtsK. *Science* **307**, 586–590 (2005).
15. Strick, T.R., Allemand, J.-F., Bensimon, D., Bensimon, A. & Croquette, V. The elasticity of a single supercoiled DNA molecule. *Science* **271**, 1835–1837 (1996).
16. Strick, T.R., Allemand, J.-F., Bensimon, D. & Croquette, V. Behavior of supercoiled DNA. *Biophys. J.* **74**, 2016–2028 (1998).
17. Sase, I., Miyata, H., Ishiwata, S. & Kinosita, K. Axial rotation of sliding actin filaments revealed by single-fluorophore imaging. *Proc. Natl. Acad. Sci. USA* **94**, 5646–5650 (1997).
18. Ali, M.Y. *et al.* Myosin V is a left-handed spiral motor on the right-handed actin helix. *Nat. Struct. Biol.* **9**, 464–467 (2002).
19. Singleton, M.R., Sawaya, M.R., Ellenberger, T. & Wigley, D.B. Crystal structure of T7 gene 4 ring helicase indicates a mechanism for sequential hydrolysis of nucleotides. *Cell* **101**, 589–600 (2000).
20. Hishida, T., Han, Y.-W., Fujimoto, S., Iwasaki, H. & Shinagawa, H. Direct evidence that a conserved arginine in RuvB AAA+ ATPase acts as an allosteric effector for the ATPase activity of the adjacent subunit in a hexamer. *Proc. Natl. Acad. Sci. USA* **101**, 9573–9577 (2004).
21. Wang, J.C. DNA supercoiling and its effects on the structure of DNA. *J. Cell Sci.*, 21–29 (1984).
22. Zechiedrich, E.L. *et al.* Roles of topoisomerases in maintaining steady-state DNA supercoiling in *Escherichia coli*. *J. Biol. Chem.* **275**, 8103–8113 (2000).
23. Bath, J., Wu, L.J., Errington, J. & Wang, J.C. Role of *Bacillus subtilis* SpoIIIE in DNA transport across the mother cell-prespore division septum. *Science* **290**, 995–997 (2000).
24. Perals, K., Cornet, F., Merlet, Y., Delon, I. & Louarn, J.M. Functional polarization of the *Escherichia coli* chromosome terminus: the dif site acts in chromosome dimer resolution only when located between long stretches of opposite polarity. *Mol. Microbiol.* **36**, 33–43 (2000).
25. Bouchiat, C. *et al.* Estimating the persistence length of a worm-like chain molecule from force-extension measurements. *Biophys. J.* **76**, 409–413 (1999).
26. Efron, B. & Tibshirani, R. Statistical data analysis in the computer age. *Science* **253**, 390–395 (1991).

La lotte de Méditerranée pochée à l'huile d'olive noire, côtes et feuilles de moutarde

Michel Bras

Ingrédients (4 personnes) : Lotte de méditerranée 1,2 kg de lotte

Préparer la lotte et bien la dénerver. Lever les filets et la tronçonner en quatre parts.

400 g d'olives noires à la grecque Dénoyauter les olives. Les ranger sur une plaque et les glisser dans un four réglé à 80 řC. Les laisser le temps nécessaire pour qu'elles soient sèches (environ une nuit ou plus).

Huile noire de cuisson 100 g d'olives noires sèches 1,5 dl d'huile d'olive Le résultat sera encore meilleur si vous multipliez les proportions par 4 ou plus. Mixer fortement l'huile d'olive et les olives sèches. Réserver.

Huile noire de présentation 80 g d'olives noires sèches 8 cl d'huile d'olive Le résultat sera encore meilleur si vous multipliez les proportions par 4 ou plus. Mixer fortement l'huile d'olive et les olives sèches. Réserver.

Moutarde 1 pied de moutarde Quantité suffisante de sel

au dernier moment Poudre de graines de moutarde Olives sèches hachées Quantité suffisante de beurre

Séparer les côtes des feuilles. Les laver et les cuire séparément à l'eau bouillante salée. Refroidir dans l'eau glacée.

Au dernier moment Dans une sauteuse, verser 4 cuillères d'huile noire de cuisson. Chauffer modérément et y placer la lotte. Procéder à une cuisson douce - presque pochée - afin d'éviter à l'huile de se décomposer. Arroser fréquemment la lotte à l'aide d'une cuillère. Sonder la lotte avec une fine brochette. La lotte est prête lorsque le centre du pavé de lotte est tiède. La laisser se détendre. À la découpe, on doit avoir une belle couleur blanc nacré. Trop cuite, la lotte sera cotonneuse. Refendre la lotte afin de visualiser le côté nacré. Chauffer la moutarde au beurre. Dresser harmonieusement la moutarde et la lotte en épurant la présentation au maximum. Tacher les assiettes d'huile "noire" de présentation, d'olives sèches hachées ainsi que de poudre de moutarde.

http://www.michel-bras.com/

Troisième partie

Fluorescence

Chapitre 1

Introduction

Lors de mon recrutement en 1999 une partie de mon projet de recherche, en continuité avec les projets précédents, portait sur l'étude de l'influence de la force sur l'activité enzymatique, pouvant aussi être celle d'un moteur. Brièvement il s'agit de modifier, par une action mécanique, les conformations d'une enzyme pour en modifier son activité et étudier par cette méthode la relation structure/activité de l'enzyme.

Le choix de la technique de mesure de détection de l'activité enzymatique s'est naturellement porté vers la fluorescence : c'est une méthode qui peut être très sensible et d'un point de vue expérimental un certain nombre d'enzymes très utilisées comme la HRP (Horse Radish Peroxidase) ou la βgalactosidase, peuvent produire de la fluorescence en catalysant leur réaction. De plus la détection de molécules uniques est complémentaire des micromanipulations pour l'étude des interactions ADN-protéine. Développer un système de visualisation de molécules uniques était donc un point expérimental important, pour mon acquisition de compétences et pour le développement des thématiques qui m'intéressent.

Pour observer des molécules uniques il existe trois méthodes répandues: excitation biphotonique, onde évanescente, microscopie confocale. Dans les trois cas on augmente le rapport signal sur bruit en limitant la région d'excitation et/ou de détection de la fluorescence. Dans un premier temps nous avons fait le choix d'utiliser la microscopie biphotonique comme méthode d'excitation permettant de visualiser des molécules uniques. L'achat, onéreux, d'un laser Ti:Sa permettant cette excitation a été fait en commun entre le LPS et l'équipe du département de chimie de L. Jullien.

1.1 Principe de l'excitation biphotonique

L'excitation biphotonique repose sur une transition électronique induite par deux photons absorbés simultanément. Pour observer les mêmes longueurs d'onde d'émission de fluorescence dans le visible qu'en microscopie classique il faut donc exciter dans l'infrarouge pour observer de la fluorescence dans le visible. Ceci suppose que deux photons IR arrivent en même temps sur la molécule à exciter donc une grande densité de photons d'où l'utilisation de laser pulsé. La nécessité de cette forte densité de photons fait qu'en pratique l'excitation se produit sur un faisceau focalisé et plus précisément au point focal d'un objectif. Pour l'observation de molécules uniques cela a l'avantage de ne produire de photons que dans une faible zone de l'espace ce qui réduit le bruit de fond (figure 1.1). C'est en fait un

confocal intrinsèque. Par ailleurs la séparation spectrale entre l'excitation et l'émission permet une bonne séparation des deux sources de photodétection ce qui permet de diminuer le bruit du à de l'excitation mal filtrée. Les inconvénients sont le prix et un photobleaching plus important.

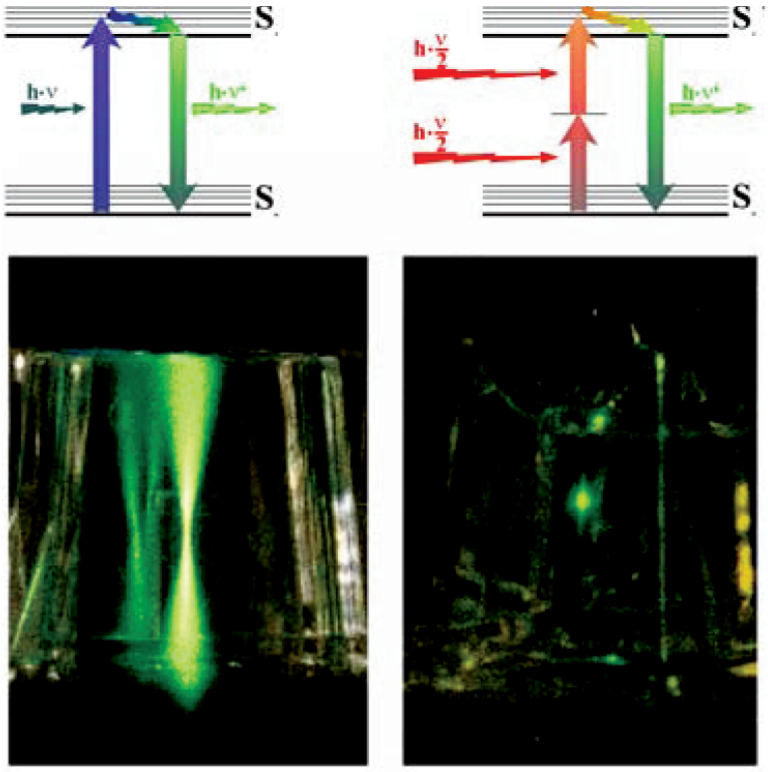

FIG. 1.1 – *L'excitation biphotonique repose sur l'absoprtion de deux photons IR simultanés par opposition à la fluorescence classique ou un seul photon est absorbé. Cette contrainte implique que la fluorescence ne peut être excitée qu'au point focal de l'objectif alors qu'a un photon tout un cône est excité.*

Chapitre 2

Mesure de sections efficaces d'absorption à deux photons

Pour commencer à utiliser la fluorescence nous avons débuté avec une tâche plus simple que l'observation de molécules uniques avec la mise en place d'un dispositif de mesure de section efficace d'absorption à deux photons. Le but du montage est de mesurer le nombre de photons que peut émettre une molécule en fonction du flux de photons incidents lors d'une excitation biphotonique. L'intérêt est double : d'une part pour pouvoir à terme observer des molécules uniques il faudra de bons fluorophores, c'est à dire des fluorophores avec une grande section efficace d'absorption à deux photons, d'autre part la relation entre la structure d'une molécule et sa capacité à absorber à deux photons n'est pas très bien connue et il est donc intéressant de développer une approche entre chimie et physique où il y a un couplage entre la synthèse chimique de molécules et la mesure de ses propriétés.

Nous avons donc construit un dispositif basé sur l'un des nombreux excellents travaux de l'équipe de W.W. Webb [54], permettant cela dont l'utilisation a permis les résultats présentés dans l'article suivant. Il va sans dire que je n'ai rien à voir avec la partie synthèse...ma contribution étant centrée sur la construction et l'acquisition des données deux photons avec E. Cogné.

FULL PAPER

Diaroyl(methanato)boron Difluoride Compounds as Medium-Sensitive Two-Photon Fluorescent Probes

Emmanuelle Cogné-Laage,[a] Jean-François Allemand,*[a, b] Odile Ruel,[a] Jean-Bernard Baudin,[a] Vincent Croquette,[b] Mireille Blanchard-Desce,[c] and Ludovic Jullien*[a]

Abstract: This paper evaluates the use of diaroyl(methanato)boron difluoride compounds for designing efficient fluorescent probes through two-photon absorption. Three different pathways allowing for the syntheses of symmetrical and dissymmetrical molecules are reported. The stable diaroyl(methanato)-boron difluoride derivatives can be easily obtained in good yields. They exhibit a large one-photon absorption that is easily tuned in the near-UV range. Their strong fluorescence emission covers the whole visible domain. In addition to these attractive linear properties, several diaroyl(methanato)-boron difluoride derivatives possess significant cross sections for two-photon absorption. The derived structure–property relationships are promising for designing new generations of molecules relying on the diaroyl(methanato)boron difluoride backbone.

Keywords: boron · fluorescent probes · structure–activity relationships · two-photon absorption

Introduction

Extrinsic fluorophores are increasingly used as reporter molecules for labeling, for probing environments, for evaluating intramolecular distances or molecular motions, and so forth.[1] Relatively small molecules exhibiting large fluorescence quantum yields are always sought after for such applications. In addition, other features have to be considered in answer to specific questions. A high sensitivity of the photophysical features to the surrounding medium is favored to evaluate the polarity or the viscosity of molecular environments. For fluorescence-depolarization experiments, fluorophores with well-defined electronic-transition dipoles in a molecular frame are preferred. Despite extensive studies, few series of molecules satisfy these criteria, as revealed by the catalog contents of the main purchasers of fluorescent molecular probes; therefore, searching for new series of fluorescent species is still an important issue. In fact, the lack of appropriate fluorescent labels or probes that cover the whole UV/Vis-wavelength range is regarded as critical for the development of promising experiments that rely on the observation of singly fluorescent molecules.[2] Finally, the growing interest in fluorescence imaging based on two-photon excitation[3,4] requires the identification of fluorophores exhibiting large cross sections for multiple-photon absorptions.[5,6]

In relation to the preceding paragraph, one of the most recently developed fluorescent chromophores is 4,4-difluoro-4-bora-3a-azonia-4a-aza-s-indacene (BODIPY) (Scheme 1).[7–11] BODIPY-based fluorophores exhibit spectral features that make them especially attractive when the excitation is performed in the 500–600 nm range, thus producing a fluorescence emission at 500–650 nm. Their molar absorption coefficient is very high ($\varepsilon > 8 \times 10^4\ \mathrm{M}^{-1}\mathrm{cm}^{-1}$) along with their fluorescence quantum yield (ϕ_F) that is close to one, even in water. For imaging, such properties are well suited for fluorescence microscopy relying on one-photon excitation, in which they compete with most fluorescein and rhodamine derivatives. In contrast, BODIPY-based

[a] Dr. E. Cogné-Laage, Dr. J.-F. Allemand, Dr. O. Ruel, Dr. J.-B. Baudin, Prof. Dr. L. Jullien
Département de Chimie (C.N.R.S. U.M.R. 8640)
École Normale Supérieure, 24 rue Lhomond
75231 Paris Cedex 05 (France)
Fax: (+33) 1-44-32-33-25
E-mail: Jean-Francois.Allemand@ens.fr
Ludovic.Jullien@ens.fr

[b] Dr. J.-F. Allemand, Dr. V. Croquette
Département de Physique (C.N.R.S. U.M.R. 8550)
École Normale Supérieure, 24 rue Lhomond
75231 Paris Cedex 05 (France)
Fax: (+33) 1-44-32-34-92
E-mail: Jean-Francois.Allemand@ens.fr

[c] Dr. M. Blanchard-Desce
Université de Rennes 1, Institut de Chimie (C.N.R.S. U.M.R. 6510)
Campus scientifique de Beaulieu, 35042 Rennes (France)

Supporting information for this article is available on the WWW under http://www.chemeurj.org/ or from the author. It contains Figures 1Sa, 1Sb, 2S, and 3S.

 DOI: 10.1002/chem.200305321

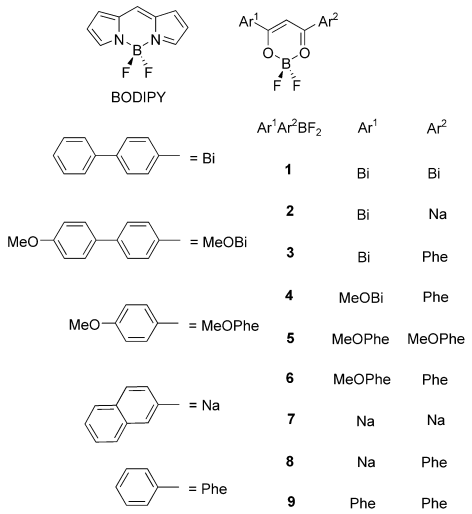

$Ar^1Ar^2BF_2$	Ar^1	Ar^2
1	Bi	Bi
2	Bi	Na
3	Bi	Phe
4	MeOBi	Phe
5	MeOPhe	MeOPhe
6	MeOPhe	Phe
7	Na	Na
8	Na	Phe
9	Phe	Phe

Scheme 1. Generic structures of the BODIPY and the diaroyl(methanato)boron difluoride $Ar^1Ar^2BF_2$ compounds prepared during this study.

fluorophores are less satisfactory when two-photon excitation is used. For instance, the two-photon fluorescence absorption (TPA) cross section (δ) of the disodium salt of 4,4-difluoro-1,3,5,7,8-pentamethyl-4-bora-3a,4a-diaza-s-indacene-2,6-disulfonic acid is about two and ten times lower than the TPE cross sections of fluorescein and rhodamine B, respectively.[12]

Aiming at keeping the satisfactory aspects of the BODIPY chromophores while improving their features toward two-photon absorption, we became interested in a series of diaroyl(methanato)boron difluoride compounds ($Ar^1Ar^2BF_2$ **1**–**9**), with structures related to BODIPY (Scheme 1). β-Diketone–boron difluoride complexes have been known for more than 75 years;[13] nevertheless, the diaroyl series remains largely unexplored, excepting the investigations performed on the parent compound of this series, dibenzoyl(methanato)boron difluoride (**9**), whose emission[14,15] and reactivity[16] of the singlet excited state have been investigated. Some related compounds were reported to exhibit attractive absorption and emission features, such as large molar absorption coefficients, or large fluorescence quantum yields.[17–20] In particular, the range of absorption wavelengths (ca. 350–500 nm) is especially suitable for two-photon excitation with femtosecond Ti–sapphire pulsed lasers that can be tuned between 700 and 1100 nm.

The present paper is organized as follows: We first describe three different synthetic pathways to access the diaroyl(methanato)boron difluoride derivatives **1**–**9**. Some photophysical properties of these compounds are then reported and discussed (one- and two-photon absorption, steady-state fluorescence emission). In view of the possible use of $Ar^1Ar^2BF_2$ compounds as labels, we also examined both the dependence of the emission features upon the environment and the chemical stability of the present fluorescent molecules.

Abstract in French: *Cet article évalue l'intérêt de complexes difluoroboroniques de diaroyl-β-dicétones dans l'élaboration de sondes fluorescentes après excitation à deux photons. Trois différentes voies de synthèse de dérivés symétriques et dissymétriques sont décrites. Elles permettent d'obtenir de grandes quantités de complexes avec de bons rendements. Ces composés présentent une absorption intense à un photon, accordable dans le proche UV. Leur forte émission de fluorescence couvre la gamme du visible. En sus de ces intéressantes propriétés linéaires, certains des complexes difluoroboroniques de diaroyl-β-dicétones synthétisés possèdent une importante section efficace d'absorption à deux photons. Les relations structure-propriétés obtenues permettent d'envisager le développement de molécules performantes construites à partir du squelette étudié.*

Results and Discussion

Synthesis: To derive structure–property relationships, we synthesized eight compounds differing in 1) the aryl backbones: phenyl (Phe), biphenyl (Bi), and naphthalene (Na), 2) the aromatic substituents: H, or methoxy (MeO), and 3) their symmetry ($Ar^1 = Ar^2$ or $Ar^1 \neq Ar^2$). The diaroyl(methanato)boron difluoride compounds ($Ar^1Ar^2BF_2$ **1**–**9**) were easily obtained in good yields from the reaction of boron trifluoride/diethyl ether (BF_3/Et_2O) with the corresponding 1,3-diketones (Ar^1Ar^2) in benzene or dichloromethane (Scheme 2).[21] The Ar^1Ar^2 derivatives were synthesized by three different pathways (Scheme 2).

Diketones BiBi, BiNa, MeOBiPhe, MeOPhePhe, NaNa, and NaPhe were prepared in three steps according to pathway A. In the first step, the ethyl aroyl acetates 1 A-Ar^1 (1 = step 1, A = pathway A, Ar^1 = Bi or Na) were obtained from condensation of the dianion of monoethyl malonate with aroyl chloride.[22] The monoanions from the 1 A-Ar^1 species were then condensed with the appropriate aroyl chloride to yield 2 A-BiBi, 2 A-BiNa, 2 A-MeOBiPhe, 2 A-MeOPhePhe, 2 A-NaNa, and 2 A-NaPhe.[23] Finally, the 2 A-Ar^1Ar^2 compounds were decarboxylated in the presence of sodium chloride in DMSO to yield the desired diketones.[24]

BiPhe was synthesized in three steps (pathway B). The condensation of 4-acetylbiphenyl with benzaldehyde first provided the chalcone 1-biphenyl-4′-yl-3-phenylprop-2-enone 1 B-BiPhe.[25] This compound was subsequently brominated[26] to yield 2 B-BiPhe, which finally gave BiPhe after elimination under basic conditions.[27] Lastly, MeOPheMeOPhe was directly obtained in one step from acylation of ethenyl acetate by 4-methoxybenzoyl chloride (pathway C).[28]

Chemical stability against hydrolysis: During experiments performed in our laboratory, some BODIPY derivatives were prone to color fading in the presence of water. For example, during preparation of egg lecithin vesicles by detergent removal, the signal arising from a BODIPY-labeled

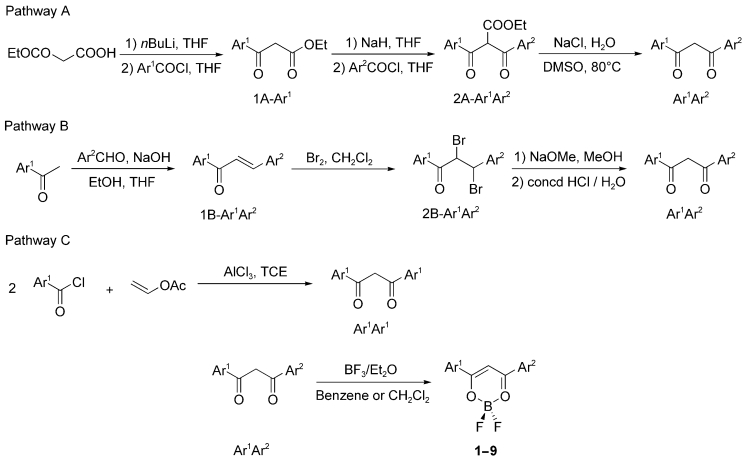

Scheme 2. Pathways for syntheses of the target compounds $Ar^1Ar^2BF_2$ **1–9**.

lipid essentially disappeared in less than 12 h, even when protected from light with aluminium foil. This behavior probably originates from slow hydrolysis of the boron difluoride bridge. In view of the structural similarity between the BODIPY dyes and the present $Ar^1Ar^2BF_2$ series, we investigated the stability of the series towards water hydrolysis. In view of the poor water solubility of the presently synthesized $Ar^1Ar^2BF_2$ compounds, we considered incorporating some of them into micelles that are known to remain quite permeable to water molecules, while solubilizing hydrophobic molecules. Compounds **4** and **7** were dissolved in an aqueous solution of α-D-octylglucopyranoside (OG 25 mM), which forms micelles above 23 mM at room temperature,[29,30] to yield dye solutions (80 μM). The resistance to hydrolysis was evaluated by following the fluorescence emission (vide infra) as a function of time at room temperature. In fact, no significant drop of the signal was noticed over a few days, so it was concluded that $Ar^1Ar^2BF_2$ compounds are rather stable. The better resistance to hydrolysis of the present series could be related to the greater affinity of boron to oxygen, compared with nitrogen.[31,32]

Table 1. Single-photon absorption maxima (λ_{max}), steady-state fluorescence emission maxima (λ_{em}), molar absorption coefficients for single-photon absorption ($\varepsilon(\lambda_{max})\pm5\%$ [$\mu M^{-1}cm^{-1}$]), fluorescence quantum yields ($\phi_F\pm5$ [%]), Stokes shift values ($\Delta\nu$), two-photon excitation spectra maxima (λ^2_{max}), two-photon excitation cross sections ($\delta_{max}\pm20\%$ in GM; $1\,GM=10^{-50}cm^4s(photon-molecule)^{-1}$) for the $Ar^1Ar^2BF_2$ derivatives in dichloromethane at 298 K.

Ar^1Ar^2	λ_{max} [nm]	$\varepsilon(\lambda_{max})$ [$\mu M^{-1}cm^{-1}$]	λ_{em} [nm]	ϕ_F [%]	$\Delta\nu$ [cm^{-1}]	λ^2_{max} [nm]	δ_{max} [GM]
1	411	75000	458	50	2500	795	30
2	416	45000	473	35	2900	745	60
3	394	61000	450	70	3160	775	30
4	410	59000	540	75	5900	835	200
5	410	89000	436	85	1050	785	20
6	396	62000	431	85	2050	787	25
7	420	47000	476	40	2800	775	85
8	398	40000	482	35	4380	805	30
9	364	46000	395	20	2150	–[a]	< 5

[a] The signal remained in the 2—3 GM range between 700 nm and 750 nm.

Linear absorption and emission properties: Derivatives **1–9** exhibit a strong one-photon absorption ($\varepsilon > 50000\,M^{-1}cm^{-1}$) in the 350–450 nm range (Figure 1 and Table 1). The corresponding band is rather narrow (50–75 nm at half-width). This band was interpreted as corresponding to a $\pi\rightarrow\pi^*$ transition in the parent compound **9**.[14,33] As anticipated, the maximum one-photon absorption (λ_{max}) is redshifted when the conjugation path length is increased. Linear dependence of the absorption on concentration without any spectrum alteration was observed in dichloromethane in the 1–20 μM range, suggesting that only monomeric species are present in this concentration range, as reported for **9**.[15] We investigated the solvatochromism of some $Ar^1Ar^2BF_2$ derivatives by recording the UV/Vis absorption spectra in several solvents (Table 2 and Figure 2a and b). The correlation between the transition energy associated with light absorption and the empirical parameter $E_T(30)$ (representing solvent polarity)[34] is displayed in Figure 2a for **3**, **8**, and **9**. It is reasonably linear except for a few deviating points originating from the solvent dependence of the largest vibronic band used to determine the absorption maximum. The observed slopes are negative (positive solvatochromism). In the absence of any evidence suggesting the formation of aggregates (except for **4** and **7** in cyclohexane), this result was interpreted as revealing an increase of molecular-dipole

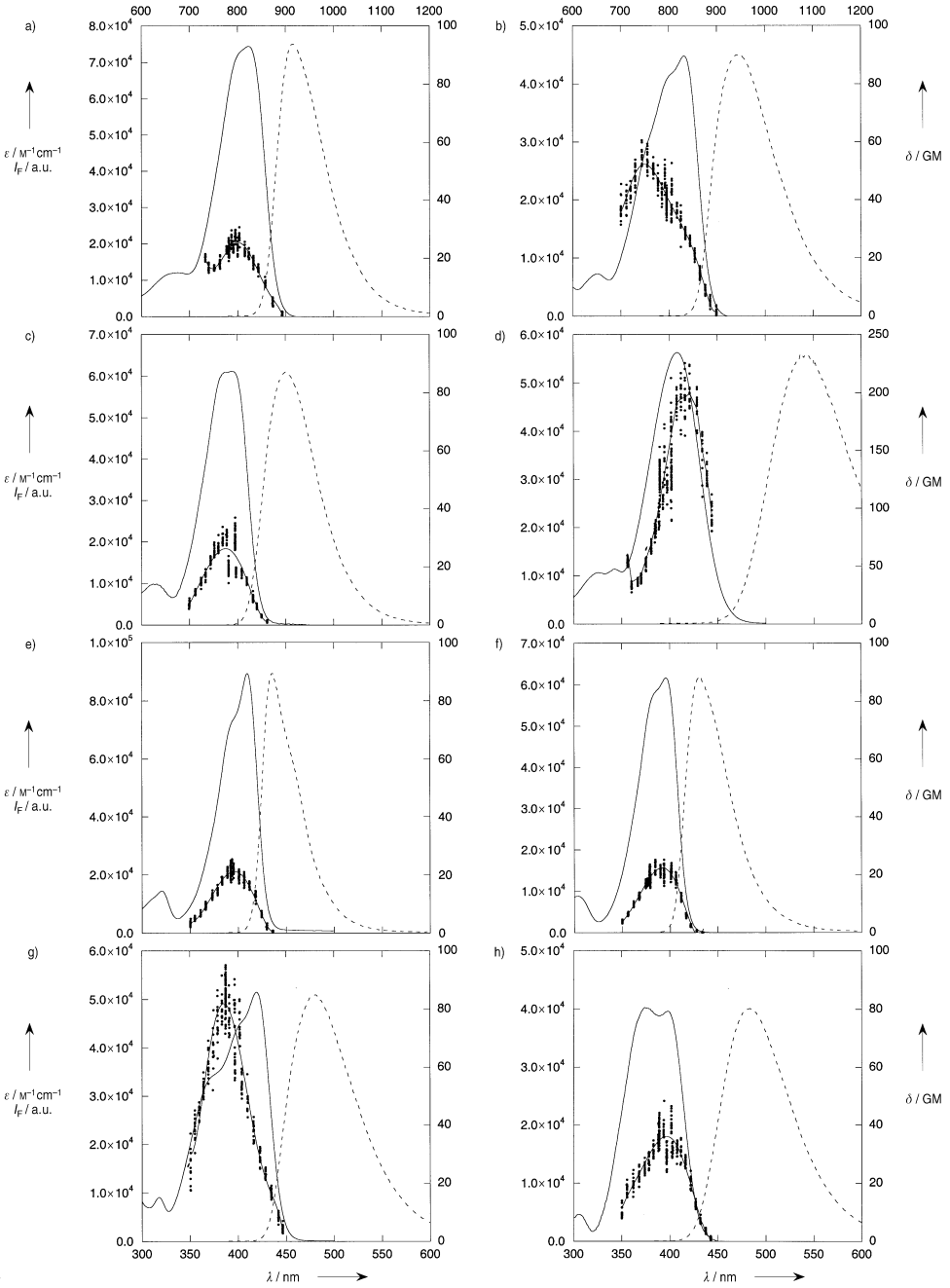

Figure 1. Single-photon absorption (molar absorption coefficient ε in $M^{-1}cm^{-1}$, solid line), steady-state fluorescence emission (fluorescence emission intensity I_F in arbitrary units, dotted line), and two-photon excitation spectra (clouds of points) of a)–h) **1–8**, respectively, in dichloromethane at 298 K. Spectra a)–h) all have the same scale unless stated otherwise.

Table 2. Solvatochromism of some $Ar^1Ar^2BF_2$ derivatives. UV/Vis single-photon absorption and emission features under different conditions. Maxima of absorption λ_{max} [nm], molar absorption coefficients $\varepsilon(\lambda_{max})\pm5\%$ [$\mu M^{-1}cm^{-1}$], steady-state fluorescence emission λ_{em} [nm], and fluorescence quantum yields $\phi_F\pm5$ [%]. Also see Table 1.

Ar^1Ar^2	Acetone, 42.2[a]	Acetonitrile, 45.6[a]	Cyclohexane, 30.9[a]	DMSO, 45.1[a]	Ethanol, 51.9[a]	OG micelles
3	385/51 000/451/50	385/60 000/468/65	375/52 000/408/15	406/60 000/469/1	378/45 000/454/40	–
4	–	–	394/–[b]/432/–[b]	420/56 000/610/15	–	–[c]/–[c]/566/40[d]
7	–	–	409/–[b]/420/–[b]	–	–	–[c]/–[c]/510/50[d]
8	397/41 000/501/50	370/38 000/523/50	395/39 000/407/35	373/38 000/502/30	406/41 000/530/1	
9	364/46 000/394/10	364/45 000/402/10	359/43 000/407/5	371/46 000/405/1	371/46 000/405/ < 1	

[a] $E_T(30)$ values from ref. [34]. [b] The Ar^1Ar^2 compounds were sometimes insoluble or only partially soluble in cyclohexane. In the latter case, only λ_{max} and λ_{em} are indicated. [c] The light scattering induced by the presence of the OG micelles prevented extraction of reliable data from the absorption spectrum. [d] The fluorescence quantum yields of **4** and **7** in OG micelles were crudely evaluated using Equation (1) under the assumption that the absorbances of the micellar solutions at the excitation wavelength were identical to the corresponding CH_2Cl_2 solutions at the same concentration.

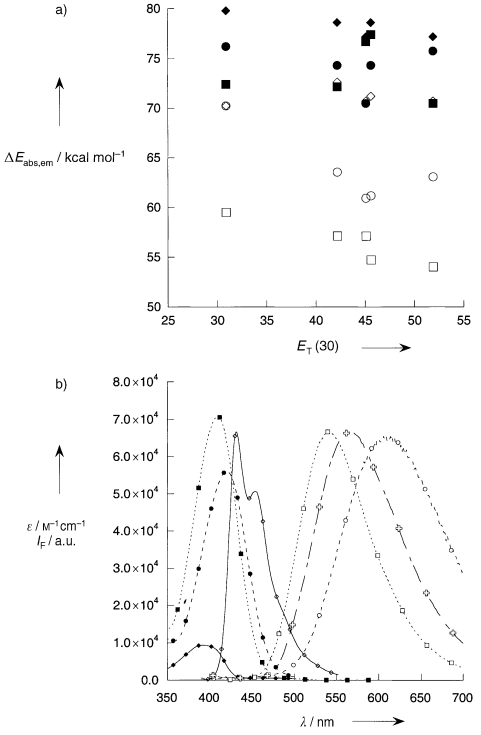

Figure 2. a) Dependence of the transition energies associated with the processes of absorption ($\Delta E_{abs}=hc/\lambda_{abs}$, filled markers) and emission ($\Delta E_{em}=hc/\lambda_{em}$, empty markers) on the empirical parameter $E_T(30)$ representing solvent polarity[34] for **3** (circles), **8** (squares), and **9** (diamonds); b) single-photon absorption (molar absorption coefficient ε in $M^{-1}cm^{-1}$, filled markers) and steady-state fluorescence emission (fluorescence emission intensity I_F in arbitrary units, empty markers) of **4** in cyclohexane (diamonds), dichloromethane (squares), DMSO (circles), and OG micelles (crosses) at 298 K.

moment upon light absorption. These observations are in accordance with the donor–acceptor structure of the $Ar^1Ar^2BF_2$ molecules. In fact, **9** possesses a ground dipole moment of 6.7 debye;[21] the BF_2 moiety has a withdrawal effect, whereas the aromatic rings act as donating groups.

Compounds **1**–**9** are strongly fluorescent in the 400–550 nm range in dichloromethane at 298 K (Figure 1 and Table 1). The fluorescence quantum yields are good-to-excellent for the most conjugated molecules ($0.35<\phi_F<0.85$).

As observed for one-photon absorption, fluorescence emission becomes redshifted when the solvent polarity is increased, consistent with an increase of dipole moment upon excitation (Table 2). In addition, a more pronounced solvatochromism is observed for the emission than for the absorption, as revealed by an increase of the Stokes shift with increasing polarity for the derivatives bearing the most donating groups (Table 2). The large Stokes shift values can be related to a major reorganization of the solvent shell during the excitation lifetime. Interestingly, **4** exhibits both the larger Stokes shift values (220 cm^{-1} in cyclohexane, 5900 cm^{-1} in dichloromethane, 7400 cm^{-1} in DMSO), as well as the most definite fluorescence solvatochromism (Figure 2b). This behavior can be attributed to a large nuclear reorganization after excitation prior to emission, in addition to a significant electronic redistribution occurring upon excitation. Within this framework, the more pronounced features of **4** can be tentatively interpreted as resulting from the larger donor character of the methoxybiphenyl moiety, leading to a larger excited-state dipole.[35]

The sensitivity of the fluorescence maxima to the solvent polarity makes such compounds attractive as polarity probes. From this point of view, the fluorescence characteristics of **4** suggest that α-D-octylglucopyranoside (OG) acts as a medium of intermediate polarity between dichloromethane and dimethylsulfoxide (Tables 1 and 2). In fact, although being structurally related to cyclohexane, the micellar core is strongly permeable to polar water molecules. In addition to the shift of the emission band, the solvent was found to exert a significant influence on the fluorescence quantum yield, hence supporting the view of $Ar^1Ar^2BF_2$ molecules as polarity reporters.

The fluorescence quantum yields were highest in dichloromethane and considerably decreased in polar media, such as DMSO (Tables 1 and 2). The fluorescence quantum yields in OG micelles are difficult to evaluate owing to light scattering precluding the evaluation of sample absorbances; nevertheless, the crude estimates derived suggest the corresponding quantum yields are intermediary between apolar and polar media. A possible explanation to account for such sensitivity to polarity relies on the presence of two excited

states whose energy would be solvent dependent: a non-fluorescent excited state arising from a $n\rightarrow\pi^*$ transition, and a fluorescent excited state arising from $\pi\rightarrow\pi^*$. Such an explanation was already proposed in closely related series, to discuss the relationships between molecular conformation and photophysical features.[36]

As a partial conclusion, the linear properties of the present $Ar^1Ar^2BF_2$ series satisfactorily compare with the corresponding existing fluorescent series such as stilbene, coumarin, or pyrene derivatives, which exhibit comparable photophysical features.

Two-photon absorption properties: In contrast to single-photon absorption, two-photon absorption is a nonlinear optical process causing a molecule to simultaneously absorb two photons to access an excited state. As a consequence, the two-photon absorption is related quadratically to light intensity. Provided that satisfactory chromophores will be available, the favorable features of two-photon absorption are anticipated to be useful for application in various fields, such as two-photon fluorescence microscopy,[3,37,38] two-photon-induced biological caging investigations,[39,40] and optical limiting.[41–46] Despite work already reported dealing with the same issue, there is still a need to accumulate experimental data to derive relevant structure–property relationships for optimizing two-photon absorption.[46–58]

Two-photon excitation spectra of **1**–**9** were recorded in dichloromethane at 298 K with a home-built set up relying on the design of Webb et al.[60] (see Figures 1S–3S in the Supporting Information and Experimental Section). Figure 1a–h displays the spectra (for **1**–**8**) together with the corresponding single-photon absorption and fluorescence emission spectra. The quadratic dependence of two-photon-excited fluorescence of the compounds listed in this paper was checked at several wavelengths (see Figure 3S in the Supporting Information for a typical example); it revealed satisfactory behavior over the 20–200 mW range. The position of the two-photon absorption maximum ($\lambda_{max}^{(2)}$) and the peak two-photon absorptivity maximum (δ_{max}) are summarized in Table 1. The observed values of $\lambda_{max}^{(2)}$ satisfactorily compare with twice the corresponding values of λ_{max}; this suggests that the same excited states are reached regardless of the excitation mode. Such an observation goes against the behavior of symmetrical molecules, such as fluorescein, but is in line with other reports making use of a comparable technique on unsymmetrical donor–acceptor compounds. For instance, coumarin 307 is reported to exhibit $\lambda_{max}^{(2)}=800$ nm in methanol[12] and $\lambda_{max}=395$ nm in ethanol.[61] In the present series, the δ_{max} range from 20 to 200 GM (1 GM = 10^{-50} cm^4 s (photon−molecule)$^{-1}$).

The effectiveness of electron-donating substituents on the aryl group to increase the two-photon fluorescence absorptivity (δ_{max}), is supported by the trend observed in both series of 1) dissymmetrically substituted molecules: **6** (25) versus **9** (<5) and **4** (200) versus **3** (30) and 2) symmetrically substituted molecules: **5** (20) versus **9** (<5). Thus, much lower TPA values are observed in the absence of donating substituents on the aryl moieties, suggesting that the dipolar contribution is a dominant effect, as observed in other push–pull systems.[47,54,55] We observe that the substituent effect is much more pronounced in the case of the elongated derivative **4**, leading to an increase of nearly one order of magnitude in the TPA response. This effect can be tentatively attributed to a synergetical effect between donating substituent and conjugated linker length, as observed for optical nonlinearities of push–pull derivatives.[62]

The nature and length of the aryl moieties also influences the TPA response. Increasing its donating strength or its size leads to an increase of the TPA response, as indicated by the comparison of 1) symmetrical molecules in the series **9** (<5), **1** (30), and **7** (85) and 2) dissymmetrical molecules in the series **9** (<5), **3** (30), and **8** (30), as well as in the series **6** (25) and **4** (200). It should be stressed that the length effect is much more pronounced in the case of a dissymmetrical compound with a donating substituent, leading again to an order of magnitude increase of the TPA cross section. We conclude from this observation that the distinctly larger TPA characteristics of **4**, among the nine related derivatives, could be related to the major electronic redistribution occurring upon excitation (vide supra), supporting the role of the dominant dipolar contribution. In contrast, the present investigation suggests that symmetrization of the structure does not bring any distinct advantage. In fact, δ_{max} values are identical for the couples (**1**,**3**) and (**5**,**6**).

Conclusion

We have prepared a series of novel fluorophores of definite interest for various applications in biological imaging (TPEF microscopy, microenvironment probes). Their absorption and emission properties have been investigated, demonstrating that these molecules can be used as sensitive fluorescent probes of micropolarity. These new fluorochromes combine large fluorescence quantum yields and enhanced chemical stability against hydrolysis in aqueous environment, as compared to the most popular BODIPY probes. Their TPA cross-section action has been determined using an original experimental protocol. Structure–property relationships have been derived providing evidence that their TPA cross sections can be significantly enhanced in elongated dissymmetrical derivatives bearing an electron-donating group. These combined features of the new series of fluorophores provide an interesting route towards optimized TPA fluorophores/probes for various applications.

Experimental Section

General procedures: Anhydrous solvents were freshly distilled before use. Column chromatography (CC): silica gel 60 (0.040–0.063 mm) Merck or silica gel SDS. Analytical: TLC: silica gel plates (Merck), detection by UV (254 nm); melting point: Büchi 510; ^{1}H NMR spectra: AM-250 Bruker, chemical shifts in ppm related to the protonated solvent as internal reference (^{1}H: $CHCl_3$ in $CDCl_3$, 7.27 ppm, CHD_2SOCD_3 in CD_3SOCD_3, 2.49 ppm; ^{13}C: $^{13}CDCl_3$ in $CDCl_3$, 76.9 ppm, $^{13}CD_3SOCD_3$ in CD_3SOCD_3, 39.6 ppm); coupling constants (J) in Hz; mass spectrometry (chemical ionization with NH_3) was performed at the Service de Spectro-

métrie de masse de l'ENS; microanalyses were obtained from the Service de Microanalyses de l'Université Pierre et Marie Curie, Paris. Acyl chlorides were prepared from the corresponding acids by reaction with thionyl chloride.[65] Compound **9** was synthesized according to the presently reported procedure starting from the commercially available β-diketone PhePhe.

Syntheses of the diketones Ar^1Ar^2 along pathway A

Ethyl 3-(biphenyl-4′-yl)-3-oxo propionate (1A-Bi): Butyllithium in hexane (1 M, 16 mL) was added dropwise to a cooled (−78 °C) solution of monoethyl malonate (1.32 g, 10 mmol; 2 equiv) in THF (40 mL) with a crystal of 2,2′-bipyridine as indicator.[22] The solution was allowed to warm to −5 °C and stirred for 15 min. After cooling (−70 °C), biphenyl-4-carbonyl chloride (1.08 g, 5 mmol) in THF (5 mL) was slowly added. The cooling bath was removed and the mixture was stirred for 1 h. The mixture was poured into diethyl ether (35 mL) and hydrochloric acid (15 mL, 1 M). The organic phase was separated and washed with saturated sodium hydrogencarbonate, then dried over magnesium sulfate. After filtration and evaporation, the crude product was purified by CC (cyclohexane/dichloromethane (C_6H_{12}/CH_2Cl_2), gradient 40:60 to 0:100) to yield 1A-Bi as a white powder (942 mg, 70 %). M.p. 76 °C; ^{1}H NMR (250 MHz, $CDCl_3$, 25 °C, TMS): $\delta = 1.27$ (t, $^3J(H,H) = 7.2$ Hz, 3H), 4.02 (s, 2H), 4.23 (q, $^3J(H,H) = 7.2$ Hz, 2H), 7.32–7.52 (m, 3H), 7.54–7.74 (m, 4H), 7.97–8.07 ppm (m, 2H); ^{13}C NMR (63 MHz, $CDCl_3$, 25 °C, TMS) (CE: enol-ester tautomer; CK: keto-ester tautomer): $\delta = 14.1$, 14.3, 46.0 (CK), 60.3, 61.5, 87.3 (CE), 126.5, 127.1, 127.2, 127.3, 127.4, 127.9, 128.4, 128.9, 129.0, 129.1, 132.3, 134.8, 139.6, 140.1, 144.0, 146.4, 167.5, 171.1, 173.2, 192.1 ppm; MS (CI, NH_3): *m/z* (%): 286 (24) [M^++18], 269 (100) [M^++1], 197 (40).

Ethyl naphthalene-2-carbonyl acetate (1A-Na):[66] Same procedure as for 1A-Bi, but with naphthalene-2-carbonyl chloride (952.5 mg, 5 mmol). Purified by CC (C_6H_{12}/CH_2Cl_2, 50:50 to 0:100). 1A-Na obtained as a white powder (930 mg, 76 %). ^{1}H NMR (250 MHz, $CDCl_3$, 25 °C, TMS) (HE: enol-ester tautomer; HK: keto-ester tautomer): $\delta = 1.27$ (t, $^3J(H,H) = 7.15$ Hz, 3HK), 1.36 (t, $^3J(H,H) = 7.15$ Hz, 3HE), 4.13 (s, 2HK), 4.24 (q, $^3J(H,H) = 7.15$ Hz, 2HK), 4.30 (q, $^3J(H,H) = 7.15$ Hz, 2HE), 5.82 (s, 1HE), 7.48–7.70 (m, 2HK+2HE), 7.74–8.07 (m, 4HK+4HE), 8.37 (brs, 1HE), 8.47 (brs, 1HK), 12.69 ppm (s, 1HE); ^{13}C NMR (63 MHz, $CDCl_3$, 25 °C, TMS) (CE: enol-ester tautomer; CK: keto-ester tautomer): $\delta = 14.2$, 14.4, 46.1 (CK), 60.4, 61.5, 87.9 (CE), 122.6, 123.9, 126.7 (2C), 126.8, 127.0, 127.6, 127.7, 127.9, 128.3, 128.7, 128.9, 129.1, 129.7, 130.6, 132.5, 132.7, 133.5, 134.7, 135.7, 167.7, 171.3, 173.3, 192.5 ppm.

Ethyl benzoylnaphthoyl acetate (2A-NaPhe): A solution of ethyl benzoyl acetate (960 mg, 5 mmol) dissolved in THF (2 mL) was added dropwise to a suspension of sodium hydride (220 mg, 5.5 mmol) in THF (3 mL), under an atmosphere of nitrogen at 0 °C.[23] The mixture was stirred until the hydrogen evolution ceased (10 min). Naphthalene carbonyl chloride (952 mg, 5 mmol) in THF (5 mL) was then added and the stirring continued at RT for 16 h. THF was evaporated and the mixture was hydrolyzed with sulfuric acid (2 M, 10 mL). The residue was extracted three times with CH_2Cl_2 and the organic phase was washed with water. After drying (magnesium sulfate), the solvent was evaporated and the crude residue was washed several times with cyclohexane/diethyl ether (50:50, 3 mL) to yield 2A-NaPhe as a white powder (986 mg, 58 %). M.p. 121 °C; ^{1}H NMR (250 MHz, $CDCl_3$, 25 °C, TMS): $\delta = 1.24$ (t, $^3J(H,H) = 7.1$ Hz, 3H), 4.31 (q, $^3J(H,H) = 7.1$ Hz, 2H), 6.36 (s, 1H), 7.4–7.52 (m, 2H), 7.52–7.68 (m, 3H), 7.82–8.04 (m, 6H), 8.44 ppm (brs, 1H); ^{13}C NMR (63 MHz, $CDCl_3$, 25 °C, TMS): $\delta = 14.0$, 62.5, 64.5, 123.9, 127.2, 127.9, 128.7, 129.0, 129.2, 129.8, 130.7, 132.5, 133.1, 134.1, 135.7, 136.0, 165.9, 190.7, 190.9 ppm; MS (DEI): *m/z* (%): 346 (3) [M^+], 300 (14), 155 (100), 127 (38), 105 (45), 77 (14); elemental analysis calcd (%) for $C_{22}H_{18}O_4$ (346): C 76.28, H 5.24; found: C 76.33, H 5.14.

Ethyl di(biphenyl-4-carbonyl) acetate (2A-BiBi): Same procedure as for 2A-NaPhe, but with ethyl biphenyl-4-carbonyl acetate (804 mg, 3 mmol), sodium hydride (132 mg, 3.3 mmol), biphenyl-4-carbonyl chloride (650 mg, 3 mmol). Compound 2A-BiBi was obtained as colorless crystals after recrystallization in ethanol (1.27 g, 94 %). M.p. 163 °C; ^{1}H NMR (250 MHz, $CDCl_3$, 25 °C, TMS): $\delta = 1.28$ (t, $^3J(H,H) = 7.1$ Hz, 3H), 4.33 (q, $^3J(H,H) = 7.1$ Hz, 2H), 6.24 (s, 1H), 7.37–7.53 (m, 6H), 7.58–7.67 (m, 4H), 7.67–7.74 (m, 4H), 7.98–8.07 ppm (m, 4H); ^{13}C NMR (63 MHz, $CDCl_3$, 25 °C, TMS): $\delta = 14.0$, 62.5, 64.6, 127.3, 127.6, 128.5, 129.0, 129.3, 134.3, 139.6, 146.8, 165.8, 190.5 ppm; MS (CI, NH_3): *m/z* (%): 466 (8) [M^++18], 449 (37) [M^++1], 377 (100), 269 (78), 198 (28); elemental analysis calcd (%) for $C_{30}H_{24}O_4$ (448): C 80.34, H 5.54; found: C 78.06, H 5.55.

Ethyl 3-(2-naphthyl)-3-oxo-2-(biphenyl-4-carbonyl) propionate (2A-BiNa): Same method as for 2A-NaPhe, but using ethyl naphthalene-2-carbonyl acetate (795 mg, 3.28 mmol), and biphenyl-4-carbonyl chloride (710 mg, 3.28 mmol). Compound 2A-BiNa was obtained as colorless crystals after recrystallization in ethanol (478 mg, 35 %). M.p. 154 °C; ^{1}H NMR (250 MHz, $CDCl_3$, 25 °C, TMS): $\delta = 1.27$ (t, $^3J(H,H) = 7.1$ Hz, 3H), 4.33 (q, $^3J(H,H) = 7.1$ Hz, 2H), 6.38 (s, 1H), 7.37–7.74 (m, 9H), 7.84–8.04 (m, 6H), 8.47 ppm (brs, 1H); ^{13}C NMR (63 MHz, $CDCl_3$, 25 °C, TMS): $\delta = 14.0$, 62.5, 64.6, 123.9, 127.1, 127.3, 127.6, 127.8, 128.5, 129.0, 129.1, 129.3, 129.8, 130.7, 132.4, 133.0, 134.3, 135.9, 139.5, 146.7, 165.8, 190.3, 190.6 ppm; MS (CI, NH_3): *m/z* (%): 440 (33) [M^++18], 424 (34) [M^++2], 423 (100) [M^++1]; elemental analysis calcd (%) for $C_{28}H_{22}O_4$ (422): C 79.60, H 5.25; found: C 79.59, H 5.23.

Ethyl 3-(4′-methoxybiphenylyl)-3-oxo-2-benzoyl propionate (2A-MeOBiPhe): Same method as for 2A-NaPhe, but with ethyl benzoyl acetate (960 mg, 5 mmol), 4′-methoxybiphenylcarbonyl chloride (1.23 g, 5 mmol) to yield 2A-MeOBiPhe as white crystals after washing several times with C_6H_{12}/Et_2O (50:50) and after recrystallization in ethanol (1.105 g, 54 %). M.p. 135 °C; ^{1}H NMR (250 MHz, $CDCl_3$, 25 °C, TMS): $\delta = 1.26$ (t, $^3J(H,H) = 7.1$ Hz, 3H), 3.87 (s, 3H), 4.25 (q, $^3J(H,H) = 7,1$ Hz, 2H), 6.22 (s, 1H), 6.98–7.03 (m, 2H), 7.43–7.70 (m, 7H), 7.90–8.02 ppm (m, 4H); ^{13}C NMR (63 MHz, $CDCl_3$, 25 °C, TMS): $\delta = 14.0$, 55.4, 62.4, 64.4, 114.5, 126.9, 128.4, 128.6, 130.0, 129.3, 131.8, 133.6, 134.0, 135.6, 146.3, 160.1, 165.8, 190.1, 190.7 ppm; MS (CI, NH_3): *m/z* (%): 420 (25) [M^++18], 403 (71) [M^++1], 331 (100), 299 (41); elemental analysis calcd (%) for $C_{25}H_{22}O_5$ (402): C 74.61, H 5.51; found: C 74.08, H 5.54.

Ethyl benzoyl-4-methoxybenzoyl acetate (2A-MeOPhePhe): Same method as for 2A-NaPhe, but with ethyl benzoyl acetate (960 mg, 5 mmol) and 4-methoxybenzoyl chloride (853 mg, 5 mmol). Compound 2A-MeOPhePhe was obtained as white crystals after recrystallization in ethanol (1.25 g, 76 %). M.p. 104 °C; ^{1}H NMR (250 MHz, $CDCl_3$, 25 °C, TMS): $\delta = 1.25$ (t, $^3J(H,H) = 7.1$ Hz, 3H), 3.87 (s, 3H), 4.29 (q, $^3J(H,H) = 7.1$ Hz, 2H), 6.14 (s, 1H), 6.88–6.99 (m, 2H), 7.43–7.53 (m, 2H), 7.56–7.65 (m, 1H), 7.87–7.96 ppm (m, 4H); ^{13}C NMR (63 MHz, $CDCl_3$, 25 °C, TMS): $\delta = 14.0$, 55.6, 62.4, 64.4, 114.2, 128.8, 128.9, 131.1, 133.9, 135.7, 164.2, 165.9, 189.0, 190.7 ppm; MS (CI, NH_3): *m/z* (%): 344 (42) [M^++18], 327 (100) [M^++1], 279 (51); elemental analysis calcd (%) for $C_{19}H_{18}O_5$ (326): C 69.92, H 5.56; found: C 69.78, H 5.57.

Ethyl di(naphthalene-2-carbonyl) acetate (2A-NaNa): Same method as for 2A-NaPhe, but with ethyl naphthalene-2-carbonyl acetate (930 mg, 3.84 mmol) and naphthalene-2-carbonyl chloride (731.5 mg, 3.84 mmol). Compound 2A-NaNa was obtained as a white powder after washing several times with C_6H_{12}/Et_2O 50:50 (1.02 g, 67 %). M.p. 150 °C; ^{1}H NMR (250 MHz, $CDCl_3$, 25 °C, TMS): $\delta = 1.26$ (t, $^3J(H,H) = 7.12$ Hz, 3H), 4.33 (q, $^3J(H,H) = 7.12$ Hz, 2H), 6.50 (s, 1H), 7.49–7.69 (m, 4H), 7.81–8.07 (m, 8H), 8.48 ppm (brs, 2H); ^{13}C NMR (63 MHz, $CDCl_3$, 25 °C, TMS): $\delta = 14.0$, 62.5, 64.7, 123.9, 127.1, 127.8, 129.0, 129.1, 129.8, 130.7, 132.5, 133.1, 135.9, 165.9, 190.6 ppm; MS (CI, NH_3): *m/z* (%): 414 (3) [M^++18], 397 (11) [M^++1], 260 (60), 243 (100); elemental analysis calcd (%) for $C_{26}H_{20}O_4$ (396): C 78.77, H 5.085; found: C 78.74; H 5.19.

1-(2-Naphthyl)-3-phenylpropane-1,3-dione (NaPhe): A solution of ethyl benzoylnaphthoyl acetate (692 mg, 2 mmol), water (72 mg, 4 mmol; 2 equiv) and sodium chloride (120 mg, 2.2 mmol; 1.1 equiv) in DMSO (2 mL) was heated at 140 °C until the release of carbon dioxide ceased.[24] After cooling to room temperature, water was added and the mixture was extracted with ethyl acetate and cyclohexane (1:1). The organic phase was washed three times with water, then dried over magnesium sulfate. After filtration and evaporation of the solvent, NaPhe was obtained as a white solid after recrystallization in ethanol (510 mg, 93 %). M.p. 98 °C (ref. [67] 99 °C); ^{1}H NMR (250 MHz, $CDCl_3$, 25 °C, TMS): $\delta = 4.77$ (s, 2H), 7.45–7.65 (m, 5H), 7.87–8.11 (m, 6H), 8.55 ppm (brs, 1H); ^{13}C NMR (63 MHz, $CDCl_3$, 25 °C, TMS): $\delta = 93.5$, 123.2, 126.8, 127.2, 127.8, 128.1, 128.3, 128.5, 128.7, 129.4, 132.5, 132.75, 132.8, 135.3, 135.6, 185.5, 185.8 ppm.

1,3-Di(biphenyl-4-yl)propane-1,3-dione (BiBi): Same method as for NaPhe, but with ethyl di(biphenyl-4-carbonyl) acetate (248 mg,

0.55 mmol). Compound BiBi was obtained as pale yellow plates (172 mg, 83%). M.p. 220°C (ref. [68] 218–220°C); ^{1}H NMR (250 MHz, $CDCl_3$, 25°C, TMS):δ=6.95 (s, 1H), 7.37–7.54 (m, 6H), 7.57–7.82 (m, 8H), 8.04–8.13 (m, 4H), 14.58–14.76 ppm (m, 1H); ^{13}C NMR (63 MHz, $CDCl_3$, 25°C, TMS): δ=93.2, 127.3, 127.4, 127.8, 128.2, 129.0, 134.4, 140.0, 145.3, 185.3 ppm.

1-(Biphenyl-4′-yl)-3-(2-naphthyl)propane-1,3-dione (BiNa): Same method as for NaPhe, but with ethyl 3-(2-naphthyl)-3-oxo-2-(biphenyl-4-carbonyl) propionate (336 mg, 0.8 mmol). Compound BiNa was obtained as colorless crystals after recrystallization in ethanol (140 mg, 50%). ^{1}H NMR (250 MHz, $CDCl_3$, 25°C, TMS): δ=7.06 (s, 1H), 7.37–7.72 (m, 7H), 7.75 (d, ^3J(H,H)=8.4 Hz, 2H), 7.86–8.10 (m, 4H), 8.13 (d, ^3J(H,H)=8.4 Hz, 2H), 8.57 (brs, 1H), 14.60 ppm (brs, 1H); ^{13}C NMR (63 MHz, $CDCl_3$, 25°C, TMS): δ=64.7, 123.9, 127.1, 127.3, 127.6, 127.9, 128.5, 129.0, 129.1, 129.3, 129.8, 130.7, 132.5, 133.1, 134.4, 136.0, 139.6, 146.7, 165.8, 190.3, 190.6 ppm.

(4′-Methoxybiphenylyl)-3-phenylpropane-1,3-dione (MeOBiPhe): Same method as for NaPhe, but with ethyl benzoyl-4-methoxybenzoyl acetate (1.08 g, 2.7 mmol). Compound MeOBiPhe was obtained as pale yellow crystals after recrystallization in ethanol (515 mg, 57%). M.p. 176°C; ^{1}H NMR (250 MHz, $CDCl_3$, 25°C, TMS): δ=3.87 (s, 3H), 6.90 (s, 1H), 6.98–7.06 (m, 2H), 7.44–7.66 (m, 5H), 7.65–7.72 (m, 2H), 7.97–8.09 ppm (m, 4H); ^{13}C NMR (63 MHz, $CDCl_3$, 25°C, TMS): δ=55.4, 93.0, 114.4, 126.7, 127.2, 127.8, 128.3, 128.7, 132.3, 132.4, 133.6, 135.7, 144.8, 159.9, 185.4, 185.5 ppm; MS (CI, NH_3): *m/z* (%): 348 (2) [M^++18], 331 (100) [M^++1]; elemental analysis calcd (%) for $C_{22}H_{18}O_3$ (330): C 79.98, H 5.49; found: C 79.82, H 5.69.

1-(4-Methoxyphenyl)-3-phenylpropane-1,3-dione (MeOPhePhe): Same method as for NaPhe, but with ethyl benzoyl 4-methoxybenzoyl acetate (654 mg, 2 mmol). Compound MeOPhePhe was obtained as colorless crystals after recrystallization in ethanol (393 mg, 77%). M.p. 137°C; ^{1}H NMR (250 MHz, $CDCl_3$, 25°C, TMS): δ=3.89 (s, 3H), 6.80 (s, 1H), 6.95–7.04 (m, 2H), 7.43–7.60 (m, 3H), 7.94–8.06 ppm (m, 4H); ^{13}C NMR (63 MHz, $CDCl_3$, 25°C, TMS): δ=55.5, 92.4, 114.0, 127.0, 128.2, 128.6, 129.3, 132.1, 135.6, 163.3, 184.0, 186.2 ppm; MS (CI, NH_3): *m/z* (%): 272 (21) [M^++18], 256 (37) [M^++2], 255 (100) [M^++1]; elemental analysis calcd (%) for $C_{16}H_{14}O_3$ (254): C 75.57, H 5.55; found: C 75.56, H 5.65.

1,3-Di(2-naphthyl)propane-1,3-dione (NaNa): Same method as for NaPhe, but with ethyl di(naphthalene-2-carbonyl) acetate (792 mg, 2 mmol). Compound NaNa was obtained as colorless crystals after recrystallization in ethanol (501 mg, 77%). M.p. 171°C (ref. [69] 172°C); ^{1}H NMR (250 MHz, $CDCl_3$, 25°C, TMS): δ=7.16 (s, 1H), 7.51–7.68 (m, 4H), 7.84–8.20 (m, 8H), 8.60 (brs, 2H), 14.58 ppm (brs, 1H); ^{13}C NMR (63 MHz, $CDCl_3$, 25°C, TMS): δ=93.6, 123.3, 126.6, 127.6, 128.2, 128.4, 128.5, 129.4, 132.8, 132.9, 135.4, 185.6 ppm.

Syntheses of the diketones Ar^1Ar^2 along pathway B

1-Biphenyl-4′-yl-3-phenylprop-2-enone (1 B-BiPhe):[25] Sodium hydroxide (5M, 4 mL) was slowly added to a heated (50°C) solution of benzaldehyde (1.06 g, 10 mmol) and 4-acetylbiphenyl (1.96 g, 10 mmol) in ethanol (50 mL) and THF (10 mL). The mixture was stirred for 20 h at room temperature. After evaporation of the solvents, the residue was extracted with CH_2Cl_2. The organic phase was washed several times with water and was dried (magnesium sulfate). After filtration and evaporation of the solvent, 1 B-BiPhe was obtained as a white solid (2.67 g, 94%) that was used without further purification for the following step. ^{1}H NMR (250 MHz, $CDCl_3$, 25°C, TMS): δ=7.35–7.53 (m, 6H), 7.60 (d, ^3J(H,H)=15.7 Hz, 1H), 7.58–7.78 (m, 6H), 7.86 (d, ^3J(H,H)=15.7 Hz, 1H), 8.06–8.17 ppm (m, 2H).

1-(Biphenyl-4-yl)-2,3-dibromo-3-phenylpropanone (2 B-BiPhe): An excess of bromine (0.75 mL, 20 mmol) in CH_2Cl_2 (7.5 mL) was slowly added at RT to a solution of 1 B-BiPhe (2.67 g, 9.4 mmol) in CH_2Cl_2 (30 mL).[26] The mixture was stirred for 80 min. After evaporation of the solvent, 2 B-BiPhe was obtained as a white solid (4.17 g) that was used without further purification for the following step. ^{1}H NMR (250 MHz, $CDCl_3$, 25°C, TMS): δ=5.67 (d, ^3J(H,H)=11.3 Hz, 1H), 5.88 (d, ^3J(H,H)=11.3 Hz, 1H), 7.34–7.64 (m, 8H), 7.60–7.70 (m, 2H), 7.72–7.82 (m, 2H), 8.12–8.23 ppm (m, 2H).

1-(Biphenyl-4-yl)-3-phenylpropane-1,3-dione (BiPhe): Sodium methylate (460 mg, 18.8 mmol; 2 equiv) in methanol (6 mL) was added to a suspension of 2 B-BiPhe (4.17 g, 9.4 mmol) in methanol (30 mL).[27] After being under reflux for 2 h, concentrated hydrochloric acid (0.5 mL) was added to the mixture. Reflux was continued for 5 min and water (5 mL) was added. After evaporation of the solvent, the crude residue was purified by CC (C_6H_{12}/CH_2Cl_2 75:25 to 30:70) to yield BiPhe as a white solid (620 mg, 21%). M.p. 111°C (ref. [69] 112°C); ^{1}H NMR (250 MHz, $CDCl_3$, 25°C, TMS): δ=6.91 (s, 1H), 7.37–7.63 (m, 8H), 7.60–7.70 (m, 2H), 7.68–7.78 (m, 4H), 7.93–8.12 (m, 4H), 14.73 ppm (brs, 1H); ^{13}C NMR (63 MHz, $CDCl_3$, 25°C, TMS): δ=93.1, 127.0, 127.15, 127.2, 127.25, 127.3, 127.7, 128.1, 128.2, 128.7, 128.9, 128.95, 130.1, 132.4, 134.3, 135.6, 139.9, 145.2, 145.6, 185.3, 185.7 ppm.

Syntheses of the diketones Ar^1Ar^2 along pathway C

1,3-Di(4-methoxyphenyl)propane-1,3-dione (MeOPheMeOPhe):[28] A suspension of 4-methoxybenzoyl chloride (1.67 g, 9.8 mmol) and aluminium chloride (1.4 g, 10.25 mmol) in tetrachloroethane (5 mL) was stirred at 55°C for 2 h. Then, ethenyl acetate (430 mg, 5 mmol) was added and the mixture was further stirred at 55°C for 20 h. After cooling to room temperature, hydrochloric acid (2M, 2 mL) and water (20 mL) were successively added. After extraction with ethyl acetate, the organic phase was washed with sodium hydrogencarbonate and water. After drying (magnesium sulfate) and filtration, the organic solvent was evaporated to yield MeOPheMeOPhe as pale yellow crystals after recrystallization in ethanol (357 mg, 25%). M.p. 114°C (ref. [28] 116–117°C); ^{1}H NMR (250 MHz, $CDCl_3$, 25°C, TMS): δ=3.89 (s, 6H), 6.74 (s, 1H), 6.93–7.02 (m, 4H), 7.92–8.01 ppm (m, 4H); ^{13}C NMR (63 MHz, $CDCl_3$, 25°C, TMS): δ=55.5, 91.5, 114.0, 128.2, 129.1, 131.4, 163.0, 184.6 ppm.

Syntheses of the $Ar^1Ar^2BF_2$ compounds

Compound 1: A solution of BiBi (276 mg, 0.73 mmol) and BF_3/Et_2O (0.14 mL, 1.1 mmol) in benzene (2 mL) was heated to reflux for 1 h.[21] After evaporation of the solvent, **1** was obtained as yellow crystals after recrystallization in benzene (230 mg, 74%). M.p. >290°C; ^{1}H NMR (250 MHz, $CDCl_3$, 25°C, TMS): δ=7.28 (s, 1H), 7.40–7.57 (m, 6H), 7.66–7.72 (m, 4H), 7.76–7.84 (m, 4H), 8.21–8.31 ppm (m, 4H); ^{13}C NMR (63 MHz, $CDCl_3$, 25°C, TMS): δ=93.3, 127.4, 127.8, 128.9, 129.1, 129.6, 130.8, 139.2, 148.1, 182.4 ppm; ^{19}F NMR (235 MHz, $CDCl_3$, 25°C, $CFCl_3$): δ=−140.24 (75%), −140.17 ppm (25%); MS (CI, NH_3): *m/z* (%): 442 (100) [M^++18], 405 (18), 361 (5); elemental analysis calcd (%) for $C_{27}H_{19}BF_2O_2$ (424): C 76.44, H 4.51; found: C 76.45, H 4.51.

Compound 2: Same procedure as for **1**, but with BiNa (140 mg, 0.4 mmol) and BF_3/Et_2O (0.05 mL, 1.1 mmol). **2** was obtained as yellow crystals after recrystallization in benzene (113 mg, 71%). M.p. 258°C; ^{1}H NMR (250 MHz, $CDCl_3$, 25°C, TMS): δ=7.39 (s, 1H), 7.43–7.57 (m, 3H), 7.57–7.64 (m, 4H), 7.82 (d, ^3J(H,H)=8.5 Hz, 2H), 7.91–7.92 (m, 1H), 7.92–8.04 (m, 1H), 8.03–8.09 (m, 1H), 8.10–8.17 (m, 1H), 8.30 (d, ^3J(H,H)=8.5 Hz, 2H), 8.81 ppm (brs, 1H); ^{13}C NMR (100 MHz, $CDCl_3$, 25°C, TMS): δ=93.6, 123.5, 127.3, 127.4, 127.7, 127.9, 128.9, 129.1, 129.1, 129.6, 129.8, 130.0, 130.65, 131.6, 132.5, 136.5, 139.5, 148.0, 182.4, 182.6 ppm; ^{19}F NMR (235 MHz, $CDCl_3$, 25°C, $CFCl_3$): δ=−140.185 (75%), −140.12 ppm (25%); MS (CI, NH_3): *m/z* (%): 416 (100) [M^++18], 379 (23), 351 (1), 335 (1); elemental analysis calcd (%) for $C_{25}H_{17}BF_2O_2$ (398): C 75.40, H 4.30; found: C 75.20, H 4.31.

Compound 3: Same method as for **1**, but with BiPhe (620 mg, 2.1 mmol) and BF_3/Et_2O (0.27 mL, 2.1 mmol) in CH_2Cl_2 (20 mL). **3** was obtained as orange crystals after recrystallization in benzene (556 mg, 76%). M.p. 228°C; ^{1}H NMR (250 MHz, $CDCl_3$, 25°C, TMS): δ=7.25 (s, 1H), 7.40–7.63 (m, 5H), 7.63–7.77 (m, 3H), 7.77–7.83 (m, 2H), 8.13–8.21 (m, 2H), 8.21–8.28 ppm (m, 2H); ^{13}C NMR (63 MHz, $CDCl_3$, 25°C, TMS): δ=93.3, 127.3, 127.7, 128.9, 129.1, 129.2, 129.6, 130.5, 132.0, 135.2, 139.1, 148.1, 182.7, 182.9 ppm; ^{19}F NMR (235 MHz, $CDCl_3$, 25°C, $CFCl_3$): δ=−140.20 (75%), −140.14 ppm (25%); MS (CI, NH_3): *m/z* (%): 366 (100) [M^++18], 329 (8), 300 (8), 285 (7); elemental analysis calcd (%) for $C_{21}H_{15}BF_2O_2$ (348): C 72.45, H 4.34; found: C 72.36, H 4.40.

Compound 4: Same method as for **1**, but with MeOBiPhe (330 mg, 1 mmol) and BF_3/Et_2O (0.14 mL, 1.1 mmol). **4** was obtained as a yellow powder after recrystallization in benzene (160 mg, 42%). M.p. 245°C; ^{1}H NMR (250 MHz, [D_6]DMSO, 25°C, TMS): δ=3.81 (s, 3H), 7.01–7.12 (m, 2H), 7.59–7.72 (m, 2H), 7.77–7.88 (m, 3H), 7.90–8.01 (m,2H), 7.97 (s, 1H), 8.33–8.49 ppm (m, 4H); ^{13}C NMR (63 MHz, [D_6]DMSO, 25°C, TMS): δ=55.7, 94.7, 115.0, 127.0, 129.0, 129.6, 129.8, 130.6, 130.7, 131.8, 136.1, 147.2, 160.6, 182.2, 182.4 ppm; ^{19}F NMR (235 MHz, $CDCl_3$ ($CFCl_3$), 25°C, $CFCl_3$): δ=−140.25 (67%), −140.19 ppm (33%); MS (CI,

NH_3): *m*/*z* (%): 396 (100) [M^++18], 359 (9), 331 (8); elemental analysis calcd (%) for $C_{22}H_{17}BF_2O_3$ (378): C 68.87, H 4.53; found: C 69.73, H 4.70.

Compound ***5***: Same method as for **1**, but with MeOPheMeOPhe (284 mg, 1 mmol) and BF_3/Et_2O (0.14 mL, 1.1 mmol). **5** was obtained as yellow crystals after recrystallization in benzene (283 mg, 85%). M.p. 236°C; ^{1}H NMR (250 MHz, $CDCl_3$, 25°C, TMS): $\delta = 3.93$ (s, 6H), 6.97–7.06 (m, 4H), 7.02 (s, 1H), 8.10–8.19 ppm (m, 4H); ^{13}C NMR (63 MHz, $CDCl_3$, 25°C, TMS): $\delta = 55.8$, 91.5, 114.6, 124.6, 131.3, 165.3, 180.9 ppm; ^{19}F NMR (235 MHz, $CDCl_3$, 25°C, $CFCl_3$): $\delta = -141.53$ (75%), −141.47 ppm (25%); MS (CI, NH_3): *m*/*z* (%): 350 (92) [M^++18], 313 (100), 269 (1); elemental analysis calcd (%) for $C_{17}H_{15}BF_2O_4$ (332): C 61.48, H 4.55; found: C 61.62, H 4.63.

Compound ***6***: Same method as for **1**, but with MeOPhePhe (254 mg, 1 mmol) and BF_3/Et_2O (0.14 mL, 1.1 mmol). **6** was obtained as yellow crystals after recrystallization in benzene (125 mg, 41%). M.p. 216°C; ^{1}H NMR (250 MHz, $CDCl_3$, 25°C, TMS): $\delta = 3.94$ (s, 3H), 7.00–7.09 (m, 2H), 7.11 (s, 1H), 7.51–7,61 (m, 2H), 7.65–7.73 (m, 1H), 8.09–8.21 ppm (m, 4H); ^{13}C NMR (63 MHz, $CDCl_3$, 25°C, TMS): $\delta = 55.8$, 92.5, 114.7, 124.2, 128.6, 129.1, 131.7, 132.4, 134.7, 165.8, 181.6, 182.4 ppm; ^{19}F NMR (235 MHz, $CDCl_3$, 25°C, $CFCl_3$): $\delta = -140.84$ (75%), −140.78 ppm (25%); MS (CI, NH_3): *m*/*z* (%): 320 (58) [M^++18], 283 (18), 166 (100); elemental analysis calcd (%) for $C_{16}H_{13}BF_2O_3$ (302): C 63.62, H 4.34; found: C 63.71, H 4.31.

Compound **7**: Same method as for **1**, but with NaNa (324 mg, 1 mmol) and BF_3/Et_2O (0.14 mL, 1.1 mmol). **7** was obtained as a yellow powder after recrystallization in benzene (264 mg, 71%). M.p. >276°C; ^{1}H NMR (250 MHz, [D_6]DMSO, 25°C, TMS): $\delta = 7.73$–7.97 (m, 4H), 8.18–8.26 (m, 2H), 8.27–8.43 (m, 4H), 8.37 (s, 1H), 8.49–8.58 (m, 2H), 9.30 ppm (brs, 2H); ^{13}C NMR (63 MHz, [D_6]DMSO, 25°C, TMS): $\delta =$ 95.2, 123.9, 127.6, 127.9, 128.7, 129.1, 130.1, 130.2, 132.1, 132.2, 136.2, 182.1 ppm; ^{19}F NMR (235 MHz, $CDCl_3$ ($CFCl_3$), 25°C, $CFCl_3$): $\delta =$ −143.32 (75%), −143.30 ppm (25%); MS (CI, NH_3): *m*/*z* (%): 390 (100) [M^++18], 353 (9), 309 (9); elemental analysis calcd (%) for $C_{23}H_{15}BF_2O_2$ (372): C 74.22, H 4.06; found: C 74.26, H 4.01.

Compound ***8***: Same method as for **1**, but with NaPhe (274 mg, 1 mmol) and BF_3/Et_2O (0.14 mL, 1.1 mmol). **8** was obtained as a yellow powder (261 mg, 81%). M.p. 229°C; ^{1}H NMR (250 MHz, $CDCl_3$, 25°C, TMS): $\delta = 7.34$ (s, 1H), 7.48–7.75 (m, 5H), 7.85–8.14 (m, 4H), 8.14–8.22 (m, 2H), 8.76 ppm (brs, 1H); ^{13}C NMR (63 MHz, $CDCl_3$, 25°C, TMS): $\delta =$ 93.7, 123.4, 127.5, 127.9, 128.9, 129.1, 129.2, 129.8, 130.0, 131.6, 132.0, 132.5, 135.2, 136.5, 182.9 ppm; ^{19}F NMR (235 MHz, $CDCl_3$, 25°C, $CFCl_3$): $\delta = -140.03$ (75%), −139.98 ppm (25%); MS (CI, NH_3): *m*/*z* (%): 340 (100) [M^++18], 303 (12), 275 (45), 259 (63); elemental analysis calcd (%) for $C_{19}H_{13}BF_2O_2$ (322): C 70.85, H 4.07; found: C 70.72, H 4.10.

UV/Vis spectroscopic measurements: All experiments were performed at 293 K in spectroscopic grade solvents. UV/Vis absorption spectra were recorded on a Kontron Uvikon-930 spectrophotometer. Molar absorption coefficients were extracted, while checking the validity of the Beer–Lambert law. Corrected fluorescence spectra were obtained from a Photon Technology International LPS 220 spectrofluorimeter. The concentrations of solutions for fluorescence measurements were adjusted so that the absorption was below 0.15 at the excitation wavelength. The overall fluorescence quantum yields ϕ_F were calculated from the relation shown in Equation (1):

$$\phi_F = \phi_{ref} \frac{A_{ref}(\lambda_{exc})}{A(\lambda_{exc})} \frac{D}{D_{ref}} \left(\frac{n}{n_{ref}}\right)^2 \quad (1)$$

in which the subscript *ref* stands for standard samples, $A(\lambda_{exc})$ is the absorbance at the excitation wavelength, *D* is the integrated emission spectrum, and *n* is the refractive index for the solvent. The uncertainty in the experimental value of ϕ_F was estimated to be ±10%. The standard fluorophore for the quantum yield measurements was quinine sulfate in 0.1 M H_2SO_4 with $\phi_S = 0.50$.[70]

Samples for solvatochromism and stability studies were prepared in the following manner: Fixed volumes of a stock solution of dye in dichloromethane were transferred into pyrex hemolysis tubes. The volatile solvent was evaporated under a fume hood for one whole night or under vacuum for one hour. For solvatochromism investigations, the appropriate amount of desired spectroscopic grade solvent (Aldrich, except for the CH_2Cl_2 which was freshly home-distilled over calcium hydride) was added to each tube and the mixture was sonicated. For experiments involving micelles, β-octylglucopyranoside was added to stock solutions of dye before evaporation of dichloromethane. Transparent micellar solutions were obtained after addition of ultra-pure water and brief sonication (final concentration in detergent 25 mM).

Measurements of the cross sections for two-photon absorption

Method: In the absence of photobleaching, the photon flux $F(t)$ emitted under two-photon excitation is proportional to the fluorophore concentration *c* (assumed to be homogeneous and stationary) and to the square of the incoming power $I(\vec{r},t)$ [Eq. (2)]:

$$F(t) = \frac{1}{2}\alpha\phi_F\delta c \int_v I^2(\vec{r},t)\,dV \quad (2)$$

in which ϕ_F is the fluorescence quantum yield (assumed to remain identical to the value determined by the study of the linear photophysical properties), δ is the two-photon absorption cross section to be measured (in $cm^4 s(photon-molecule)^{-1}$) and α is the set-up detection efficiency. During an acquisition, the amount of fluorescence detected is shown by using Equation (3):

$$\langle F(t)\rangle = \frac{1}{2}\alpha\phi_F\delta c\langle P^2(t)\rangle \int_v S(\vec{r})\,dV \quad (3)$$

in which $S(\vec{r})$ is the temporal distribution of the incident light and $P(t)$ is the instantaneous photon flux for the sample ($photon\,s^{-1}$).

The signal detected is proportional to $\langle P^2(t)\rangle$, whereas most detectors are sensitive to $\langle P(t)\rangle^2$. An accurate measurement of δ thus requires the determination of the temporal structure of the excitation beam and its second-order temporal coherence: $g^{(2)} = \langle P^2(t)\rangle/\langle P(t)\rangle^2$. This is usually achieved by calibration at each wavelength by using a known standard, such as fluorescein or rhodamine, which causes heavy and repetitive manipulations. An alternative elegant method has been described by Xu et al.[60] By adding a Michelson interferometer to the laser path, the usual set up is transformed into an autocorrelator, using the fluorescent sample as the quadratic medium (Figure 1Sa and 1Sb in the Supporting Information). The major interest of this set-up configuration is evidently to get rid of the otherwise necessary determination of the pulse temporal shape, for this information is now intrinsically contained in the interference pattern. The only unknown quantity remaining is the α factor that may be determined by calibration at one single wavelength. In the interference conditions it was then shown that [Eq. (4)]:

$$\delta = \frac{\left(\int_{-T}^{T} F(t)\,dt\right) - 2\,TF_\infty}{2\alpha cA\phi_F\left[\int_{-\infty}^{+\infty} P(t)\,dt\right]^2} \quad (4)$$

in which T is the integration time ($2T$ larger than the interference pattern width). $A = \int_v S^2(\vec{r})\,dV \approx 2.55/\lambda$ when overfilling the back-aperture of the focusing lens (in the case of a plane wave truncated by an aperture, giving an Airy diffraction pattern). F_∞ is the mean fluorescence signal without any interference; it is then simply twice the fluorescence generated by one pulse from one of the Michelson paths. It was also shown that the ratio between the fluorescence maximum and F_∞ must be 8:1, which is also a probe for the quadratic dependence on the excitation power.

Set up and data treatment: The experiments were performed at room temperature in spectroscopic grade dichloromethane at 10^{-4} M. Freshly prepared solutions were sealed in square capillary tubes (1 mm × 1 mm; VitroCom, USA), kept at +5°C, and away from light afterwards.

The scheme of the home-made experimental set up was inspired from ref. [60] (Figure 1Sa and 1Sb in the Supporting Information). The excitation source was a pulsed Ti–sapphire laser (MIRA - Coherent, USA) pumped at 532 nm by a Nd-YVO_4 laser (VERDI - Coherent, USA). This femtosecond laser delivered pulses in the near-infrared region from 690 to 1000 nm.

The Michelson interferometer consisted of a beamsplitter (BS) and two corner-cubes (Figure 1Sb). One corner-cube (CC_1) was fixed on the diaphragm of a loudspeaker powered by a low-frequency generator. A continuous He-Ne laser was also included in the interferometer to calibrate the diaphragm displacement. The resulting interference pattern was recorded at the end of the Michelson interferometer on a photodiode (PD_1). Typical pulse widths at the sample were less than 200 fs.

After a beam-expander 6× (BE, Melles Griot), the IR laser beam overfilled the back aperture of the lens (Nikon, 20×, N.A. 0.35), which collimates it onto the sample. A lens focused most of the excitation beam on a second photodiode (PD_2; the fraction collected remains unchanged with wavelength). A long-pass dichroic filter (DC, Chroma, USA) separated the fluorescence in the visible range from the excitation light. After a set of short-pass filters (from Melles Griot or OmegaOptics), the remaining IR background (from elastic or inelastic scattering) was totally removed and the pure fluorescence emission was divided by a beam-splitter to be detected on two photomultiplier tubes (PMT_1, R1527P, and PMT_2, RC135 - Hamamatsu, Japan). PMT_2 is a photon-counting tube, but its minimal integration delay is limited to 10 ms, hence requiring the auxiliary use of PMT_1 with a faster rate cut energy-dependent signal. The signals of the two photodiodes and the fluorescence in energy and in photon counts from the two PMTs were thus recorded as functions of time on a PC, thanks to the acquisition card PCI-DAS1602/16 (ComputerBoards, USA), with a maximum acquisition rate of 200 kHz. The signals were then corrected by the sensitivities of the detectors given by the manufacturers. For PD_2, the excitation wavelength was first determined by the following method: both interference signals from the two photodiodes were treated by the Hilbert transform (HT) method. The phase of the HT was integrated as a function of time, and the slope was proportional to the interference spatial frequencies, that is, to the wavelength. The ratio of the slopes for the excitation IR to the He-Ne then gave the ratio between the wavelengths; the signal of the He-Ne on PD_2 was used as the reference wavelength ($\lambda_{He\text{-}Ne} = 632.8$ nm). With this determination of the excitation wavelength, we then referred to the constructor sensitivity charts to extract the required correction factor. For the two PMs, the correction was taken at the maximum emission, determined by fluorimetry (vide supra). We also checked that the correction was modified within the experimental uncertainty when integrating it on the whole emission spectrum.

The value of δ was computed according to Equation (4), directly from the input signals: PD_2 leads to $\langle P(t)\rangle$, PM_1 and PM_2 supply $F(t)$ and F_∞ (Figure 2S in the Supporting Information). To optimize its determination, the acquisition is triggered on the GBF signal, and the final value of δ was averaged over 15 to 20 successive acquisitions. The whole spectrum was obtained for steps in the wavelength between 5 and 10 nm, which corresponds to the width of the excitation wavelength distribution. It is then calibrated on one wavelength by comparison to fluorescein, whose TPA cross sections have been tabulated.[71] The accuracy of the measurements were first validated with rhodamine, whose spectrum was consistent with the one published.[12] The method was then applied to the newly synthesized chromophores.

[1] B. Valeur, *Molecular Fluorescence Principles and Applications*, Wiley-VCH, Weinheim, **2002**.
[2] For a recent review see, for example: W. E. Moerner, *J. Phys. Chem. B* **2002**, *106*, 910–927.
[3] C. Xu, W. Zipfel, J. B. Shear, R. M. Williams, W. W. Webb, *Proc. Natl. Acad. Sci. USA* **1996**, *93*, 10763–10768.
[4] R. M. Williams, W. R. Zipfel, W. W. Webb, *Curr. Opin. Chem. Biol.* **2001**, *5*, 603–608.
[5] M. Göppert-Mayer, *Ann. Phys.* **1931**, *9*, 273–294.
[6] D. M. Friedrich, *J. Chem. Educ.* **1982**, *59*, 472–481.
[7] A. Treibs, F.-H. Kreuzer, *Liebigs Ann. Chem.* **1968**, *718*, 208–223.
[8] E. Vos de Wael, J. A. Pardoen, J. A. van Koeveringe, J. Lugtenburg, *Recl. Trav. Chim. Pays-Bas* **1977**, *96*, 306–309.
[9] H. J. Wories, J. H. Koek, G. Lodder, J. Lugtenburg, R. Fokkens, O. Driessen, G. R. Mohn, *Recl. Trav. Chim. Pays-Bas* **1985**, *104*, 288–291.
[10] R. P. Haugland, H. C. Kang, *Chemically Reactive Dipyrromethene-boron Difluoride Dyes*, US 4774339, **1988**.
[11] H. C. Kang, R. P. Haugland, *Ethenyl-Substituted Dipyrromethene-boron Difluoride Dyes and Their Synthesis*, US 5187288, **1993**.
[12] C. Xu, W. W. Webb, *J. Opt. Soc. Am. B* **1996**, *13*, 481–491.
[13] G. T. Morgan, R. B. Tunstall, *J. Chem. Soc.* **1924**, *125*, 1963–1967.
[14] H. D. Hilge, E. Birckner, D. Fassler, M. V. Kozmenko, M. G. Kuz'min, H. Hartmann, *J. Photochem.* **1986**, *32*, 177–189.
[15] Y. L. Chow, X. Cheng, C. I. Johansson, *J. Photochem. Photobiol. A* **1991**, *57*, 247–255.
[16] See, for example: Y. L. Chow, S.-S. Wang, C. I. Johansson, Z.-L. Liu, *J. Am. Chem. Soc.* **1996**, *118*, 11725–11732.
[17] H.-D. Ilge, D. Fassler, H. Hartmann, *Z. Chem.* **1984**, *24*, 218–219.
[18] H.-D. Ilge, D. Fassler, H. Hartmann, *Z. Chem.* **1984**, *24*, 292–293.
[19] H. Hartmann, T. Schumann, R. Dusi, U. Bartsch, H.-D. Ilge, *Z. Chem.* **1986**, *26*, 330–331.
[20] M. Halik, H. Hartmann, *Chem. Eur. J.* **1999**, *5*, 2511–2517.
[21] N. M. D. Brown, P. Bladon, *J. Chem. Soc. A* **1969**, 526–532.
[22] W. Wierenga, H. I. Skulnick, *J. Org. Chem.* **1979**, *44*, 310–311.
[23] G. A. Reynolds, C. R. Hauser, *Org. Synth.* **1963**, *4*, 708–710.
[24] A. P. Krapcho, A. J. Lovey, *Tetrahedron. Lett.* **1973**, *12*, 957–960.
[25] D. E. Applequist, R. D. Gdanski, *J. Org. Chem.* **1981**, *46*, 2502–2510.
[26] T. W. Abbott, D. Althousen, *Org. Synth.* **1943**, *2*, 270–271.
[27] C. F. H. Allen, R. D. Abell, J. B. Normington, *Org. Synth.* **1921**, *1*, 205–207.
[28] F. Dayer, H. L. Dao, H. Gold, H. Rode-Gowa, H. Dahn, *Helv. Chim. Acta* **1974**, *57*, 2201–2209.
[29] *Liposomes a Practical Approach* (Ed.: R. R. C. New), Oxford University Press, Oxford, New York, Tokyo, **1990**.
[30] L.-Z. He, V. Garamus, B. Niemeyer, H. Helmholz, R. Willumeit, *J. Mol. Liq.* **2000**, *89*, 239–249.
[31] K. F. Purcell, J. C. Kotz, *Inorganic Chemistry*, Holt–Saunders International Editions, **1977**.
[32] N. N. Greenwood, A. Earnshaw, *Chemistry of the Elements*, 2nd ed., Butterworth Heinemann, Oxford, Auckland, Boston, Johannesburg, Melbourne, New Delhi, **1997**.
[33] V. E. Karasev, O. A. Korotkikh, *Zh. Neorg. Khim.* **1986**, *31*, 869–872.
[34] C. A. Reichardt, *Solvents and Solvent Effects in Organic Chemistry*, 2nd ed., VCH, Weinheim, Basel, Cambridge, New York, **1988**.
[35] We note that the large amplitude of the fluorescence solvatochomism might be related to a charge-transfer phenomenon coupled to a molecular change of geometry in the excited state in the polar environment. Such behavior would be reminiscent of the Twisted Intramolecular Charge Transfer occurring in some donor–acceptor derivatives. See, for example: W. Rettig, *Angew. Chem.* **1986**, *98*, 969–986; *Angew. Chem. Int. Ed. Engl.* **1986**, *25*, 971–988.
[36] G. Haucke, P. Czerney, H.-D. Ilge, D. Steen, H. Hartmann, *J. Mol. Struct.* **1990**, *219*, 411–416.
[37] W. Denk, J. H. Strickler, W. W. Webb, *Science* **1990**, 248, 73–76.
[38] J. D. Bhawalkar, A. Shih, S. J. Pan, W. S. Liou, J. Swiatkiewicz, B. A. Reinhardt, P. N. Prasad, P. C. Cheng, *Bioimaging* **1996**, *4*, 168–178.
[39] E. D. Brown, J. B. Shear, S. R. Adams, R. Y. Tsien, W. W. Webb, *Biophys. J.* **1999**, *76*, 489–499.
[40] T. Furuta, S. S.-H. Wang, J. L. Dantzker, T. M. Dore, W. J. Bybee, E. M. Callaway, W. Denk, R. Y. Tsien, *Proc. Natl. Acad. Sci. USA* **1999**, *96*, 1193–1200.
[41] G. S. He, G. C. Xu, P. N. Prasad, B. A. Reinhardt, J. C. Bhatt, R. McKellar, A. G. Dillard, *Opt. Lett.* **1995**, *20*, 435–437.
[42] G. S. He, J. D. Bhawalkar, C. F. Zhao, P. N. Prasad, *Appl. Phys. Lett.* **1995**, *67*, 2433–2435.
[43] J. D. Bhawalkar, G. S. He, P. N. Prasad, *Rep. Prog. Phys.* **1996**, *59*, 1041–1070.
[44] J. E. Ehrlich, X. L. Wu, I.-Y. S. Lee, Z.-Y. Hu, H. Röckel, S. R. Marder, J. W. Perry, *Opt. Lett.* **1997**, *22*, 1843–1845.

[45] J. W. Perry, S. Barlow, J. E. Ehrlich, A. A. Heikal, Z.-Y. Hu, I.-Y. S. Lee, K. Mansour, S. R. Marder, H. Röckel, M. Rumi, S. Thayumanavan, X.-L. Wu, *Nonlinear Opt.* **1999**, *21*, 225 – 243.

[46] M. Rumi, J. E. Ehrlich, A. A. Heikal, J. W. Perry, S. Barlow, Z. Hu, D. McCord-Maughon, T. C. Parker, H. Röckel, S. Thayumanavan, S. R. Marder, D. Beljonne, J.-L. Brédas, *J. Am. Chem. Soc.* **2000**, *122*, 9500 – 9510.

[47] a) G. S. He, L. Yuan, N. Cheng, J. D. Bhalwalkar, P. N. Prasad, L. L. Brott, S. J. Clarson, B. A. Reinhardt, *J. Opt. Soc. Am. B* **1997**, *14*, 1079 – 1087; b) B. A. Reinhardt, L. L. Brott, S. J. Clarson, A. G. Dillard, J. C. Bhatt, R. Kannan, L. Yuan, G. S. He, P. N. Prasad, *Chem. Mater.* **1998**, *10*, 1863 – 1874; c) O.-K. Kim, K.-S. Lee, H. Y. Woo, K.-S. Kim, G. S. He, J. Swiatkiewicz, P. N. Prasad, *Chem. Mater.* **2000**, *12*, 284 – 286; d) G. S. He, T.-C. Lin, P. N. Prasad, R. Kannan, R. A. Vaia, L.-S. Tan, *J. Phys. Chem. B* **2002**, *106*, 11 081 – 11 084; e) S.-J. Chung, T.-C. Lin, K.-S. Kim, G. S. He, J. Swiatkiewicz, P. N. Prasad, G. A. Baker, F. V. Bright, *Chem. Mater.* **2001**, *13*, 4071 – 4706; f) A. Adronov, J. M. J. Frechet, G. S. He, K.-S. Kim, S.-J. Chung, J. Swiatkiewicz, P. N. Prasad, *Chem. Mater.* **2000**, *12*, 2838 – 2841.

[48] a) T. Kogej, D. Beljonne, F. Meyers, J. W. Perry, S. R. Marder, J.-L. Brédas, *Chem. Phys. Lett.* **1998**, *298*, 1 – 6; b) M. Albota, D. Beljonne, J.-L. Brédas, J. E. Ehrlich, J.-Y Fu, A. A. Heikal, S. E. Hess, T. Kogej, M. D. Levin, S. R. Marder, D. McCord-Maughon, J. W. Perry, H. Röckel, M. Rumi, G. Subramamian, W. W. Webb, X.-L. Wu, C. Xu, *Science* **1998**, *281*, 1653 – 1656.

[49] K. D. Belfield, D. J. Hagan, E. W. van Stryland, K. J. Schafer, R. A. Negres, *Org. Lett.* **1999**, *1*, 1575 – 1578.

[50] P. Norman, Y. Luo, H. Ågren, *J. Chem. Phys.* **1999**, *111*, 7758 – 7765.

[51] S. K. Pati, T. J. Marks, M. A. Ratner, *J. Am. Chem. Soc.* **2001**, *123*, 7287 – 7291.

[52] A. Abbotto, L. Beverina, R. Bozio, A. Facchetti, C. Ferrante, G. A. Pagani, D. Pedron, R. Signorini, *Org. Lett.* **2002**, *4*, 1495 – 1498.

[53] T. D. Poulsen, P. K. Fredericksen, M. Jorgensen, K. V. Mikkelsen, P. R. Ogilby, *J. Phys. Chem. A* **2001**, *105*, 114 888 – 111 495.

[54] a) L. Ventelon, L. Moreaux, J. Mertz, M. Blanchard-Desce, *Chem. Commun.* **1999**, 2055 – 2056; b) L. Ventelon, L. Moreaux, J. Mertz, M. Blanchard-Desce, *Synth. Met.* **2002**, *127*, 17 – 21; c) L. Ventelon, S. Charier, L. Moreaux, J. Mertz, M. Blanchard-Desce, *Angew. Chem.* **2001**, *113*, 2156 – 2159; *Angew. Chem. Int. Ed.* **2001**, *40*, 2098 – 2101; d) O. Mongin, L. Porrès, L. Moreaux, J. Mertz, M. Blanchard-Desce, *Org. Lett.* **2002**, *4*, 719 – 722; e) M. Barzoukas, M. Blanchard-Desce, *J. Chem. Phys.* **2000**, *113*, 3951 – 3959; f) M. Barzoukas, M. Blanchard-Desce, *Nonlinear Opt.* **2001**, *27*, 209 – 218.

[55] a) B. R. Cho, K. H. Son, S. H. Lee, Y.-S. Song, Y.-K. Lee, S.-J. Jeon, J. H. Choi, H. Lee, M. Cho, *J. Am. Chem. Soc.* **2001**, *123*, 10 039 – 10 045; b) W.-H. Lee, M. Cho, S.-J. Jeon, B. R. Cho, *J. Phys. Chem. A* **2000**, *104*, 11 033 – 11 040; c) W.-H. Lee, H. Lee, J. A. Kim, J. H. Choi, S.-J. Jeon, B. R. Cho, *J. Am. Chem. Soc.* **2001**, *123*, 10 658 – 10 667.

[56] a) P. Norman, Y. Luo, H. Ågren, *Opt. Commun.* **1999**, *168*, 297 – 303; b) P. Norman, Y. Luo, H. Ågren, *Chem. Phys. Lett.* **1998**, *296*, 8 – 18; c) P. Macak, Y. Luo, P. Norman, H. Ågren, *J. Chem. Phys.* **2000**, *113*, 7055 – 7061.

[57] Y. Morel, A. Imia, P. Najechalski, Y. Kervella, O. Stephan, P. L. Baldeck, C. Andraud, *J. Chem. Phys.* **2001**, *114*, 5391 – 5396.

[58] M. Drobizhev, A. Karotki, A. Rebane, C. W. Spangler, *Opt. Lett.* **2001**, *26*, 1081 – 1083.

[59] S.-J. Chung, K.-S. Kim, T.-C. Lin, G. S. He, J. Swiatkiewicz, P. N. Prasad, *J. Phys. Chem. B* **1999**, *103*, 10 741 – 10 745.

[60] C. Xu, J. Guild, W. W. Webb, W. Denk, *Opt. Lett.* **1995**, *20*, 2372 – 2374.

[61] G. A. Reynolds, K. H. Drexhage, *Opt. Commun.* **1975**, *13*, 222 – 225.

[62] See, for example: a) S. R. Marder, L.-T. Cheng, B. G. Tiemann, A. C. Friedli, M. Blanchard-Desce, J. W. Perry, J. Skindhøj, *Science* **1994**, *263*, 511 – 514; b) M. Blanchard-Desce, V. Alain, P. V. Bedworth, S. R. Marder, A. Fort, C. Runser, M. Barzoukas, S. Lebus, R. Wortmann, *Chem. Eur. J.* **1997**, *3*, 1091 – 1104; c) V. Alain, S. Rédoglia, M. Blanchard-Desce, S. Lebus, K. Lukaszuk, R. Wortmann, U. Gubler, C. Bosshard, P. Günter, *Chem. Phys.* **1999**, *245*, 51 – 71.

[63] C. Eggeling, J. Widengren, R. Rigler, C. A. M. Seidel, *Anal. Chem.* **1998**, *70*, 2651 – 2659.

[64] C. Eggeling, J. Widengren, R. Rigler, C. A. M. Seidel, *Applied Fluorescence in Chemistry, Biology and Medicine*, Springer, Berlin, Heidelberg, New York, Chapter 10, pp. 195 – 240.

[65] H. H. Bosshard, R. Mory, M. Schmid, H. Zollinger, *Helv. Chim. Acta* **1959**, *42*, 1653 – 1658.

[66] V. H. Wallingford, A. H. Homeyer, D. M. Jones, *J. Am. Chem. Soc.* **1941**, *63*, 2252 – 2254.

[67] R. B. Shenoi, R. C. Shah, T. S. Wheeler, *J. Chem. Soc.* **1940**, 247 – 251.

[68] J. Kuthan, *Collect. Czech. Chem. Commun.* **1979**, *75*, 2409 – 2416.

[69] L. Wolf, C. Troeltzsch, *J. Prakt. Chem.* **1962**, *17*, 69 – 77.

[70] J. N. Demas, G. A. Crosby, *J. Phys. Chem.* **1971**, *75*, 991 – 1024.

[71] M. A. Albota, C. Xu, W. W. Webb, *Appl. Opt.***1998**, *37*, 7352 – 7356.

Received: July 10, 2003
Revised: September 10, 2003 [F5321]

Chapitre 3

FCS et mesure de constantes cinétiques

Avec l'amélioration des détecteurs de photons la technique de Fluorescence Correlation Spectroscopie a pris un essor important. Cette technique se sert des corrélations temporelles du signal de fluorescence émis dans une région de l'espace pour en déduire les modifications des paramètres des molécules présentes dans ce volume. L'exemple le plus simple est celui de la diffusion : une molécule commence à donner un signal lorsqu'elle pénètre dans la zone d'excitation et elle n'en donne plus quand elle en sort par diffusion. Le temps caractéristique de traversée dans le volume d'excitation donnera , en connaissant la taille de ce dernier , la constante de diffusion de la molécule. La modification de la fluorescence peut être dû à de la diffusion mais également à une réaction chimique qui transformerait une molécule fluorescente en une molécule non fluorescente ou bien encore la fixation d'une protéine fluorescente sur un ADN , qui verrait sa constante de diffusion modifiée, ou un processus de FRET entre deux fluorophores présents sur deux protéines interagissants, etc. (voir par exemple Zander, Enderlein, Keller, Single molecule detection in solution, Wiley)

Un élément important de cette technique est que la qualité des signaux de corrélations dépend du nombre de photons par molécule (voir par exemple Zander, Enderlein, Keller, Single molecule detection in solution, Wiley). C'est en ce sens une technique de molécule unique, même si le signal observé peut être la somme de celui émis par des centaines de molécules.

L'équipe de L. Jullien ayant besoin de cette technique, *a priori* potentiellement utile pour mesurer des constantes cinétiques, et celle-ci pouvant m'être utile pour mesurer des interactions ADN-protéines ou des activités enzymatiques [55, 56, 57] nous avons décider d'implémenter cette technique au laboratoire. Cela s'est avéré d'autant plus utile que comme je l'ai dit c'est à la fois une technique de molécule unique mais qui peut également fonctionner avec le signal provenant de nombreuses molécules, donc c'est un pas supplémentaire vers l'observation de molécules uniques tout en en évitant certaines difficultés.

Le montage que nous avons développé a donné pour le moment lieu essentiellement à des mesures de coefficients de diffusion [58, 59]. L'article suivant décrit des résultats plus complexes et, à mon avis, plus jolis, sur la mesure de constantes cinétiques.

J|A|C|S
ARTICLES
Published on Web 10/18/2005

Reactant Concentrations from Fluorescence Correlation Spectroscopy with Tailored Fluorescent Probes. An Example of Local Calibration-Free pH Measurement

Sandrine Charier,[†] Adrien Meglio,[†] Damien Alcor,[†] Emmanuelle Cogné-Laage,[†] Jean-François Allemand,[†,‡] Ludovic Jullien,[*,†] and Annie Lemarchand[§]

Contribution from the Département de Chimie (CNRS UMR 8640), École Normale Supérieure, 24, rue Lhomond, 75231 Paris Cedex 05, France, the Département de Physique (CNRS UMR 8550), École Normale Supérieure, 24, rue Lhomond, 75231 Paris Cedex 05, France, and the Laboratoire de Physique Théorique de la Matière Condensée (CNRS UMR 7600), Université Pierre et Marie Curie, 4, place Jussieu, 75252 Paris Cedex 05, France

Received June 14, 2005; E-mail: Ludovic.Jullien@ens.fr

Abstract: The present account is concerned with the measurement of local reactant concentrations by observing specific fluorescent probes in fluorescence correlation spectroscopy (FCS). The Theoretical Analysis section revisits the photophysical, thermodynamic, and kinetic information that is contained in the corresponding FCS correlation curves. In particular, we examine the conditions under which FCS is revealed as a superior tool to measure concentrations of reactive species. Careful molecular engineering of the specific fluorescent probes that simultaneously integrates photophysical, thermodynamic, and kinetic constraints will be required to benefit most from FCS. We illustrate the FCS titration approach with a series of fluorescent probes that we tailored to measure pH at around 4−6 by FCS after two-photon excitation. We show that an optimal design allows one to access pH without any preliminary calibrations such as the determination of the protonation constant or the photophysical properties of the fluorescent probe.

1. Introduction

There is a growing interest in the determination of the spatial and temporal distribution of individual components in chemical and biological systems. In principle, the concentration H in a component $\mathscr{H}$ can be deduced from measuring the local and instantaneous intensity of a signal that arises from its atoms or its characteristic groups (fluorescence emission is used here for illustration).[1−3] One can also use its reactivity and perform titrations with $\mathscr{H}$-specific reagents; this may overcome limitations intrinsic to the $\mathscr{H}$ structure. For instance, even when $\mathscr{H}$ is nonfluorescent such as in the present experimental system, $\mathscr{H}$ titration can rely on fluorescence emission if reaction 1 of

$$\mathscr{AH} \rightleftharpoons \mathscr{A} + \mathscr{H} \qquad (1)$$

$\mathscr{H}$ with a fluorescent reagent $\mathscr{A}$ yields a product, $\mathscr{AH}$, that exhibits a different brightness.

Using the latter strategy, a first approach to access H consists of converting, in concentration terms, the intensity of fluorescence emission that arises from the illuminated volume at a given wavelength. Then, to extract H requires knowledge of (i) the characteristics of the instrumental setup, (ii) the total concentration C in the fluorescent reagent, (iii) the properties of absorption and emission of $\mathscr{AH}$ and $\mathscr{A}$, and (iv) the equilibrium constant of reaction 1.

On the basis of the ratio of the emission intensities at two different wavelengths, the more favorable ratiometric determination of H no longer requires the knowledge of (i) and (ii) but still requires that of (iii) and (iv).[2,3] A similar approach relies on a biexponential analysis of the decay of fluorescence emission; H is then determined after evaluation of the amplitude of the terms associated to $\mathscr{AH}$ and $\mathscr{A}$, respectively.[4]

Data (i)−(iv) are generally derived from preliminary calibrations that are not always relevant to all the situations such as, for instance, those encountered in biology. Living cells are optically heterogeneous: the shape of the illuminated volume and the collection factor of the experimental setup are difficult to evaluate from calibrations. The concentration C often remains unknown in vivo. Eventually, the photophysical features of $\mathscr{AH}$ and $\mathscr{A}$, as well as the thermodynamic properties of reaction 1, can be significantly altered in biological media. In fact, analyses yielding H with more "robust" prerequisites would represent attractive improvements.

* Fax: (+33) 1 44 32 33 25.
[†] Département de Chimie, École Normale Supérieure.
[‡] Département de Physique, École Normale Supérieure.
[§] Université Pierre et Marie Curie.

(1) Cantor, C. R.; Schimmel, P. R. *Biophysical Chemistry*; Part II; Freeman: New York, 1980.
(2) Lakowicz, J. R. *Principles of Fluorescence Spectroscopy*; Plenum Press: New York, 1999.
(3) Valeur, B. *Molecular Fluorescence Principles and Applications*: Wiley VCH: Weinheim, New York, Chichester, Brisbane, Singapore, Toronto, 2002.
(4) See, for instance: Draxler, S.; E.L., M.; Lippitsch, M.; Leiner, J.-P. *Sens. Actuators, B* **1993**, *11*, 421−424.

10.1021/ja053909w CCC: $30.25

The analysis of density fluctuations in an open system at equilibrium provides a rich body of information related to concentrations. Thermodynamics is contained in the fluctuation amplitude, whereas kinetics lies in the time-dependent decay of the correlation of the fluctuations.[5−7] Techniques making use of fluctuation analysis are robust; they do not require any signal calibration, but only the knowledge of the system extent. Fluorescence correlation spectroscopy (FCS) is a technique relying on the preceding principle.[8−17] In relation to the titration issue, solution-based[18] FCS has been theoretically evaluated[9,19−22] and experimentally used[10,19−27] to measure rate constants in a medium that contains a fluorescent probe exchanging between two states of different brightness when it reacts with a species of interest. Possible FCS applications to titrations were already addressed for the proton[19,23−27] and the calcium(II) ion.[23]

The FCS titration approach is especially significant. It is noninvasive, and it can thus be performed in living cells[28−30] by using tiny amounts of fluorescent indicators, either permeant or synthesized in vivo (the green fluorescent protein GFP or its mutants, for instance). In addition, FCS may yield local concentrations at micrometer resolution that can be obtained either intrinsically with two-photon excitation or by using a pinhole when FCS relies on one-photon excitation.

As attractive as it is, the FCS titration approach is nevertheless rather constraining (vide infra). In particular, it requires carefully designed fluorescent probes that integrate specific photophysical, thermodynamic, and kinetic requirements. If one excepts pH and pOH jump molecules that exploit the properties of excited states,[31] the kinetic aspect is rather unusual in molecular engineering of fluorescent probes. In contrast, it is crucial here. In fact, FCS opportunities surely merit the work to address such a new challenge.

In the present report, we evaluate FCS to access the local concentration in a reactant $\mathscr{K}$ with a fluorescent reagent $\{\mathscr{AK},\mathscr{A}\}$. In section 2 and in the Supporting Information, we revisit the theoretical treatment of the correlation functions of fluorescence emission in such a situation. In addition to previous analyses,[9,19−22] we examine the following: (i) the observation of the reactivity of the ground or of the excited state of $\{\mathscr{AK},\mathscr{A}\}$ (this point is especially important because those reactivities can considerably differ such as, for instance, in the case of fluorescent pH probes[32−34] that are used for experimental illustration); (ii) the most favorable approximation to access tractable expressions of the correlation functions; (iii) the experimental constraints to access *H* with FCS. FCS is shown to be a superior tool to measure concentrations of reactive species provided that appropriate fluorescent probes are available: selectivity is at the highest because both the thermodynamics and the kinetics of reaction 1 are used to obtain the reactant concentration.[35] In addition, preliminary calibrations can sometimes even be avoided. To evaluate the preceding theoretical results, section 3 makes use of three fluorescent probes that we recently designed to measure pH in the 3−7 range by ratiometric means.[36,37] We first measure and analyze their kinetics of proton exchange by FCS after two-photon excitation. We then demonstrate that one can use them to efficiently estimate pH around 4−6 by FCS after two-photon excitation without preliminary calibration. Despite this favorable result, we suggest that further improvements will still be necessary to reliably extract pH in unknown media from FCS measurements. Section 4 is devoted to the conclusion.

2. Theoretical Analysis

In FCS, one observes and analyzes the fluctuations of the number of photons $n(\vec{r}, t)$ collected from fluorescent molecules that are contained in a tiny illuminated volume V (typically 1 fL) delimited by focusing a laser beam (see Supporting Information Figure 1S for the presentation of the setup used in the group). Thanks to the intrinsic sensitivity of fluorescence, one can observe very dilute solutions (less than 1 nM) that cause large fluctuations $\delta n(\vec{r}, t)$ around average values $\overline{n(\vec{r})}$: at 1 nM with $V = 1$ fL, $\delta n(\vec{r}, t) \approx \overline{n(\vec{r})}$. A FCS setup generally computes the autocorrelation function of fluorescence emission, defined in eq 2, that gives the time average of the products of

$$G(\tau) = \frac{\langle \delta n(\vec{r}, 0)\, \delta n(\vec{r}, \tau) \rangle}{\overline{n(\vec{r})}\ \overline{n(\vec{r})}} \qquad (2)$$

(5) Diu, B.; Guthmann, C.; Lederer, D.; Roulet, B. *Physique Statistique*; Hermann: Paris, 1989.
(6) Berne, B. J.; Pecora, R. *Dynamic Light Scattering with Applications to Chemistry, Biology, and Physics*; Dover: Mineola, NY, 2000.
(7) van Kampen, N. G. *Stochastic Processes in Physics and Chemistry*, 5th ed.; Elsevier: Amsterdam, 2004.
(8) Magde, D.; Elson, E. L.; Webb, W. W. *Phys. Rev. Lett.* **1972**, *11*, 705−708.
(9) Elson, E. L.; Magde, D. *Biopolymers* **1974**, *13*, 1−27.
(10) Magde, D.; Elson, E. L.; Webb, W. W. *Biopolymers* **1974**, *13*, 29−61.
(11) Thompson, N. L. Fluorescence Correlation Spectroscopy. *Topics in Fluorescence Spectroscopy, Techniques*; Lakowicz, J., Ed.; Plenum Press: New York, 1991; Vol. 1, pp 337−410.
(12) *Fluorescence Correlation Spectroscopy*; Rigler, R., Elson, E. S., Eds.; Springer Series in Chemical Physics; Springer-Verlag, Berlin, 2001.
(13) Elson, E. L. *Traffic* **2001**, *2*, 789−796.
(14) Chen, Y.; Müller, J.-D.; Eid, J.-S.; Gratton, E. In *New Trends in Fluorescence Spectroscopy, Applications to Chemical and Life Sciences*; Valeur, B., Brochon, J.-C., Eds.; Springer Series on Fluorescence, Methods and Applications; Springer: Berlin, 2001; pp 277−296.
(15) Thompson, N. L.; Lieto, A. M.; Allen, N. W. *Curr. Opin. Struct. Biol.* **2002**, *12*, 634−641.
(16) Krichevsky, O.; Bonnet, G. *Rep. Prog. Phys.* **2002**, *65*, 251−297.
(17) Hess, S. T.; Huang, S.; Heikal, A. A.; Webb, W. W. *Biochemistry* **2002**, *41*, 697−705.
(18) Here, we do not consider the situation where at least one reactant is immobilized such as in, for instance: Lieto, A. M.; Cush, R. C.; Thompson, N. L. *Biophys. J.* **2003**, *85*, 3294−3302.
(19) Widengren, J.; Terry, B.; Rigler, R. *Chem. Phys.* **1999**, *249*, 259−271.
(20) Lamb, D. C.; Schenk, A.; Röcker, C.; Scalfi-Happ, C.; Nienhaus, G. U. *Biophys. J.* **2000** *79*, 1129−1138.
(21) Bismuto, E.; Gratton, E.; Lamb, D. C. *Biophys. J.* **2001**, *81*, 3510−3521.
(22) Hom, E. F. Y.; Verkman, A. S. *Biophys. J.* **2002**, *83*, 533−546.
(23) Widengren, J.; Rigler, R. *J. Fluoresc.* **1997**, *7*, 211S-213S.
(24) Widengren, J.; Rigler, R. *Cell. Mol. Biol.* **1998**, *44*, 857−879.
(25) Haupts, U.; Maiti, S.; Schwille, P.; Webb, W. W. *Proc. Natl. Acad. Sci. U.S.A.* **1998**, *95*, 13573−13578.
(26) Schwille, P.; Kummer, S.; Heikal, A. A.; Moerner, W. E.; Webb, W. W. *Proc. Natl. Acad. Sci. U.S.A.* **2000**, *97*, 151−156.
(27) Hess, S. T.; Heikal, A. A.; Webb, W. W. *J. Phys. Chem. B* **2004**, *108*, 10138−10148.
(28) Berland, K. M.; So, P. T. C.; Gratton, E. *Biophys. J.* **1995**, *68*, 694−701.
(29) Schwille, P.; Haupts, U.; Maiti, S.; Webb, W. W. *Biophys. J.* **1999**, *77*, 2251−2265.
(30) Gennerich, A.; Schild, D. *Biophys. J.* **2000**, *79*, 3294−3306.
(31) For a recent reference, see, for instance: Moscovitch, D.; Noivirt, O.; Mezer, A.; Nachliel, E.; Mark, T.; Gutman, M.; Fibich, G. *Biophys. J.* **2004**, *87*, 47−57.
(32) Förster, T. *Z. Elektrochem.* **1950**, *54*, 42−46.
(33) (a) Weller, A. *Z. Elektrochem.* **1952**, *56*, 662−668. (b) Weller, A.; *Z. Phys. Chem. Neue Folge* **1955**, *3*, 238−254. (c) Weller, A. *Z. Phys. Chem. Neue Folge* **1958**, *17*, 224−245.
(34) Schulman, S. G. *Molecular Luminescence Spectroscopy, Methods and Applications*; Wiley-Interscience: New York, Chichester, Brisbane, Toronto, Singapore, 1988; Part 2.
(35) Winkler-Oswatitsch, R. W.; Eigen, M. *Angew. Chem., Int. Ed. Engl.* **1979**, *18*, 20−49.
(36) Charier, S.; Ruel, O.; Baudin, J.-B.; Alcor, D.; Allemand, J.-F.; Meglio, A.; Jullien, L. *Angew. Chem., Int. Ed. Eng.* **2004**, *43*, 4785−4788.
(37) Charier, S.; Ruel, O.; Baudin, J.-B.; Alcor, D.; Allemand, J.-F.; Meglio, A.; Jullien, L.; Valeur, B. *Chem. Eur.*−*J.*, accepted for publication.

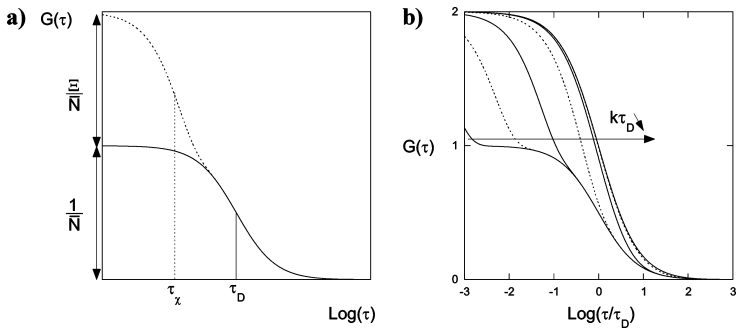

Figure 1. (a) Principle of extraction of a reactant concentration from an autocorrelation curve recorded from a reactive mixture (dotted line). Fitting with eq 3 provides $\overline{N}$ and τ_D from the term $G_D(\tau)$ related to the diffusion (solid line), and Ξ and τ_χ from the term related to chemistry. After calibration of the beam waist, $\overline{N}$ and τ_D yield the total concentration C in fluorescent probe $\{\mathcal{M},\mathcal{A}\}$ on one hand and either the $\{\mathcal{M},\mathcal{A}\}$ diffusion coefficient d or the local viscosity on the other hand. In contrast, Ξ depends on $\overline{H}$, K, and the relative brightness $Q = (\mathcal{Q}_{\mathcal{MH}}/\mathcal{Q}_{\mathcal{A}})$, whereas τ_χ depends on $\overline{H}$, K, and one of the rate constants k or k'. If K and Q are known, Ξ yields $\overline{H}$. If one rate constant, k or k', is additionally known, $\overline{H}$ can be also extracted from τ_χ. (b) Theoretical dependence of the autocorrelation function $G(\tau)$ on adimensional time τ/τ_D as calculated from eq 3 for different values of $k\tau_D$: 10^3, 10^2, 10, 1, 10^{-1}, 10^{-2}, and 10^{-3}. Parameter values for the calculation are $\overline{N} = 1$, $\omega = 10$, $\overline{H} = K$, and $Q = \infty$.

the intensity fluctuations normalized by the product of the average intensities.

***G*(τ) for a Reactive System with Three Reactants.** To extract the relevant thermodynamic and kinetic parameters from FCS data, the experimental autocorrelation function $G(\tau)$ has to be fitted with theoretical expressions. When the reactive system involves more than two reactants, assumptions are required to obtain approximate analytical expressions of the autocorrelation function $G(\tau)$ (see Supporting Information).

We first use the steady-state approximation: the fastest processes are relaxed at the time scale of the slowest ones. Then, the typical nanosecond range for the lifetime of singlet excited states as well as the hundred-nanoseconds time resolution of the autocorrelator in a current FCS setup led us to conclude that, although relying on the analyses of the fluctuations of the fluorescence intensity from excited states, FCS reveals the reactivity of virtual averaged species that involve both the ground and the excited states (see Supporting Information). In fact, the autocorrelation functions essentially contain rate and thermodynamic constants associated with ground states in most encountered experimental situations (see Supporting Information). This conclusion is especially significant because the rate constants of chemical reactions can sometimes be considerably altered by the nature, ground or excited, of the state (rate constants for proton exchange reactions can be changed by 10 orders of magnitude, for instance).[32−34]

We are now interested in getting $G(\tau)$ for a system submitted to reaction 1. k and k' designate the rate constants of the forward and backward processes, and $K = k/k'$, the equilibrium constant of reaction 1. $\overline{H}$ is the average concentration in $\mathcal{H}$ in the illuminated volume V, and $C = A\overline{H} + A$. In relation with titrating $\mathcal{H}$ with a fluorescent reagent $\{\mathcal{MH},\mathcal{A}\}$ in the most general case, we assume that $\mathcal{H}$ is not fluorescent. In addition, we consider that the diffusion coefficients of $\mathcal{MH}$ and $\mathcal{A}$ are identical and equal to d. This approximation is satisfactory as long as $\mathcal{H}$ is small enough. For instance, the acidic and basic states of a pH indicator exhibit similar shape and size. In addition, the small difference in charge between both states is not expected to alter the diffusion coefficient by different coupling with the cloud of the counterions at any relevant ionic strength.[1]

Lamb et al. introduced a simple approximate analytical expression of $G(\tau)$ when $C \ll \overline{H}$.[20] In FCS, this condition should be often fulfilled because sensitive detectors such as avalanche photodiodes make measurements possible down to the nanomolar range in $\{\mathcal{M},\mathcal{A}\}$: a large range of $\mathcal{H}$ concentrations is thus accessible (see Supporting Information). Then,

$$G(\tau) = G_D(\tau)\,[1 + \Xi\, e^{-(\tau/\tau_\chi)}] \tag{3}$$

with

$$G_D(\tau) = \frac{1}{\overline{N}}\left(1 + \frac{\tau}{\tau_D}\right)^{-1}\left(1 + \frac{\tau}{\omega^2\tau_D}\right)^{(-1/2)} \tag{4}$$

and

$$\Xi = \frac{K}{\overline{H}}\left(\frac{Q-1}{Q + \frac{K}{\overline{H}}}\right)^2 \tag{5}$$

where $\overline{N} = CV$, $\tau_D = \omega_{xy}^2/(4d\nu)$, $\omega = (\omega_z/\omega_{xy})$, and $Q = \mathcal{Q}_{\mathcal{MH}}/\mathcal{Q}_{\mathcal{A}}$ designate, respectively, the average number of $\{\mathcal{MH},\mathcal{A}\}$ molecules contained in the illuminated volume V, the diffusion time of $\{\mathcal{MH},\mathcal{A}\}$ through the beam waist described as 3D-Gaussian with ω_{xy} diameter and ω_z height (ν is equal to 1 for one-photon excitation and to 2 for two-photon excitation), the aspect ratio of the 3D-Gaussian volume V, and the ratio of the effective brightness, $\mathcal{Q}_{\mathcal{MH}}$ and $\mathcal{Q}_{\mathcal{A}}$, associated to the states $\mathcal{MH}$ and $\mathcal{A}$. $G(\tau)$ is the product of the diffusive term, $G_D(\tau)$, and of the term in square brackets associated with the chemical relaxation. Figure 1a displays a typical prediction for the $G(\tau)$ function from eq 3. In particular, Figure 1a makes explicit the significance of $\overline{N}$ and Ξ and of τ_D and τ_χ to, respectively, determine the amplitude and the time dependence of the $G(\tau)$ function.

Measuring Reactant Concentrations by FCS. In the following, we assume that $C \ll \overline{H}$ to be able to use the simple analytical expression (eq 3) to extract the concentration $\overline{H}$ sought from correlation functions of $\{\mathcal{MK},\mathcal{M}\}$ fluorescence emission.

A. General Case. As shown in Figure 1a, fitting the experimental data with eq 3 should provide $\overline{N}$ and τ_D from the term $G_D(\tau)$ related to the diffusion and Ξ and τ_χ from the term related to chemistry.[38]

A fruitful interpretation of $\overline{N}$ and τ_D requires a preliminary calibration of the illuminated volume V. This can be done by using a reference fluorophore such as fluorescein at a known concentration. Then, $\overline{N}$ and τ_D yield the total concentration in $\{\mathcal{MK},\mathcal{M}\}$, $C = \overline{N}/V$, on one hand and the diffusion coefficient of $\{\mathcal{MK},\mathcal{M}\}$, $d = \omega_{xy}^2/(4\nu\tau_D)$, on the other hand.

In contrast, Ξ depends on $\overline{H}$, on K, and on the relative brightness Q, whereas τ_χ depends on $\overline{H}$, on K, and on one of the rate constants, k or k' ($\tau_\chi \approx [k + k'\overline{H}]^{-1}$ in the present region of approximation). If K and $\overline{H}$ are known, it is possible to determine the rate constants k and k' from the measurement of τ_χ. Conversely, if K and Q are known, Ξ yields $\overline{H}$. If one rate constant, k or k', is additionally known, $\overline{H}$ can also be extracted independently from τ_χ.

As far as Ξ analysis only is concerned, FCS satisfactorily compares with ratiometric methods because both the thermodynamic (K) and the photophysical (Q) information is required to extract $\overline{H}$ from the experimental data. FCS alternatively yields $\overline{H}$ from τ_χ if the thermodynamic and rate constants of reaction 1 are known. Under such a condition, FCS should be at the most selective because $\overline{H}$ measurement relies on both thermodynamic and kinetic data from reaction 1.[35] This point is a major advantage if one deals with a mixture of species that can interact with the fluorescent indicator.

As a general conclusion, FCS provides more observables than the classical methods evoked in the Introduction to measure $\overline{H}$. Nevertheless, preliminary calibrations are still required in the most general case.

B. "Calibration-Free" Approach. In fact, FCS reveals its definitive advantages only after proper design of the $\{\mathcal{MK},\mathcal{M}\}$ fluorescent reagent. As an example related to the experimental part of the present work, we first assume that either $\mathcal{Q}_{\mathcal{MK}}$ or $\mathcal{Q}_{\mathcal{M}}$ is equal to zero ($\mathcal{MK}$ or $\mathcal{M}$ appears nonfluorescent *on the detecting channels*). For instance, reaction 1 can be accompanied by the quenching or the shift of the emission of the fluorescent reagent. Second, we suppose that the reaction of $\mathcal{M}$ with $\mathcal{K}$ is limited by the diffusion (vide infra). Then, a good order of magnitude of the rate constant k' can be derived from the respective diffusion coefficients of $\mathcal{M}$ (d) (extracted from the diffusive term $G(\tau)$ in eq 4) and $\mathcal{K}$ (D):

$$k' \approx 4\pi N_A(d + D)a \qquad (6)$$

where N_A and a, respectively, designate the Avogadro number and a captured length in the 1 nm range.[39] If k' is known, both Ξ and τ_χ only depend on $\mathcal{K}$ and K. Consequently, the simultaneous measurement of Ξ and τ_χ should now yield, without any preliminary calibration, not only the desired $\mathcal{K}$ concentration but also the value of the thermodynamic constant K.

Constraints on Measuring Concentrations by FCS. The preceding paragraph suggests that FCS could be extremely attractive to measure concentrations: this noninvasive technique can yield local concentrations at the micrometer resolution without calibration in the best cases. In fact, its impact will strongly depend on the proper design of fluorescent reagents. This section examines different types of constraints on accessing reactant concentrations by FCS.

A. Amplitude of Ξ. To be used for analysis, the amplitude of the chemical term, Ξ, must be large enough (see eq 3). Figure 2a displays the dependence of Ξ on $\log_{10}(K/\overline{H})$ and on $\log_{10} Q$. In the following, we assume the solutions to be ideal and we denote $\mathrm{pH} = -\log_{10} \overline{H}$ and $\mathrm{p}K = -\log_{10} K$ in relation to the following experimental illustration.

FCS does not reveal the occurrence of reaction 1 when the brightnesses of $\mathcal{MK}$ and $\mathcal{M}$ are identical: For $Q = 1$, $\Xi = 0$ over the whole range of pH−pK. Ξ is appreciably large only in symmetrically related zones of the two quadrants in the (Q, pH−pK) space ($\Xi \approx 1$ under our experimental conditions).[40] In these two zones, the large value of Ξ is associated with occurrences of transitions from the darkest state that is present in the largest amount to the minor brightest state.

B. Statistical Accuracy. In practice, the intrinsic noise of the experimental setup limits the statistical accuracy of FCS experiments. In fact, FCS experiments provide reliable information related to the fluorescent probe only when $\overline{N}$ is larger than the equivalent number of molecules, $\overline{N'}$, associated to the background fluorescence.[41]

If Ψ and Ψ_{min}, respectively, designate the photon fluxes from the illuminated volume V that originates from the $\overline{N}$ fluorescent probe molecules and that gives rise to a signal equal to the intrinsic noise at the detecting unit, then

$$\frac{\overline{N'}}{\overline{N}} = \frac{\Psi_{min}}{\Psi} = \frac{1 + \dfrac{K}{\overline{H}}}{\varphi\overline{N}\mathcal{Q}_{\mathcal{M}}\left(Q + \dfrac{K}{\overline{H}}\right)}\Psi_{min} \qquad (7)$$

where φ is the photon collection factor of the setup. Note that $\overline{N'}$ depends on the pH-dependent average brightness of the fluorescent probe.

The preceding subsection emphasized that the measurement of reactant concentrations by FCS can only be performed when the brightest state is in a low amount. Unfortunately, the gain in the fluctuation amplitude is counterbalanced by a corresponding drop of statistical accuracy due to the low average brightness under such conditions. For instance, when $Q \gg (K/\overline{H}) \gg 1$, increasing the pH−p$K$ by one unit also increases $\overline{N'}$ by a factor of 10 because $((\mathcal{Q}_{\mathcal{M}}/1) + (K/\overline{H}))(Q + (K/\overline{H})) \approx (\mathcal{Q}_{\mathcal{MK}}/(K/\overline{H}))$.

(38) ω does not significantly affect $G(\tau)$ and cannot be reliably extracted from the fit. See ref 14.
(39) Berry, R. S.; Rice, S. A.; Ross, J. *Physical Chemistry*, 2nd ed.; Oxford University Press: Oxford, U.K., 2000.
(40) For a given relative brightness, Q, two different $\overline{H}$ values give noticeably the same Ξ value; in principle, it should not be possible to extract pH−pK from Ξ without ambiguity. In fact, the constraint on the intensity of fluorescence emission should forbid the observation of the branch attached to pH values significantly departing from pK (vide infra).
(41) Koppel, D. E. *Phys. Rev. A* **1974**, *10*, 1938−1945.

The condition $\overline{N} \geq \overline{N'}$ is equivalent to

$$\left(\frac{1}{1+Q}\right)\left(\frac{Q+\frac{K}{\overline{H}}}{1+\frac{K}{\overline{H}}}\right) \geq \frac{\Psi_{\min}}{\varphi\overline{N}(\mathcal{Q}_{\mathcal{MR}}+\mathcal{Q}_{\mathcal{A}})} \equiv \alpha^{-1} \qquad (8)$$

Figure 2b displays for different values of α the domain in which eq 8 is fulfilled in the (pH−pK, $\log_{10} Q$) space (α ≈ 10 under our experimental conditions). Significant experiments can be essentially performed in the two quadrants, $Q > 1$ and pH < pK and $Q < 1$ and pH > pK.

To enlarge the extent of the relevant domain, one could first imagine increasing $\overline{N}$. Unfortunately, this would reduce the total amplitude of the FCS autocorrelation function that inversely depends on $\overline{N}$ (see eqs 3 and 4). With the currently available detecting systems, $C \approx 10-10^3$ nM seems rather optimal. In principle, one could also improve the collection factor and the instrumental response to enlarge φ. Eventually, one can increase the brightness of the fluorescent probe by engineering its absorption and emission properties.

Comparison between Figure 2a and 2b is useful to analyze the domains in which the measurement of reactant concentrations can be performed by FCS. Figure 2c displays the typical zone that can be investigated with our experimental setup by using the following fluorescent pH probes. The best results should be eventually obtained in the range pH ≈ pK.

C. Kinetic Window. In fact, stringent kinetic constraints also have to be taken into account. Figure 1b illustrates the theoretical evolution of the autocorrelation function $G(\tau)$ as a function of the normalized time τ/τ_D for different relaxation times τ_χ of reaction 1; in relation to the preceding paragraphs, the calculations were performed at pH = pK, where $\tau_\chi = 1/(2k) = 1/(2k'\overline{H})$.

As long as $\tau_\chi \leq \tau_D$ (i.e., $k\tau_D \geq 1$), the autocorrelation function exhibits two thresholds at τ_χ and τ_D that are associated with the regression of the fluctuations from chemical and diffusional origins, respectively. The amplitudes of these two contributions are, respectively, equal to $\Xi/\overline{N}$ and $1/\overline{N}$ (see also Figure 1a). In the corresponding region, both thermodynamic and kinetic information on reaction 1 can be extracted from the autocorrelation function. In contrast, when $\tau_\chi \gg \tau_D$ (i.e., $k\tau_D \ll 1$), the autocorrelation function exhibits only one threshold at τ_D with an amplitude that is equal to $(1 + \Xi)/\overline{N}$. As anticipated from the absence of a chemical reaction at the time scale of the diffusion through the beam waist in the corresponding region, this behavior corresponds to a nonreactive mixture of $\mathcal{MR}$ and $\mathcal{A}$: only the thermodynamic constant of reaction 1 can be extracted from the autocorrelation function.

In relation to measuring the concentration $\overline{H}$ by FCS, the region $\tau_\chi \leq \tau_D$ is more favorable because both kinetic and thermodynamic information can be exploited. To reach this region, it is possible to play with τ_D or with τ_χ. From an instrumental point of view, it is possible to enlarge τ_D by playing with ω_{xy}. In relation to the engineering of the fluorescent probe, it is difficult to tune τ_D because the diffusion coefficient of the fluorescent probe is only poorly dependent on its structure in the limit of acceptable ranges of size. In fact, τ_D for "small" molecules under typical conditions can be hardly larger than 1 ms with one-photon excitation FCS and 0.1 ms with two-photon excitation FCS. In contrast, molecular design of the fluorescent probe should favor the increase of k' to reduce τ_χ as much as possible at pH = pK.

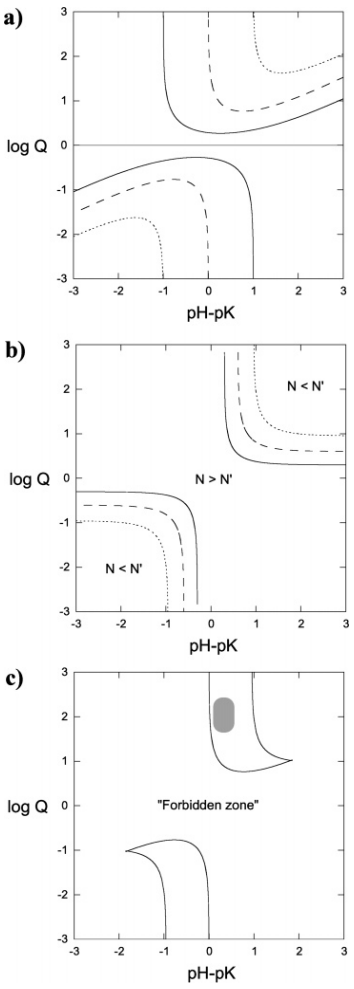

Figure 2. (a) Contour plot of the amplitude Ξ of the chemical term in the autocorrelation function $G(\tau)$ on pH−pK and log Q. Solid line: $\Xi = 0.1$. Dashed line: $\Xi = 1$. Dotted line: $\Xi = 10$. (b) Manifold $\overline{N} = \overline{N'}$ in the (pH−pK, log Q) space for different values of the α parameter. Solid line: $\alpha = 3$. Dashed line: $\alpha = 5$. Dotted line: $\alpha = 10$. (c) Combined diagram picturing the zones where proton concentration can be measured by FCS with the present pH fluorescent probes and with our experimental setup. The gray zone displays the domain in which experiments were performed in the present study.

Nevertheless, there is also a lower limit to the accessible relaxation time τ_χ that is fixed by the temporal resolution τ_{cor} of the autocorrelator ($\tau_{cor} = 0.1$ μs in the present FCS setup). At the τ_{cor} time scale, the fluorescent probe exchanging between the acidic and the basic states behaves as a single species and

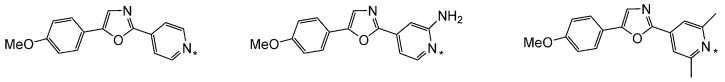

Figure 3. Fluorescent pH indicators that were used in the present study: **4-PYMPO**, **4-PYMPO−NH$_2$**, and **4-PYMPOM**. The relevant protonation site in the considered pH range is indicated with an asterisk.

chemistry is no longer visible in FCS if $\tau_\chi < \tau_{cor}$. In fact, the autocorrelation function only contains the information related to the diffusion of the fluorescent probe: it is impossible to extract the concentration $\bar{H}$ by FCS. This type of situation is illustrated in Figure 1b for $k\tau_D = 10^3$.

As a conclusion, the preceding paragraphs emphasize that the measurement of reactant concentrations by FCS is attractive but rather constraining. Ideally, a good fluorescent reagent $\{\mathscr{H},\mathscr{A}\}$ would (i) have a thermodynamic constant K in the $\bar{H}$ working range (control of Ξ amplitude), (ii) be at the brightest (control of the amplitude of fluorescence emission), (iii) exhibit a major change of fluorescence intensity upon reaction 1 (control of Ξ amplitude), (iv) yield a relaxation time τ_χ in the 1−100 μs range (constraint on the kinetic window), and (v) possibly react with $\mathscr{H}$ under control of diffusion (to avoid any calibration).

3. Application to pH Measurement by FCS after Two-Photon Excitation

The proton is probably the first reactant one could imagine to titrate by FCS.[19,23,24] Beyond the intrinsic significance of the proton, proton exchange reactions provide a wide range of thermodynamic and kinetic behaviors allowing one to find appropriate fluorescent indicators. In addition, the mechanisms governing the proton exchange reactions are rather simple and were already thoroughly examined.[42,43]

Presentation of the Fluorescent pH Indicators. We recently reported on a series of fluorescent probes for dual emission wavelength pH measurement that work in the biologically relevant 4−7 pH range.[36,37] These probes were additionally designed to fulfill, as much as possible, the requirements exposed in the preceding paragraph when two-photon excitation is used for FCS. In fact, this excitation mode is especially adapted to perform local investigations because of its intrinsic limitation of the excitation volume.[14,28]

A. Design. The thermodynamic and kinetic issues of the fluorescent probe were addressed as follows.

We ideally sought a fluorescent pH indicator that would exhibit a chemical relaxation time such that $\tau_{cor} \le \tau_\chi \le \tau_D$ with $\tau_D < 100$ μs (vide supra). We engineered $\tau_\chi \approx 10$ μs. We first considered that the reaction of a base with a proton is most often controlled by diffusion.[42,43] As explained above, this feature is especially favorable here. Respectively, denoting $\mathscr{HA}$ and $\mathscr{A}$ as the acidic and the basic states of the fluorescent pH indicator and denoting $\mathscr{H}$ as the proton, we sought $k' \approx 10^{10}$ M^{-1} s^{-1}.[42,43] In addition, we decided to work at pH = pK = pK_a (vide supra) where K_a designates the protonation constant of the fluorescent pH indicator. Taking into account that $\tau_\chi = 1/(2k) = 1/(2k'\bar{H}) \approx 10$ μs at pH = pK_a, we got pH = p$K_a \approx$ 5. Thus, we designed fluorescent pH indicators with a pK_a between 4 and 6 that would not exhibit any significant steric hindrance around the basic site to maintain the diffusion-limited rate constant for its protonation.

From a photophysical point of view, we additionally favored pH indicators exchanging between two strongly fluorescent states, $\mathscr{HA}$ and $\mathscr{A}$, with shifted emission spectra. First, this allowed us to tune the respective brightness of the exchanging states by changing the excitation wavelength and by using appropriate filters; this may find applications in dual-color fluorescence cross-correlation spectroscopy.[22,44] In addition, this feature provided a way to directly access pH from a ratiometric analysis of the fluorescence emission from the acidic and basic states of the pH indicator. In the present series of experiments, this was favorable because it is impossible to reliably measure $\bar{H}$ at neutral pH with the glass electrode of a pH meter in the absence of supporting salt at the corresponding concentrations.

Figure 3 displays the three tailored water-soluble fluorescent pH indicators that we eventually retained: **4-PYMPO**, **4-PYMPO−NH$_2$**, and **4-PYMPOM**.[36,37]

B. Photophysical Properties and Protonation Constants. In relation to the present work, the main relevant photophysical properties of the three retained pH indicators are displayed in Figure 4 and summarized in Table 1. Their absorption and emission features made them appropriate to perform FCS experiments after two-photon excitation. The typical order of magnitude of their maximal peak two-photon absorptivities in the 700−900 nm range is 60 ± 10 GM (1 GM = 10^{-50} cm^4 s (photon·molecule)$^{-1}$). They additionally exhibit a strong fluorescence emission (quantum yield of fluorescence Φ_F up to 0.8) in the 400−600 nm range for both acidic and basic states of the three pH indicators.

The ground-state pK_a of the present pH indicators is located in the 4−6 range (Table 1). In relation to the preceding paragraph, they should be appropriate to perform kinetic experiments and pH measurements relying on FCS after two-photon excitation. As explained in the Theoretical Analysis section and in the Supporting Information, here, it is important to note that FCS reveals the reactivity of the ground state of the present pH probes despite a large shift of their pK_a upon light excitation.[37]

C. Diffusion Coefficients. To evaluate the intrinsic diffusion coefficients of the fluorescent pH indicators, one can analyze the autocorrelation functions from their solutions at a pH largely departing from their pK_a. Under such conditions, the chemical contribution in eq 3 reduces to one (i.e., $\Xi = 0$). Figures 5a and 6a,b display typical experimental FCS autocorrelation curves for solutions of **4-PYMPO**, **4-PYMPO−NH$_2$**, and **4-PYMPOM** at a pH significantly lower than their pK_a, where the acidic state is essentially present. The fit according to eq 4 is satisfactory for all compounds. The extracted data, $G_D(0)$ and

(42) Eigen, M. *Angew. Chem.* **1963**, *75*, 489−508.
(43) Eigen, M.; Kruse, W.; Maas, G.; de Mayer, L. In *Progress in Reaction Kinetics;* Porter, G., Ed.; Pergamon Press: Oxford, London, Edinburgh, New York, Paris, Frankfurt, 1964, Vol. 2; pp 287−318.
(44) Schwille, P.; Meyer-Almes, F.-J.; Rigler, R. *Biophys. J.* **1997**, *72*, 1878−1886.

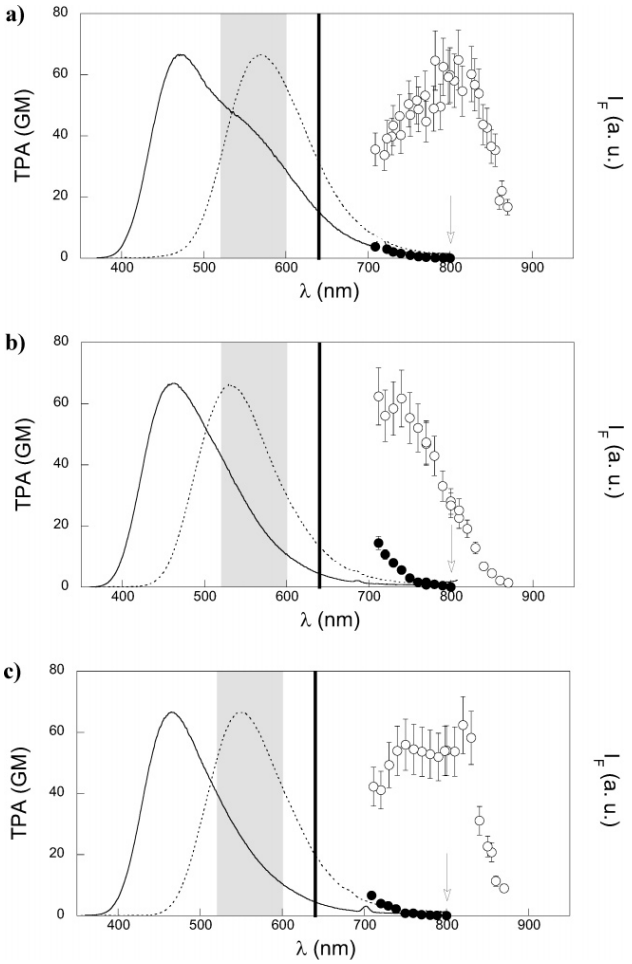

Figure 4. Photophysical properties of the present fluorescent pH indicators that are relevant for FCS after two-photon excitation. Two-photon excitation spectra $\delta(\lambda^{(2)})$ and normalized steady-state fluorescence emission $I_F(\lambda^{(1)})$ after one-photon excitation (acidic state = dotted line and empty disks; basic state = solid line and filled disks). (a) **4-PYMPO**; (b) **4-PYMPO**−$\mathbf{NH_2}$; (c) **4-PYMPOM**. Solvent: Britton-Robinson buffer[45] (acetic acid, boric acid, phosphoric acid) at 0.1 M. T = 293 K. The characteristics of dichroic mirror (thick line) and filters (gray zone) used for spectral separation of the emission light are also indicated, as well as the excitation wavelength (arrow); such conditions were used to adopt $Q = \infty$ for fitting. Adapted from ref 37.

τ_D, can be analyzed after calibration of the illuminated volume V and of the beam waist by recording the FCS autocorrelation curve from a solution of a reference fluorophore such as fluorescein at a known concentration. The extracted $G_D(0)$ value reasonably conformed to the expectation based on the nominal concentrations. In addition, the fits, respectively, provided 370 ± 30, 470 ± 30, and 440 ± 30 $\mu m^2\ s^{-1}$ for the diffusion coefficients of the acidic states of **4-PYMPO**, **4-PYMPO**−$\mathbf{NH_2}$, and **4-PYMPOM** at 293 K. Such values satisfactorily compare with the diffusion coefficient of fluorescein that is a slightly larger molecule than the present probes; under similar conditions, the diffusion coefficient of fluorescein is 300 ± 30 $\mu m^2\ s^{-1}$.[14]

In the case of **4-PYMPO**, we also measured the diffusion coefficient at a pH much above its pK_a: at pH = 12, we found a value of 400 ± 30 $\mu m^2\ s^{-1}$ at 293 K. The similarity between the values obtained for the acidic and basic states is in agreement with the similarity of the size and the shape of both states. This observation pushed us to adopt, for all the investigated pH indicators, the value of the diffusion coefficient that was measured in the acidic state where the brightness was at the largest under our experimental conditions.

D. Rate Constants for Proton Exchange. D.1. Design of the Experiments. The Theoretical Analysis section suggested that working at pH = pK_a is the most favorable to reveal the kinetic behavior of a fluorescent pH probe by FCS. Nevertheless,

Table 1. Photophysical Properties, Protonation Constants (pK_a (0.1), Diffusion Coefficients (d (30 í m^2 s^{-1}), and Rate Constants for Proton Exchange (k_{13} (10% s^{-1} and k_{31} (10% M^{-1} s^{-1}) of **4-PYMPO**, **4-PYMPO-NH$_2$**, and **4-PYMPOM**[a]

	4-PYMPO[b]	4-PYMPO–NH$_2$[b]	4-PYMPOM[b]	4-PYMPOM[c]
ì$^{(1)}_{max}$ ($_{max}$)[d]	390 (21)/332 (21)[e]	355 (23)/326 (19)[e]	380 (19)/330 (17)[e]	382 (11)/330 (14)
ì$^{(1)}_{em}$ [¼$_F$][f]	569 [0.3]/472 [0.5][e]	530 [0.7]/465 [0.8][e]	550 [0.5]/465 [0.8][e]	549 [0.4]/444 [0.8]
ì$^{(2)}_{max}$ (ä$_{2,max}$)[g]	800 (65)/710 (5)[e]	710 (60)/710 (15)[e]	800 (60)/710 (10)[e]	
pK_a (0.1	4.3[e]	5.7[e]	5.7[e]	5.3
d	370	470	440	690
10^{-4}k_{13}	80	3	1	6
10^{-10}k_{31}	1.2	1.3	1.5	3.2

[a] T) 293 K. [b] Solvent/water. [c] Solvent: acetonitrile/water 60:40 (v/v). [d] Maxima of single-photon absorption ì$^{(1)}_{max}$ (nm). Molar absorption coefficients for single-photon absorption at ì$^{(1)}_{max}$, $_{max}$ ((10%; mM^{-1} cm^{-1}). [e] From ref 37. [f] Maxima of steady-state fluorescence emission ì$^{(1)}_{em}$ (nm). Quantum yields of fluorescence ¼$_F$ ((5%). [g] Maxima of two-photon excitation spectra ì$^{(2)}_{max}$ (nm) in the investigated 700- 900 wavelength range. Two-photon excitation cross sections at ì$^{(2)}_{max}$, ä$_{2,max}$ ((20%; GM, 1 GM) 10^{-50} cm^4 s (photonåmolecule)$^{-1}$).

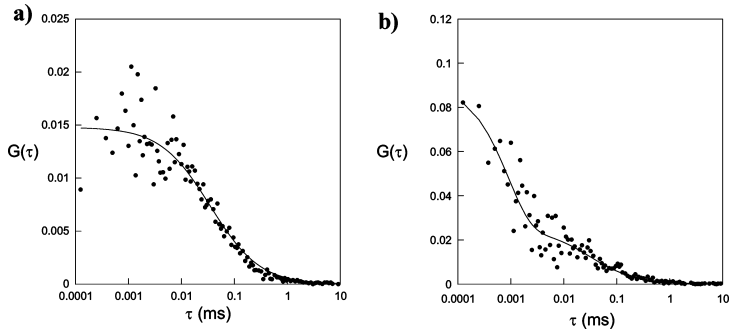

Figure 5. FCS autocorrelation curves recorded at 293 K from solutions of **4-PYMPO** (ì$^{(2)}_{exc}$) 800 nm). (a) pH) 2.0. The fit according to eq 4 yields $\overline{N/V}$) 110 (10 nM and d) 370 (30 í m^2 s^{-1}. (b) pH) 4.6. Using d) 370 (30 í m^2 s^{-1} and pK_a) 4.3, the fit with eq 3 yields $\overline{N/V}$) 75 (10 nM, pH) 4.70 (0.05, and ô$_{13}$) 0.9 (0.1 í s.

the analysis of the kinetic information from the FCS autocorrelation function requires a careful examination here. In fact, the exchange between the acidic A H and basic A states of a fluorescent pH indicator involves more than one chemical reaction, 1, and three components. The relevant minimal mechanism already implies three chemical reactions and five components (Figure 7a).[42,43,46] In the presence of a second acid-base nonfluorescent couple {Y H,Y } such as a buffer,[19,23,25-27] the minimal mechanism of proton exchange even contains six chemical reactions and seven components (Figure 7b).[42] In such a complicated dynamical system, a numerical approach could be required to extract rate constants from the experimental autocorrelation function. In fact, much simplification results from (i) considering that only the chemical reactions that involve brightness alterations can be visualized with FCS (in relation to Figure 7b, the relevant reactive channels with exchange between A H and A are 13, 23, and 33′) and (ii) applying a simplifying assumption that was already fruitfully used above: at low concentration in a fluorescent pH indicator, the concentration of most chemical species is independent of the occurrences of the conversions between the A and A H states and diffusion and chemistry are no longer correlated (see Supporting Information).

To address which relevant reactive channel had to be taken into consideration for the FCS analysis, we first noticed that, in a closed system submitted to the reactions displayed in Figure 7b, the four conservation laws (conservation of {A H,A } is A_{tot}) $\overline{AH} + \overline{A}$, conservation of {Y H,Y } is Y_{tot}) $\overline{YH} + \overline{Y}$, conservation of oxygen is O_{tot}) $\overline{H_2O} + \overline{OH}$, and the electroneutrality) imply only three independent processes.[47] In FCS, the chemical relaxation only manifests itself by three noninfinite relaxation times and it is essentially governed by the three fastest exchange processes displayed in Figure 7b. In relation to our experiments that involved fluorescent pH indicators with pK_a(A H /A) 5, we considered two different situations.

In the first situation, a diluted strong acid with pK_a(Y H /Y) < 0 fixes the pH in the 4- 6 ([pK_a(A H /A) - 1; pK_a(A H /A) + 1]) range. First, the rate constants for proton transfer between two acid- base couples are generally limited by diffusion when transfer occurs from the strongest acid to the strongest base.[42] Then, one can derive orders of magnitude for the ô$_{ij}$ associated to each reaction (see Supporting Information Table 1S; case 1). The three smallest relaxation times are ô$_{13'}$, ô$_{12}$, and ô$_{13}$ with ô$_{13'}$, ô$_{12}$ < ô$_{13}$. Second, H is essentially equal to $\overline{H}$ beyond the ô$_{13'}$ time scale. Indeed, channels 12 and 13 do not involve considerable amounts of protons at the 10^{-4}- 10^{-6} M relevant

(45) Frugoni, C. *Gazz. Chim. Ital.* **1957**, *87*, 403- 407.
(46) Here, one here assumes that the solution is dilute enough to neglect the reaction

A H + A h A + A H

(47) Lemarchand, H.; Guyot, F.; Jousset, L.; Jullien, L. *Thermodynamique de la Chimie*; Hermann: Paris, 1999.

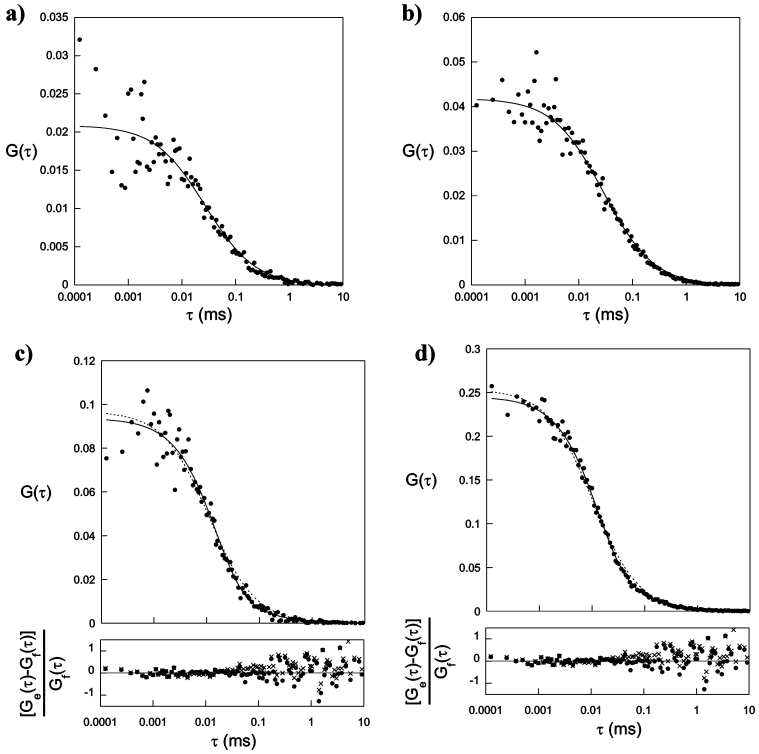

Figure 6. FCS autocorrelation curves recorded at 293 K from solutions of **4-PYMPO**−**NH_2** (a and c) or of **4-PYMPOM** (b and d) ($\lambda_{exc}^{(2)}$ = 800 nm). (a) pH = 2.0. The fit according to eq 4 yields $\bar{N}/V = 80 \pm 10$ nM and $d = 470 \pm 30$ $\mu m^2\ s^{-1}$. (b) pH = 2.0. The fit according to eq 4 yields $\bar{N}/V = 40 \pm 10$ nM and $d = 440 \pm 30$ $\mu m^2\ s^{-1}$. (c) pH = 6. Using $d = 470 \pm 30$ $\mu m^2\ s^{-1}$ and pK_a = 5.7, the fit with eq 3 (solid line) yields $\bar{N}/V = 70 \pm 10$ nM, pH = 6.0 ± 0.1, and $\tau_{13} = 25 \pm 1$ μs. (d) pH = 6. Using $d = 440 \pm 30$ $\mu m^2\ s^{-1}$ and pK_a = 5.7, the fit with eq 3 (solid line) yields $\bar{N}/V = 20 \pm 5$ nM, pH = 5.9 ± 0.1, and $\tau_{13} = 20 \pm 1$ μs. In (c) and (d), the fit with eq 4 is displayed with the dotted line and with the cross markers in the analysis of the residues.

concentrations in $\mathscr{YH}$ if $C < 1$ μM. Here, FCS reveals the kinetics of reaction 13. The approximate expression of the autocorrelation function becomes

$$G(\tau) = G_D(\tau)\left[1 + \frac{K_{13}}{\bar{H}}\left(\frac{Q-1}{Q + \frac{K_{13}}{\bar{H}}}\right)^2 e^{-(\tau/\tau_{13})}\right] \qquad (9)$$

in relation to the notations introduced in Figure 7b ($\tau_{13} = [k_{13} + k_{31}(\bar{H} + \bar{A})]^{-1} \approx [k_{13} + k_{31}\bar{H}]^{-1}$).

In the second situation, a buffer with p$K_a(\mathscr{YH}/\mathscr{Y}) \approx 5$ at a significant concentration (typically above 10 mM) is used to fix the pH in the 4−6 range. The three smallest relaxation times are now $\tau_{13'}$, $\tau_{23'}$, and $\tau_{33'}$ (see Supporting Information Table 1S; case 2). $\tau_{33'} = [k_{33'}(\bar{A} + \overline{YH}) + k_{3'3}(\overline{AH} + \bar{Y})]^{-1} \approx [k_{33'}\overline{YH} + k_{3'3}\bar{Y}]^{-1}$ is always the smallest among the three. Fluctuation amplitudes in concentrations of $\mathscr{YH}$ and $\mathscr{Y}$ can be neglected under the present experimental conditions. One eventually notices that $\bar{Y} \gg \overline{AH}$ and $\overline{YH} \gg \bar{A}$. The approximate expression of the autocorrelation function is now

$$G(\tau) = G_D(\tau)\left[1 + \frac{\bar{Y}}{K_{33'}\overline{YH}}\left(\frac{Q-1}{Q + \frac{\bar{Y}}{K_{33'}\overline{YH}}}\right)^2 e^{-(\tau/\tau_{33'})}\right] \qquad (10)$$

One notices that the amplitudes Ξ are identical in both envisaged situations because $K_{13}/\bar{H} = \bar{Y}/(K_{33'}\overline{YH})$. In contrast, the chemical relaxation time that is observed in FCS is τ_{13} in the first case whereas it is $\tau_{33'}$ in the second.

D.2. Results. The preceding considerations were significant to measure rate constants by FCS. In fact, $\tau_{33'}$ could be typically lower than the time resolution of the autocorrelator at large enough concentrations in buffer. Then, no kinetic information could be extracted from $G(\tau)$. Therefore, we generally conducted the kinetic experiments in the absence of buffer. In particular, all the solutions were degazed before FCS measurement to avoid any possible interference with the acidic and basic species arising from dissolution of carbon dioxide.

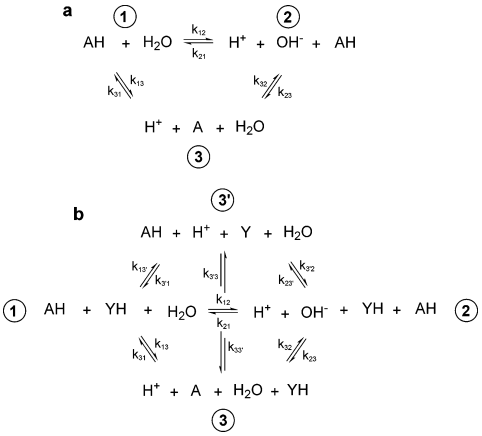

Figure 7. Reactions involved in the mechanism of dissociation/recombination of an acid−base couple, $\mathcal{AH}/\mathcal{A}$, in aqueous solution in the absence (a) or in the presence (b) of another acid−base couple, $\mathcal{YH}/\mathcal{Y}$.

We first prepared degazed unbuffered solutions of **4-PYMPO**, **4-PYMPO**−**NH$_2$**, and **4-PYMPOM** at a pH around their pK_a. Under such conditions, we extracted the pH from the fluorescence emission spectrum of each pH indicator by using a ratiometric approach relying on emission.[36,37] We also used under argon pH indicator sticks (precision: ±0.25 pH unit) or the indications of a pH meter when the latter were reliable. All indications were coherent with a precision that we estimate at 0.2 pH unit.

Figures 5b and 6c,d display typical experimental FCS autocorrelation curves for degazed solutions of **4-PYMPO**, **4-PYMPO**−**NH$_2$**, and **4-PYMPOM** at a pH around their pK_a in the absence of buffer. In relation to any chemical contribution to the correlation function, one is mainly concerned with the $G(0)$ value as well as with a possible new threshold manifesting itself in the correlation function.

For **4-PYMPO**, Figure 5b clearly evidences both features. At a similar nominal concentration of the solutions, $G(0)$ is much larger at pH = 4.6 (Figure 5b) than at pH = 2 (Figure 5a). Moreover, one notices two thresholds in the correlation function that is displayed in Figure 5b. The threshold associated with diffusion was already present in Figure 5a. In addition, there is another threshold at shorter times. To clear the origin of this second threshold, we first checked that it was not associated with the formation of the triplet state by recording FCS autocorrelation curves at different laser powers. They were essentially identical except for alterations of the signal-to-noise ratio. We also recorded the FCS autocorrelation curves from solutions of **4-PYMPO** at the same pH but in the presence of 100 mM buffer. In contrast to the experiment performed in the absence of buffer, the autocorrelation curve was essentially similar to the one recorded at pH = 2. This result was anticipated from eq 10 because $\tau_{33'}$ would be typically in the nanosecond range under such conditions. Therefore, we concluded that the second threshold displayed in Figure 5b was associated with the contribution of the reactive channel 13 to the autocorrelation function. Using $d = 370 \pm 30$ μm^2 s^{-1} and p$K_a = 4.3$,[37] we obtained the fit with eq 9 yielding $\bar{N}/V = 75 \pm 10$ nM, pH = 4.70 ± 0.05, and $\tau_{13} = 0.9 \pm 0.1$ μs. The extracted values of $\bar{N}/V$ and of pH are in line with the nominal concentration that was used during the experiment and the independent pH measurement. From pH and τ_{13}, we then derived $k_{13} = 8 \pm 1 \times 10^5$ s^{-1} and $k_{31} = 1.2 \pm 0.1 \times 10^{10}$ M^{-1} s^{-1}. k_{31} is close to the diffusion limit and is in line with the values reported for the comparable pyridine and imidazole.[42,43]

For **4-PYMPO**−**NH$_2$** and **4-PYMPOM**, the chemical signature is not as apparent as that for **4-PYMPO** in the autocorrelation curve at pH ≈ pK_a. In particular, only one threshold is visible in Figure 6c,d that were, respectively, recorded at pH = 6.1 and 6.0. Nevertheless, $G(0)$ clearly exceeds the corresponding value at a pH much lower than its pK_a for comparable nominal concentrations, and the previous observation suggests that chemical exchange is involved in the shape of the autocorrelation curves. Under such conditions, the possibility of access to the rate constants k_{13} and k_{31} depends on the relative values of τ_{13} and τ_D. As suggested by Figure 1b, the rate constants cannot be extracted anymore if $\tau_{13} \gg \tau_D$. We consequently attempted to fit the data shown in Figure 6c,d either with eq 4 (diffusion only) or with eq 9 (diffusion and chemical reaction). In fact, the fits with eq 4 reveal a systematic error that is not apparent when eq 9 is used. In the case of **4-PYMPO**−**NH$_2$**, we thus used $d = 470 \pm 30$ μm^2 s^{-1} and p$K_a = 5.7$[36,37] to extract from the fit with eq 9 $\bar{N}/V = 70 \pm 10$ nM, pH = 6.0 ± 0.1, $\tau_{13} = 25 \pm 1$ μs, $k_{13} = 3 \pm 1 \times 10^4$ s^{-1}, and $k_{31} = 1.3 \pm 0.2 \times 10^{10}$ M^{-1} s^{-1}. For **4-PYMPOM**, we correspondingly obtained with $d = 440 \pm 30$ μm^2 s^{-1} and p$K_a = 5.7$[37] $\bar{N}/V = 20 \pm 5$ nM, pH = 5.9 ± 0.1, $\tau_{13} = 20 \pm 1$ μs, $k_{13} = 3 \pm 1 \times 10^4$ s^{-1}, and $k_{31} = 1.5 \pm 0.2 \times 10^{10}$ M^{-1} s^{-1}. $\bar{N}/V$ and pH agree with the expectation from the nominal concentration and with the independent pH measurement. Noticeably, the k_{31} values observed for **4-PYMPO**−**NH$_2$** and **4-PYMPOM** are again close to the diffusion limit.[42,43] These results suggest that the presence of one ortho amino, or two ortho methyl substituents, does not significantly affect the rate of reaction of the nitrogen lone pair of the pyridine ring with the proton.

pH Measurements by FCS. A. General Case. As indicated in the Theoretical Analysis section, the issues of measuring rate constants or reactant concentrations by FCS are closely related. Thus, the autocorrelation curves displayed in Figures 5b and 6c,d can be used to illustrate how FCS should yield pH in a general case.

Provided that one considers that the pK_a and the brightness of both acidic and basic states of the pH indicator are known in the investigated medium, the analysis of the amplitude of the autocorrelation function would provide pH after fitting with eq 3. Indeed, the pH extracted from the fits in Figures 5b and 6c,d are in fair agreement with the pH value measured by other methods. Independently, pH can also be extracted from the time dependence of the autocorrelation function if one knows the pK_a and k_{31} for the fluorescent pH indicator. Ultimately, both methods can be applied to evaluate the coherence of the results if all the relevant information about the fluorescence pH indicator is available and reliable.

B. Example of Calibration-Free pH Measurement. B.1. Evaluation of the Constraints on the Fluorescent pH Indicator. The "calibration-free approach" requires that (i) the protonation of the fluorescent pH indicator is controlled by

diffusion and (ii) it is possible to find experimental conditions (excitation wavelength, optical filters, etc.) such that the fluorescence emission from one state, acidic or basic, may be neglected with regards to the other under the same conditions.

The preceding measurements in water showed that the protonation of the pyridine basic site is indeed limited by diffusion for **4-PYMPO**, **4-PYMPO−NH$_2$**, and **4-PYMPOM**. In an unknown medium, questions still arise as to whether (i) diffusion is still the limiting process for protonation and (ii) D and a in eq 6 are medium-dependent (d can be directly evaluated from the diffusion contribution in the autocorrelation function). In relation to the former question, one has to be concerned with the energy barrier associated with the solvent reorganization occurring during protonation.[48] Water is a strongly polar solvent that is anticipated to promote among the largest corresponding energy barriers. Even in water, the measured k_{31} value does not reveal the presence of such a barrier. Other conditions should be typically less polar, and the barrier should not manifest either. In relation to the latter, two main issues have to be addressed. We first notice that a should not strongly depend on the ionic strength[39] because the present probes do not involve highly charged species. In contrast, water develops a particular relation to the proton. This feature may determine too large values of D and a with regard to predictions that would only rely on the proton diameter and on the solvent viscosity.[1,39] In fact, we estimate that the k_{31} value should not depart from 1×10^{10} to 2×10^{10} M^{-1} s^{-1} by a factor exceeding a few units for most situations encountered in common liquids. In view of the logarithmic dependence of pH on proton concentration, the corresponding incertitude on k_{31} should introduce at most an error of a few tenths on the extracted pH.

We investigated the photophysical features and the significance of solvatochromism on the absorption and emission properties of **4-PYMPO** and **4-PYMPO−NH$_2$** in a preceding report.[37] **4-PYMPOM** is expected to exhibit a behavior similar to that of **4-PYMPO** because the methyl substituents generally only slightly alter photophysical properties. First, the absorption and the fluorescence emission occur at larger wavelengths for the acidic state than for the basic state (see Figure 4). In the present series, we also showed the following: (i) The maximum of single-photon absorption is not sensitive to solvent polarity for the neutral basic states, whereas it slightly drops when solvent polarity is increased for the charged acidic state. In relation to two-photon absorption, we expect a similar trend because two-photon absorption spectra generally satisfactorily compare with the one-photon absorption spectra after dividing the wavelength by a factor of 2 for unsymmetrical compounds.[49,50] (ii) The maximum of emission after single-photon absorption increases with the solvent polarity for the basic state, whereas it is not significantly sensitive to solvent polarity for the acidic state. Thus, the photophysical features brought us to conclude that one could easily find a large enough excitation wavelength to considerably and selectively excite the acidic state of the present fluorescent indicators ($\mathcal{L}_{\mathcal{A}} \gg \mathcal{L}_{\mathcal{A}}$), whatever the medium considered.

In principle, the three present fluorescent pH probes were appropriate to evaluate the calibration-free approach. Upon consideration of the similarity of their photophysical properties, the final choice would essentially rely on the proton concentration $\bar{H}$ to be measured because one ideally looks for a fluorescent pH indicator such that $\bar{H} = 10^{-pK_a}$. We retained **4-PYMPOM** for the following series of experiments.

B.2. Results. To evaluate the calibration-free approach that was evoked above, we conceived model experiments. We considered a solvent containing various amounts of a strong acid (triflic acid/CF_3SO_3H), and we aimed at using FCS and **4-PYMPOM** to determine the unknown concentrations in the proton. In parallel, we measured the protonation constant of **4-PYMPOM** and calibrated a pH meter used to monitor the proton activity in the corresponding solvent. This allowed us to evaluate the validity of the FCS results by directly measuring pH either from a ratiometric approach relying on fluorescence emission or from the pH meter indication after an appropriate calibration.

We chose to work in a mixture of water and acetonitrile to perform this series of experiments. In fact, this system remains simple for model experiments, but the corresponding solvent organization is rather controversial.[51] In particular, one cannot reasonably assume that the **4-PYMPOM** photophysical (quantum yields of fluorescence, lifetimes, etc.) and acidobasic (pK_a) properties should be identical in water and in the acetonitrile/water mixture. In such a context, **4-PYMPOM** should be a priori useless as a fluorescent pH indicator with a classical approach requiring the preliminary knowledge of the items (iii)−(iv) evoked in the Introduction.

The acetonitrile/water ratio was optimized (i) by reducing the water content to essentially suppress the protonation of the basic state of **4-PYMPOM** that occurs during the lifetime of its excited state[37] and (ii) by maintaining an as large as possible water content to facilitate the calibration of the pH meter using a glass electrode conditioned in water. We retained 60:40 (v/v) acetonitrile/water as a solvent.

Figure 8a displays a typical FCS autocorrelation curve that was recorded from a solution of **4-PYMPOM** in 60:40 (v/v) acetonitrile/water solution at an "unknown" proton concentration. In line with the calibration-free approach, the experimental data were fitted with eq 9 by taking $k_{31} = 2.0 \times 10^{10}$ M^{-1} s^{-1} as the only fixed parameter. We found $\bar{N}/V = 40 \pm 10$ nM, $\tau_D = 30$ μs, $pK_a = 5.1$, and $\bar{H} = 10 \pm 1$ μM.[52]

The extracted value of $\bar{N}/V$ was in line with the nominal **4-PYMPOM** concentration. τ_D reasonably compared with the diffusion time that was observed in the presence of an excess

(48) For an illustration of the role of solvent reorganization during a chemical reaction, see, for instance: Laage, D.; Thompson, W. H.; Blanchard-Desce, M.; Hynes, J. T. *J. Phys. Chem. A* **2003**, *107*, 6032−6046.

(49) Cogné-Laage, E.; Allemand, J.-F.; Ruel, O.; Baudin, J.-B.; Croquette, V.; Blanchard-Desce, M.; Jullien, L. *Chem.−Eur. J.* **2004**, *10*, 1445−1455.

(50) Xu, C.; Webb, W. W. *J. Opt. Soc. Am. B* **1996**, *13*, 481−491.

(51) Catalán, J.; Díaz, C.; García-Blanco, F. *Org. Biomol. Chem.* **2003**, *1*, 575−580.

(52) We performed preliminary simulations to evaluate the reliability of the parameter values that can be extracted from FCS autocorrelation curves by using eq 9. We used eq 3 to generate FCS autocorrelation curves $G_t(\tau)$ with $\bar{N} = 1$, $\omega = 10$, $\bar{H} = K$, and $Q = \infty$ for different $k\tau_D$ values. Then, we introduced some noise in the calculated autocorrelation functions to simulate "experimental" autocorrelation functions $G_e(\tau)$ by adopting the typical noise level that was observed during our present FCS measurements ($-0.1 < [G_e(\tau) - G_t(\tau)]/G_t(\tau) < 0.1$). We finally used eq 9 to fit the simulated experimental data in the 10^{-3}−10^3 range for (τ/τ_D) by using $k\tau_D$, $\bar{N}$, and ($K/\bar{H}$) as floating parameters. The results are given in Supporting Information Table 2S and Figure 4S. The values of the extracted parameters never deviate from the expected ones by more than 40% as long as $100 > k\tau_D > 0.1$. They are at the most satisfactory for $k\tau_D = 1-10$ where the threshold associated to the chemical reaction is at the most visible in the FCS autocorrelation curve.

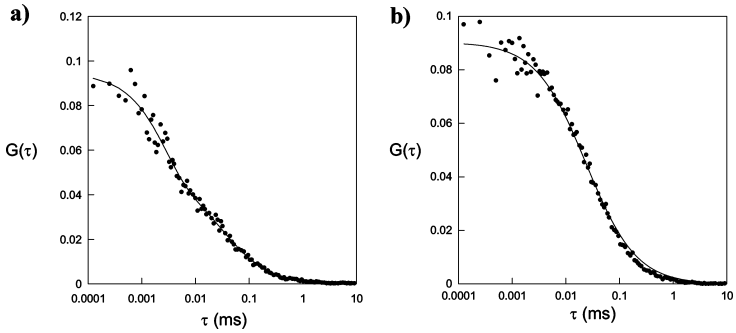

Figure 8. FCS autocorrelation curves recorded at 293 K from solutions of **4-PYMPOM** in 60:40 (v/v) acetonitrile/water solution ($\lambda_{exc}^{(2)} = 800$ nm). (a) At "unknown" proton concentration ($\lambda_{exc}^{(2)} = 800$ nm) ($\overline{H} = 6$ μM). Using $k_{31} = 2 \times 10^{10}$ M^{-1} s^{-1}, the fit with eq 3 yields $\overline{N}/V = 40 \pm 10$ nM, $\tau_D = 30$ μs, pK_a = 5.1 and $\overline{H} \approx 10 \pm 1$ μM. (b) Large excess of proton ($\overline{H} \approx 4$ mM). The fit according to eq 4 yields $\overline{N}/V = 20 \pm 5$ nM and $d = 690 \pm 30$ μm^2 s^{-1}.

of acid. In fact, we expected $\tau_D \approx 25$ μs from the 690 ± 30 μm^2 s^{-1} value of the **4-PYMPOM** diffusion coefficient that was extracted from fitting the data shown in Figure 8b with eq 4. Using the value of the **4-PYMPOM** diffusion coefficient obtained in water as a reference and considering that the diffusion coefficient is inversely proportional to medium viscosity η, we should deduce $\eta = 0.9$ Pa s for the viscosity of the unknown medium (0.6 Pa s from the reference experiment illustrated in Figure 8b). These values are in reasonable agreement with available literature data that give 0.8 Pa s for the viscosity of 60:40 (v/v) acetonitrile/water.[53]

The pK_a was independently extracted from analyzing the evolution of **4-PYMPOM** fluorescence emission in 60:40 (v/v) acetonitrile/water as a function of the concentration in triflic acid. As shown in Figure 9a, the addition of a proton promotes the drop in emission from the **4-PYMPOM** basic state and the increase of the red shifted band associated to the **4-PYMPOM** acidic state. Thus, we found p$K_a = 5.3 \pm 0.1$. This value satisfactorily compares with the value that was directly extracted from the FCS data.

To evaluate the unknown concentration in the proton independently of the FCS measurement, we relied on two different tools. We first used **4-PYMPOM** as a fluorescent pH indicator to extract the proton concentration from the ratiometric analysis in emission, displayed in Figure 9b. We also used the indication pH′ of the glass electrode of a pH meter that was preliminarily calibrated by recording the indication from standard solutions that contained known concentrations, $\overline{H}$, in the proton. We obtained $\overline{H} = 6$ μM under the conditions used to record the FCS autocorrelation curve of Figure 8a. The comparison against the FCS result is again favorable.

Eventually, we directly measured the rate constant k_{31} to evaluate the value that was taken a priori. We analyzed the dependence of $1/\tau_{13}$ on $(1 + (1/\Xi))$ in a series of experiments at different proton concentrations in 60:40 (v/v) acetonitrile/water.

$$\frac{1}{\tau_{13}} = k_{13}\left(1 + \frac{1}{\Xi}\right) \qquad (11)$$

The results are displayed in Figure 9c. Indeed, we found that τ_{13} is linearly dependent on $1 + (1/\Xi)$. In addition, we extracted $k_{31} = 3.2 \pm (0.2 \times 10^{10})$ M^{-1} s^{-1} from the slope of the linear fit displayed in Figure 9c. Such a larger value than the one found in water is in line with the low viscosity of the 60:40 (v/v) acetonitrile/water mixture. By correcting the value measured in water by the relative viscosity of the present solvent to the one of water (0.6), we expected $k_{31} \approx 2.5 \times 10^{10}$ M^{-1} s^{-1}.

In relation to the calibration-free approach, the directly measured k_{31} value is close to the one that we used a priori. To evaluate the significance of the error in using 2×10^{10} M^{-1} s^{-1} instead of $3.2 \pm (0.2 \times 10^{10})$ M^{-1} s^{-1} for the k_{31} value, we again fitted with eq 6 the data displayed in Figure 8a. As expected, we did not notice any considerable change with regards to the extracted values of $\overline{H}$ and pK_a: 6 μM and 5.2, respectively, were found.

C. Discussion. The preceding experiments confirm that FCS provides a powerful approach to measure reactant concentrations. In the case of the proton, we showed that a proper design of the fluorescent pH indicator makes it possible to measure pH between 4 and 6 with FCS after two-photon excitation. The lower limit is actually set by the present time resolution of the autocorrelator. In principle, pH indicators with pK_a around 9 would similarly open the way to pH measurements between 8 and 10. Indeed, the rate constants for reaction between the acidic states of fluorescent pH indicators and the hydroxide ion are generally limited by diffusion[42] so as to lead to results similar to the present ones after symmetry around pH = 7. In contrast, it seems difficult to cover the 6−8 pH range when FCS after two-photon excitation is used. In fact, the low concentration in the proton or in hydroxide yields $\tau_\chi > \tau_D$ under such conditions. From this point of view, FCS after one-photon excitation seems more advantageous to continuously cover the 4−10 pH range[19] because appropriate optical setup allows $\tau_\chi < \tau_D$ in the whole range of pHs.

As far as the present FCS calibration-free titration approach is concerned, we showed that it is indeed possible to extract pH without preliminary calibration from a FCS autocorrelation curve after a proper design of the fluorescent pH probe. Although rather limited in most cases, the error on the reactant concentration should mainly originate from the uncertainty on

(53) The data are provided by the Waters Company. HPLC Troubleshooting, Neue, U. D., Waters Corporation, www.waters.com.

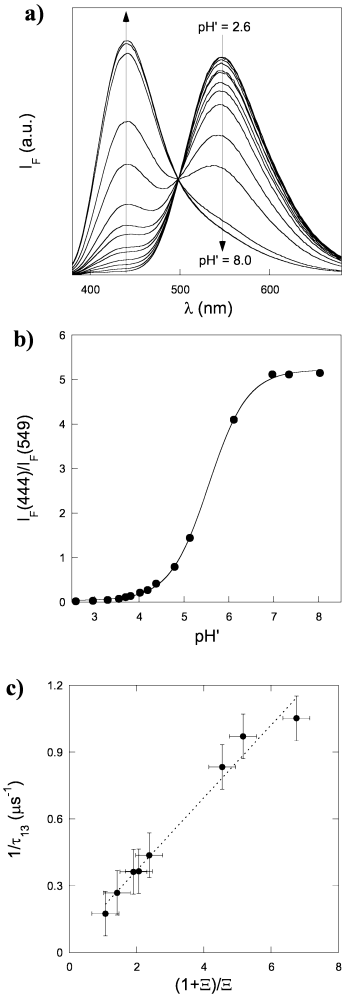

Figure 9. (a) Dependence on pH′ of the emission spectra of **4-PYMPOM** after one-photon excitation (from acidic to basic: pH′ = 2.6, 3.0, 3.3, 3.5, 3.7, 3.8, 4.0, 4.2, 4.4, 4.8, 5.1, 6.1, 7.0, 8.0). (b) Evolution on pH′ of the ratio of the fluorescence emissions at 444 and at 549 nm after one-photon excitation. Experimental data markers: fit = line. $\lambda_{exc}^{(1)}$ = 355 nm and [**4-PYMPOM**] = 5 μM. (c) Dependence of $1/\tau_{13}$ on $1/\Xi$. τ_{13} and Ξ were extracted from a series of FCS experiments at different proton concentrations. Solvent: acetonitrile/water 60:40 (v/v), T = 293 K. See text and Experimental Section.

the value of the rate constant of association of the reactant with the fluorescent probe. A satisfactory order of magnitude of this can be evaluated with eq 6 by using parameter values extracted from the autocorrelation function (*d* and *D* from the diffusion contribution that yields the local viscosity) and from the structures of the probe and of the reactant (*a* and the geometrical factors involved in *d* and *D*). Here, it is worth it to emphasize that the classical approaches for titrations with fluorescent probes rely on values of parameters (association constants and photophysical features) that cannot be easily predicted in an unknown medium on the basis of the structures of the reactant and on the probe only.

Making FCS a superior tool to measure reactant concentrations requires us to rely on the kinetic information of the FCS autocorrelation function. Beyond the photophysical and the thermodynamic aspects that may already be demanding, a proper molecular design of the kinetic properties of the fluorescent probes is a crucial issue here. Ideally, the relaxation pathways after fluctuations from equilibrium should be known and controlled, even when dealing with unknown media. In fact, it is the capability to reduce the interference of buffering species that will probably determine the impact of FCS for measuring reactant concentrations. If the information related to the buffer is lacking (like in a biological cell for instance), the buffer will "only" complicate the analysis of the kinetic content of the autocorrelation curve in the best case. Yet, it can even forbid any concentration measurement if it dominates the relaxation with a chemical relaxation time lower than the temporal resolution of the autocorrelator.

From the previous point of view, reliable pH measurement under any situation will be design demanding. In the present work, we envisaged the reduction of the rate constants involving the 33′ exchange without strongly altering k_{31} by playing with the steric hindrance around the basic site of $\mathcal{A}$. We did succeed in keeping k_{31} at the largest for the three investigated fluorescent pH indicators. In contrast, we failed to decrease enough $k_{33'}$ to measure pH by FCS in 100 mM buffered solutions with any present pH probe (if one assumes that one of the reactions in the 33′ channel is limited by diffusion,[42] the crossing between both regions governing the relaxation of the fluctuations, τ_{13} or $\tau_{33'}$, occurs as low as 10^{-4} M for a buffer with $pK_a(\mathcal{HA}/\mathcal{A})$ ≈ 5). With such nonoptimized pH probes, we had thus to totally control the composition and the reactivity of the medium in a purpose of validation of the present FCS approach to measure proton concentration: We consequently adopted rather severe experimental conditions (degazing of the solutions to avoid interference with any buffer arising from dissolution of carbon dioxide, absence of added buffer, etc.). To face the measurement of proton concentration in an unknown media, one would ideally design an improved fluorescent pH probe with a proton exchange that would occur in the 10 μs range via the 13 reactive channel without any interference of the 33′ reactive channel. At that point, it is interesting to notice that it was possible to measure rate constants for proton exchange in the green fluorescent protein (GFP) in heavily buffered media.[19,25−27] This observation suggests that coupling fluorescent pH indicators to acid−base of appropriate pK_a by a specific channel for the proton could provide attractive opportunities.

4. Conclusion

Fluorescence correlation spectroscopy clearly opens new roads for using specific fluorescent probes in the analysis of local reactant concentrations. Under many encountered situations, data treatment only involves simple analytical expressions that are derived after appropriate approximations. Under the less favorable circumstances, to extract an unknown reactant concentration from FCS data requires the same photophysical and thermodynamic information as that in a ratiometric approach. Nevertheless, the kinetic information contained in the FCS

observable may provide a distinct advantage to evaluate the coherence of the results and to improve the selectivity of the analysis. In the best cases, it is even possible to evaluate reactant concentrations in the absence of any preliminary calibration.

This report also emphasizes that the development of FCS as a powerful analytical tool will strongly depend on the availability of carefully tailored fluorescent indicators. Thermodynamic and photophysical constraints have first to be taken into account. Such criteria are rather classical to design specific fluorescent probes. Nevertheless, here probe brightness deserves special attention in relation to the submicromolar requirements of FCS, in particular, when multiphoton excitation is used. More unusual are the kinetic constraints to avoid interferences with buffering species that can alter or even cancel the relevant information contained in the FCS observable. In the present account, we engineered a series of fluorescent probes to illustrate the exciting opportunities provided by FCS after two-photon excitation to measure pH in a given range. Yet, performing reliable pH measurement in the absence of any information on buffering species is still challenging and will require further refinement in the molecular design of synthetic fluorescent probes.

5. Experimental Section

Chemicals. The syntheses of **4-PYMPO**, **4-PYMPO−NH$_2$**, and **4-PYMPOM** have already been reported elsewhere.[37] The analytical grade chemicals purchased from Aldrich were used without further purification. The 18 MΩ cm water was obtained from a Millipore setup. Acetonitrile was of spectroscopic grade.

Preparation of the Solutions. Stock solutions (50 μM) of the fluorescent pH indicators were prepared in 10^{-2} M triflic acid. These stock solutions were subsequently diluted to 100 nM in fluorescent pH indicators, either in 10^{-2} M triflic acid or in 10^{-2} M sodium hydroxide (measurement of diffusion coefficients at pH = 2 or pH = 12) or in water with pH adjustment with diluted solutions of triflic acid or sodium hydroxide (measurements at pH ≈ pK_a).

For the experiments performed in the presence of buffer, we used a Britton-Robinson buffer at 0.1 mol L^{-1} prepared according to ref 45.

Degazing was obtained by applying several freeze-thaw cycles to the solutions under a 1 mmHg vacuum. After the last cycle, the solution was settled under argon. It was eventually poured into the cell displayed in Supporting Information Figure 2S that was sealed under argon.

pH and pK_a Measurements. pH measurements were performed on a Standard pH meter PHM210-Radiometer Analytical that was calibrated with buffers at pH 4 and 7. For the measurements in the neutral solutions in the absence of any supporting salt (5 ≤ pH ≤ 7), we relied on indicator sticks (precision: ±0.25 pH unit).

To evaluate the concentration in the proton in a 60:40 (v:v) acetonitrile/water solution, we relied on the indication pH′ of the glass electrode of a pH meter that was preliminarily calibrated by recording the indication from standard solutions that contained known concentrations, $\bar{H}$, in the proton. Then, the experimental data were fitted according to a linear law. We obtained $-\log \bar{H}(M) = 8.09 \times 10^{-2} + 1.075$ pH′.

The evolutions of **4-PYMPOM** fluorescence in acetonitrile/water as a function of the concentration in the proton was analyzed with the SPECFIT/32TM Global Analysis System (Version 3.0 for 32-bit Windows systems) to extract the pK_a of the **4-PYMPOM** ground state.[54]

Spectroscopic Measurements. During the recording of the emission spectra, the temperature was regulated at 0.1 °C and was directly measured within the cuvettes.

Corrected fluorescence spectra were obtained from a Photon Technology International LPS 220 spectrofluorimeter (Photon Technology International, Monmouth Junction, NJ). Solutions for fluorescence measurements were adjusted to concentrations such that the absorption was below 0.15 at the excitation wavelength. The overall fluorescence quantum yields Φ_F were calculated from the relation in eq 12 where

$$\Phi_F = \Phi_{ref}\frac{A_{ref}(\lambda_{exc})}{A(\lambda_{exc})}\frac{S}{S_{ref}}\left(\frac{n}{n_{ref}}\right)^2 \qquad (12)$$

the subscript ref stands for standard samples. $A(\lambda_{exc})$ is the absorbance at the excitation wavelength, S is the integrated emission spectrum, and n is the refractive index for the solvent. The uncertainty in the experimental value of Φ_F was estimated to be ±10%. The standard fluorophore for the quantum yield measurements was quinine sulfate in 0.1 M H_2SO_4 with $\Phi_{ref} = 0.50$.[55]

The two-photon excitation spectra were recorded with a home-built setup[49] using the reported excitation spectrum of fluorescein for calibration.[50]

FCS Measurements. The two-photon excitation FCS setup displayed in Supporting Information Figure 1S consists of a laser source, a home-built microscope, and two avalanche photodiodes (APD).[56] The laser source is a mode-locked Ti/Sapphire laser (Mira 900, Coherent, Auburn, CA) pumped by a solid-state laser at 532 nm (Verdi, Coherent). Pumped at 5 W, the Ti/Sapphire laser generates 150 fs pulses at a 76 MHz repetition rate with about 700 mW average power output at 800 nm. The power is adjusted by means of neutral filters. The laser beam is expanded 3 times at the entrance of the microscope to reach a diameter of approximately 7 mm to fill up the back entrance of the employed objective. After the beam expander, the light is passed through a dichroic mirror and focused into the sample with a 60 times water-immersion objective (NA = 1.2, UPlanApo, Olympus). The fluorescence is collected through the same objective, reflected by the dichroic mirror, and filtered through short pass filters to absorb any possible diffused excitation infrared light. The light is then separated by a cube beam splitter with a 1:1 ratio and focused on the 200 μm^2 working surfaces of two APDs (SPCM-AQR-14, Perkin-Elmer, Vaudreuil, Canada). At the concentrations used throughout this paper, the typical signal on each APD was about 20 kHz during the experiments devoted to the measurement of the diffusion coefficients, whereas we typically obtained 6 kHz during the experiments where the chemical reaction was involved. The signal outputs of the APD modules (TTL pulses) are acquired by a digital autocorrelator module (ALV-6000, ALV, Langen, Germany) which computes online the cross-correlation function of the fluorescence fluctuations. The data are then stored in the computer and analyzed by a home-written routine which allows us to (i) select and average chosen successive acquisitions, (ii) make a least-squares fit for both single- and two-component cross-correlation functions with diffusion in two or three dimensions, and (iii) calculate the associated standard deviations.

The focused beam was assumed to adopt a 3D-Gaussian excitation profile characterized by $I = I_0 \exp[-(2(x^2 + y^2)/\omega_{xy}^2) - (2z^2/\omega_z^2)]$. It was calibrated before each measurement by using the diffusion of fluorescein in water at pH = 10 as a standard.[14] We typically obtained $\omega_{xy} \approx 0.4$ μm and $\omega_z/\omega_{xy} \approx 10$.

We investigated the dependence of the fluorescence emission as a function of the excitation power for all the compounds studied, and we chose the power to remain in the region of power-squared dependence (as a rule, the power before the entrance of the beam

(54) Gampp, H.; Maeder, M.; Meyer, C. J.; Zuberbühler, A. D. *Talanta* **1985**, *32*, 95−101. Gampp, H.; Maeder, M.; Meyer, C. J.; Zuberbühler, A. D. *Talanta* **1985**, *32*, 257−264. Gampp, H.; Maeder, M.; Meyer, C. J.; Zuberbühler, A. D. *Talanta* **1985**, *32*, 1133−1139. Gampp, H.; Maeder, M.; Meyer, C. J.; Zuberbühler, A. D. *Talanta* **1986**, *33*, 943−951.

(55) Demas, J. N.; Crosby, G. A. *J. Phys. Chem.* **1971**, *75*, 991−1024.

(56) Gosse, C.; Boutorine, A.; Aujard, I.; Chami, M.; Kononov, A.; Cogné-Laage, E.; Allemand, J.-F.; Li, J.; Jullien, L. *J. Phys. Chem. B* **2004**, *108*, 6485−6497.

expander was set to less than 60 mW). With those experimental conditions, no contribution of the triplet state to the experimental FCS curves was observed either.

A typical experiment consisted of a few hundreds of acquisitions of 2−5 s each, depending on the overall brightness, thus leading to a typical 30 min−2 h acquisition time.

Acknowledgment. This paper is dedicated to the memory of Professor André Rassat.

Supporting Information Available: Computation of the auto- and cross-correlation functions that are relevant to the present work. Experimental FCS setup (Figure 1S), sample-containing cell that was used during the present FCS experiments (Figure 2S), chemical process involving the smallest number of interconverting states that can be observed by FCS (Figure 3S), evaluation of the reliability of the parameter values that can be extracted from FCS autocorrelation curves by using eq 9 (Figure 4S), derivation of the intrinsic relaxation times τ_{ij} associated with the six chemical reactions displayed in Figure 7b (Table 1S), and evaluation of the reliability of the parameter values that can be extracted from FCS autocorrelation curves by using eq 9 (Table 2S). This material is available free of charge via the Internet at http://pubs.acs.org.

JA053909W

PIGEON " POCHE-GRILLE " LEGUMES EN VINAIGRETTE AUX ABATS

Guy Savoy

1 pigeon de 300g 3 mini-carottes 3 mini-poireaux 3 pois gourmands 5 haricots verts Petits pois et fèves 1 échalote 1 persil plat Fond blanc Huile d'olive 2 cuillères de vinaigre de xérès

1 - Préparer le pigeon (flamber, vider et brider) Hacher le foie du pigeon pour le jus.

2 - Eplucher et cuire à l'anglaise les légumes.

3 - Pocher le pigeon 3 à 4 minutes dans le fond chaud. Après, lever les filets et les cuisses.

4 - Cuire le foie du pigeon dans un sautoir. Déglacer au vinaigre de xérès, réduire et mouiller au fond blanc. Ajouter l'huile d'olive, le persil haché et l'échalote ciselée. Saler et poivrer.

5 - Griller les filets et les cuisses du pigeon côté peau. Glacer les légumes au beurre et dresser sur assiettes. Servir la vinaigrette aux abats en cassolette.

http://www.guysavoy.com/

Quatrième partie

Projet de recherche

Chapitre 1

Introduction

Les systèmes biologiques fournissent de formidables sujets d'études pour la physique. Polymères modèles, moteurs moléculaires, nanopores naturels, réseaux génétiques, repliement des protéines ou des ARNs sont autant d'exemples où l'interaction de la physique et de la biologie a donné lieux à de nombreux travaux intéressants ces dernières années.
Parmi ces sujets celui des moteurs moléculaires est celui qui me passionne le plus. Les propriétés de ces nanomachines sont étonnantes. Par exemple ils peuvent se mouvoir rapidement , compte tenu de leur taille, à faible nombre de Reynolds avec des rendements élevés (près de 100% pour la F1-ATPase, le plus petit moteur rotatif connu) en font des objets fascinants.
Il y a eu de nombreuses études, riches en résultats, sur les moteurs moléculaires impliqués dans les mouvements cellulaires (myosines, kinésines, dynéines) et des modèles physiques ont été proposé pour leur fonctionnement [60]. Cependant très peu de travaux ont porté sur les caractéristiques physiques des moteurs impliqués dans le transport d'ADN chez les procaryotes. Smith *et al.* [30] ont étudié l'encapsidation de l'ADN viral dans le phage $\phi 29$, Maier *et al.* ont pu mesurer l'incorporation d'ADN externe dans la bactérie *Bacilus subtilis*[61]. Nous même et le groupe de C. Bustamante [62, 63, 64] avons pu étudié quantitativement un moteur impliqué dans le déplacement des chromosomes lors de la division cellulaire de la bactérie *E. coli*.
Ces expériences ont en commun d'avoir mis en évidence des propriétés surprenantes pour ces moteurs. Ainsi ils sont capables d'exercer des forces plus grandes que les autres moteurs, ce qui dans le cas du virus permet d'obtenir une pression estimée à 6 MPa dans la capside, et ils sont parfois extrêment rapides (plus de $2\mu m/s$). Or ces moteurs, qui ne sont pas encore totalement caractérisés, sont impliqués dans des fonctions biologiques différentes et leur étude physique me semble être un sujet très intéressant. En particulier je pense m'intéresser au couplage translation-rotation de ces moteurs se déplaçant sur une hélice, à leur rendement et à l'influence des contraintes mécaniques sur leur activité.

Chapitre 2

Moteurs moléculaires et transfert d'ADN

2.1 Transfert d'ADN et division cellulaire

La division cellulaire chez les organismes dépourvus de noyau, comme les bactéries, est un processus qui est fortement différent de celui des eucaryotes que l'on apprend dans les cours élémentaires de biologie. Dans ces cours nous avons appris que lors de la division cellulaire on a d'abord la copie de l'ADN. Seulement ensuite il y a la séparation des chromosomes pour les déplacer dans les cellules filles. La ségrégation des chromosomes, se produit avant que les membranes cellulaires ne se séparent. Il est ainsi très improbable que la séparation finale des membranes cellulaires piège des bouts de chromosomes dans la mauvaise cellule fille. Cependant cette vision n'est pas vérifiée chez les procaryotes, où la copie de l'ADN et la ségrégation des chromosomes peuvent être concommitents. Ceci implique la nécessité d'un transport actif de l'ADN qui doit être efficace afin d'éviter de piéger l'ADN dans la mauvaise cellule fille. Chez les bactéries, une famille de moteurs moléculaires, dont les prototypes sont FtsK chez *E. coli* et SpoIIIE chez *Bacilus Subtilis* [65, 52], est impliquée dans ce transport d'ADN. Ces moteurs ont la propriété, au moment de la division cellulaire ou de la sporulation, de se placer au niveau du septum (lieu de sépération des deux cellules) (figure 2.1) et d'utiliser l'énergie chimique d'hydrolyse de l'Adénosine Tri Phosphate (ATP) pour littéralement pomper l'ADN en l'amenant dans le bon compartiment cellulaire.

Depuis quelques années nous étudions le moteur moléculaire d'*E. coli* nommé FtsK en utilisant la technique de micromanipulation des pinces magnétiques décrite plus haut. Nous avons pu montrer que c'est le plus rapide, le plus puissant moteur connu se déplaçant sur l'ADN. Il est capable de transporter plusieurs milliers de paires de bases à une vitesse $\sim 7000 bps/s$ et ceci contre des forces de tractions supérieures à $40pN$ [62]. De plus il présente l'originalité, très rare pour les moteurs moléculaires biologiques de changer de direction aléatoirement en l'absence de séquences spécifiques [62]. Enfin comme il se déplace sur une double hélice on s'attend à ce que son mouvement de translation soit couplé à de la rotation, comme on tourne autour de l'axe d'un escalier en collimaçon quand on monte cet escalier. Nous avons pu mesurer ce couplage et montré qu'il présente une valeur unique parmi tous les moteurs à ADN [63]. Généralement ce couplage induit une rotation d'un tour du moteur pour un pas hélical de l'ADN. Pour FtsK ce couplage est beaucoup plus faible (un tour de moteur pour 13.6 pas hélicaux). Nous avons pu présenter un modèle simple pour expliquer ce couplage. Pour résumé nos résultats, nous avons montré simplement que cette valeur est celle qui minimise la perturbation de la torsion présente dans l'ADN lorsque celui-ci est dans la bactérie. Ce résultat constitue un exemple de l'intérêt que peut avoir l'approche

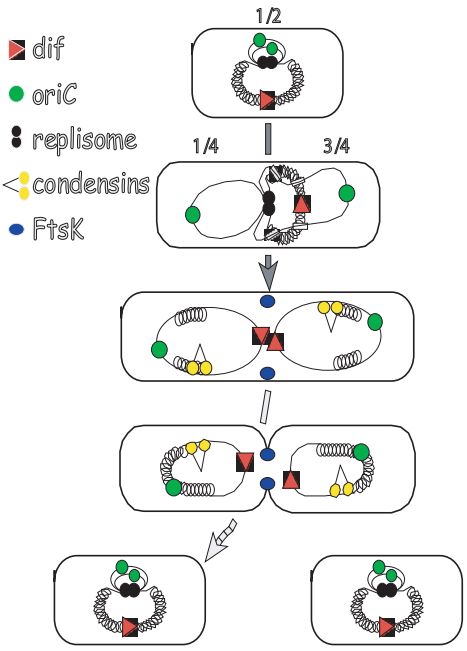

FIG. 2.1 – *Schéma simplifié de la division celullaire chez E. coli. Le génome de la bactérie est circulaire et contient 4.1Mbps. OriC est la séquence où démarre la réplication. Toute la machinerie de la répication est notée réplisome. Les condensines servent à compacter l'ADN qui sinon ne tiendrait pas dans la bactérie. La non coordination des processus cellulaires fait que la fermeture du septum peut se faire alors que les chromosomes ne sont pas encore correctement positionnés et de l'ADN peut se trouver ainsi piégé. Les séquences dif sont à l'opposé sur le chromosome de OriC. Cette région est celle qui a la plus forte probabilité d'être piégée lors de la fermture du septum. Le moteur FstK se positionne au niveau du septum et pompe l'ADN chromosomique dans le bon compartiment.*

mécanique d'un moteur moléculaire pour éclairer sa fonction biologique.

2.1.1 Mécanochimie de FtsK

Parmi les questions ouvertes les plus intéressantes d'un point de vue physique sur ce moteur se pose celle de la consommation d'ATP. Dans les conditions physiologiques l'énergie issue de son hydrolyse est d'environ $20k_BT$ soit $80pN.nm$. Par ailleurs nous avons, par une méthode statistique [62], pu mesurer son pas qui est d'environ $4nm$. Compte tenu du fait que ce moteur peut développer une force supérieure à $40pN$ cela implique que plusieurs ATP sont hydrolisées pour chaque pas. Pour mesurer l'efficacité du moteur et caractériser le couplage mécanochimique de ce moteur nous souhaitons visualiser l'hydrolyse de l'ATP (utilisation d'ATP fluorescent visualisé en ondes évanescentes) en même temps que détecterons l'activité mécanique du moteur par micromanipulation (et faire de même avec d'autres translocases).

2.1.2 Translocation de FtsK

Pour essayer de voir comment se font les contacts de FtsK sur l'ADN, en attendant la cristallisation de la protéine avec l'ADN, nous voulons voir comment se fait l'interaction avec l'ADN. En particulier voir comment FtsK passe des gaps sur son parcours. FX Barre a déjà fait des expériences préliminaires montrant le faible effet de gaps sur un des brins il nous reste à compléter cela en regardant des gaps sur l'autre brin ([35]). Enfin nous avons pu observer que FtsK avait du mal à produire de la torsion sur un ADN surenroulé positivement (alors que c'est systématique pour un ADN sous enroulé). J'aimerais donc voir si il existe un couple maximum contre lequel FtsK peut lutter.

2.1.3 FtsK membranaire

La version de FtsK que nous avons caractérisée *in vitro* est une version tronquée de la protéine présente dans la bactérie [52]. La protéine complète comprend en effet une partie hydrophobe. Dans la bactérie cette portion de la protéine permet son ancrage dans la membrane au niveau du septum. Cependant sa présence n'a pas permis jusqu'à maintenant sa purification pour des raisons de solubilité. Pour s'assurer que la protéine complète et/ou incorporée dans une membrane possède des caractéristiques similaires à celles que nous avons obtenues pour la protéine tronquée, nous souhaitons purifier la protéine complète pour la caractériser dans une vésicule lipidique et se rapprocher du système *in vivo* (fig 2.2).

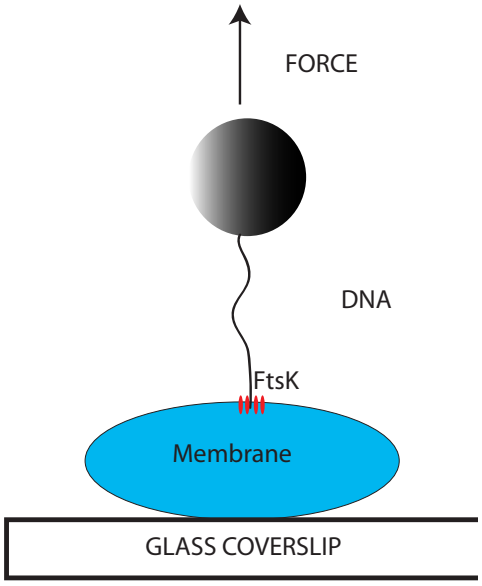

FIG. 2.2 – *In vivo FtsK étant positionnée au niveau du septum elle est donc inaccessible à la manipulation. Comme alternative expérimentale nous voulons insérer le moteur complet FtsK dans une membrane lipidique pour le caractériser dans une configuration plus proche de la situation in vivo.*

2.2 Transfert d'ADN et conjugaison bactérienne

Parmi les autres systèmes de transfert d'ADN dans les bactéries il y a le mécanisme de conjugaison [66]. Résumons ce processus pour le plasmide R388: la bactérie contient un plasmide circulaire qui code pour au moins trois protéines : TrwA, TrwB, TrwC. Lorsqu'il y a contact entre deux bactéries, une contenant le plasmide, l'autre non, un filament, un pilus, se forme entre elles. TrwA va localiser le plasmide dans la bactérie mais au voisinage de ce filament. TrwC, dite relaxase, va reconnaître une séquence d'ADN spécifique située sur le plasmide, nommée oriT, et va faire une coupure dans un des brins et commencer à les séparer (c'est une hélicase voir fig.2.3)[67]. TrWB [68], qui est un moteur hexamerique qui pompe l'ADN sous forme simple brin, envoie un des brins dans la bactérie qui ne contient pas le plasmide. Les génes présents sur ce plasmide sont ainsi transmis entre bactéries. Le même type de processus est impliqué dans la production de plantes transgéniques avec l'utilisation de *Agrobacterium tumefaciens*.
Le moteur TrwB fonctionnant sur un ADN simple brin et ne devant pas a priori former une boucle comme la version tronquée de FtsK a pu le faire dans nos expériences, il ne semble pas évident de voir fonctionner ce moteur moléculaires avec nos pinces magnétiques. Par conséquent, dans un premier temps, nous souhaitons essentiellement regarder le fonctionnement de TrwC. D'après les expériences *in vitro*, l'activité de ce moteur est controlée par le degré de torsion de l'ADN. TrwC semble en effet reconnaître la séquence oriT lorsque celle-ci adopte une structure spéciale d'ADN nommée jonction Holliday (voir fig.2.3) qui apparait si oriT est légèrement tordue dans le sens opposé au pas hélical. Elle ne fonctionne donc que si l'ADN est légèrement débobiné. Notre hypothèse est donc que c'est le couple présent dans l'ADN qui pilote l'activité du moteur. Pour cela nous comptons regarder son activité en fonction du couple dans l'ADN (que nous controlons aisément grâce à notre dispositif de pinces magnétiques). L'idée est de trouver un seuil pour l'action de l'enzyme et donc de démontrer que l'activité d'un moteur peut être régulée par un paramètre mécanique, à savoir ici la torsion dans l'ADN.

2.3 Transfert d'ADN et encapsidation virale

Un autre moteur moléculaire assurant un transfert d'ADN est présent dans les virus. Quand un virus infecte une cellule, il commence par éjecter son matériel génétique dans la cellule cible. Ensuite il se sert de la machinerie de celle-ci pour dupliquer son matériel génétique et protéique en grande quantité puis avant la lyse cellulaire finale le matériel génétique est empaqueté, grâce à un moteur moléculaire, dans une enveloppe, la capside. Cette capside va ensuite permettre le transport jusqu'à une autre cellule en protégeant le matériel génétique.

La partie d'éjection du matériel génétique a déjà fait l'objet d'études physiques tant théoriques qu'expérimentales (par exemples [69, 70, 71, 72]). Par contre la partie encapsidation n'a été caractérisée d'un point de vue mécanique et énergétique que par un seul groupe [30, 31] sur le phage $\phi 29$. En collaboration avec le groupe de L. Letellier qui est sur le point d'avoir un système d'encapsidation fonctionnel *in vitro* avec le phage T5 nous souhaitons caractériser cette encapsidation dans cet autre phage.

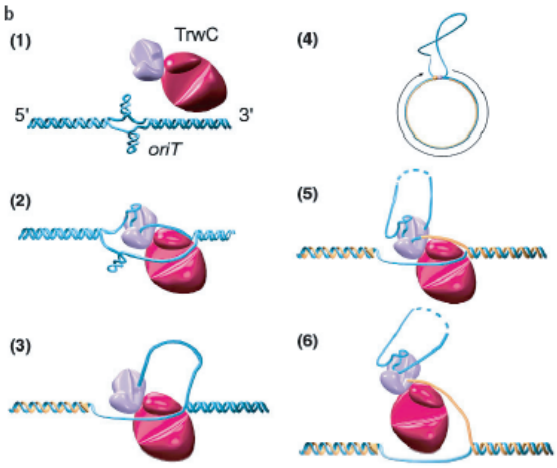

FIG. 2.3 – *Principe de fonctionnement de TrwC impliquée dans le transfert d'ADN entre bactéries. La partie bleue correspond à la partie de la protéine qui coupe l'ADN. La partie rouge correspond au bout qui sépare les brins d'ADN (partie hélicase)[67] avant que l'lun deux soit pompé dans une autre bactérie. Nous voulons vérifier que l'activité de la protéine est sensible au couple présent dans l'ADN et mesurer le seuil de déclenchement de son activité.*

2.3.1 Mécanique de l'encapsidation d'un virus

Pour cela nous voulons, de manière similaire à Smith et al. [30], fixer la capside partiellement remplie sur une surface de verre grâce à des anticorps. Avec des pinces magnétiques nous voulons ensuite tirer sur l'extrémité non encapsidée de l'ADN du phage pour excercer une contrainte mécanique qui va s'opposer à l'action du moteur et permettre sa caractérisation (FIG.2.4). Une seule expérience de ce type a donc déjà été réalisée dans le groupe de C. Bustamante en utilisant le phage $\phi 29$. Une grande diversité existe chez les phages. Il s'agira pour nous de voir si il y a des différences entre les deux phages en ce qui concerne les vitesses et forces mises en jeu compte tenu du fait que le genome du T5 est beaucoup plus grand que celui de $\phi 29$. Surtout, notre dispositif de pinces magnétiques permettra d'accéder au couplage translation/rotation du moteur qui est de manière générale un moyen invoqué pour expliquer l'incorporation de l'ADN par le moteur [73]. Dans ce modèle, placée à l'entrée de la capside se trouve une protéine, la portale, qui se comporte comme un écrou. En tournant, elle provoquerait la translation de la vis qui est ici l'ADN. Ce couplage parait d'autant plus important dans le cas du phage T5 que celui-ci a un génome qui comporte des séquences spécifiques qui, lors de l'expulsion de l'ADN lors de l'infection virale, vont être endommagées ou plus précisément "nickées" [69] (cela veut dire qu'une réaction chimique

en ces sites spécifiques va annuler le couple présent dans l'ADN).

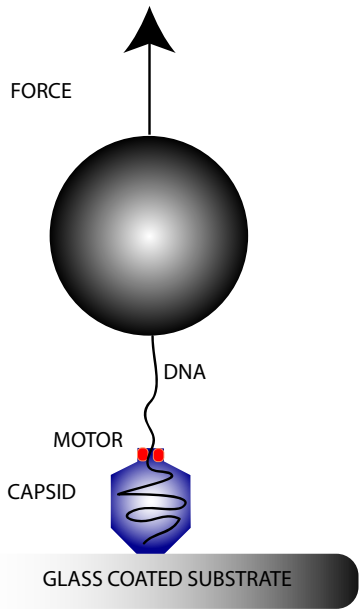

FIG. 2.4 – *Schéma de l'expérience de micromanipulation envisagée pour étudier le moteur d'encapsidation du phage T5, en particulier pour déterminer le couplage entre sa translation et sa rotation.*

Chapitre 3

Contrôle de l'activité d'une enzyme sous contrainte

Par ailleurs nous continuons le projet de recherche que j'avais commencé à développer dès la fin de ma thèse sur l'activité enzymatique sous contrainte. Comme je l'ai déjà signalé il s'agit de tirer sur une enzyme pour modifier sa structure pour regarder le rôle de celle-ci sur l'activité enzymatique. Pour détecter l'activité il s'agit d'utiliser une enzyme dont le substrat devient fluorescent après réaction. Le signal de fluoresence dépend alors de l'activité enzymatique. L'observation locale à deux photons permettant de suivre l'activité d'une enzyme isolée. J'ai consacré beaucoup de temps sur la partie instrumentation, Francesco Mosconi qui fait sa thèse sur ce sujet également, mais nous n'avons pas encore trouvé de système expérimental satisfaisant, en grande partie parce que les substrats commerciaux ne sont pas utilisables en molécule unique, un bruit de fond trop important étant présent.

Bibliographie

[1] S.B. Smith, L. Finzi, and C. Bustamante. Direct mechanical measurements of the elasticity of single DNA molecules by using magnetic beads. *Science*, 258:1122–1126, 1992.

[2] C. Bustamante, J.F. Marko, E.D. Siggia, and S. Smith. Entropic elasticity of λ-phage DNA. *Science*, 265:1599–1600, 1994.

[3] P. Cluzel, A. Lebrun, C. Heller, R. Lavery, J.-L. Viovy, D. Chatenay, and F. Caron. DNA: an extensible molecule. *Science*, 271:792 –794, 1996.

[4] S.B. Smith, Y. Cui, and C. Bustamante. Overstretching B-DNA: the elastic response of individual double-stranded and single-stranded DNA molecules. *Science*, 271:795–799, 1996.

[5] Martin Hegner, Steven B. Smith, and Carlos Bustamante. Polymerization and mechanical properties of single RecA-DNA filaments. *PNAS*, 96(18):10109–13548, 1999.

[6] J.F. Léger, J. Robert, L. Bourdieu, D. Chatenay, and J.F. Marko. RecA binding to a single double-stranded DNA molecule: a possible role of DNA conformational fluctuations. *Proc. Natl. Acad. Sci. USA*, 95:12295–12296, 1998.

[7] G.V.Shivashankar, M.Feingold, O.Kritchevsky, and A.Libchaber. RecA polymerization on double-stranded DNA by using single-molecule manipulation: the role of ATP hydrolysis. *Proc. Natl. Acad. Sci. USA*, 96:7916–7921, 1999.

[8] T. Strick, J.F. Allemand, D. Bensimon, A. Bensimon, and V. Croquette. The elasticity of a single supercoiled DNA molecule. *Science*, 271:1835 –1837, 1996.

[9] T. Strick, J.-F. Allemand, D. Bensimon, and V. Croquette. The behavior of supercoiled DNA. *Biophys. J.*, 74:2016–2028, 1998.

[10] J.-F. Allemand, D. Bensimon, R. Lavery, and V. Croquette. Stretched and overwound DNA form a Pauling-like structure with exposed bases. *Proc. Natl. Acad. Sci. USA*, 95:14152–14157, 1998.

[11] J.F. Léger, G.Romano, A. Sarkar, J. Robert, L. Bourdieu, D. Chatenay, and J.F. Marko. Structural transitions of a twisted and stretched DNA molecule. *Phys. Rev. Lett.*, 83:1066–1069, 1999.

[12] Z. Bryant, M. D. Stone, J. Gore, S. B. Smith, N. R. Cozzarelli, and C. Bustamante. Structural transitions and elasticity from torque measurements on DNA. *Nature*, 424(6946):338–41, 2003.

[13] B. M. Jaffar Ali, Roee Amit, Ido Braslavsky, Amos B. Oppenheim, Opher Gileadi, and Joel Stavans. Compaction of single DNA molecules induced by binding of integration host factor (IHF). *PNAS*, 98(19):10658–10663, 2001.

[14] D. Skoko, J. Yan, R. C. Johnson, and J. F. Marko. Low-force dna condensation and discontinuous high-force decondensation reveal a loop-stabilizing function of the protein fis. *Physical Review Letters*, 95(20), 2005.

[15] D. Skoko, B. Wong, R. C. Johnson, and J. F. Marko. Micromechanical analysis of the binding of dna-bending proteins hmgb1, nhp6a, and hu reveals their ability to form highly stable dna-protein complexes. *Biochemistry*, 43(43):13867–13874, 2004.

[16] D. Skoko, B. Wong, R. Johnson, and J. F. Marko. Irreversible binding of the dna-bending proteins hmgb1, nhp6a and huto a large dna molecule. *Biophysical Journal*, 86(1):7A–7A, 2004.

[17] A. Dawid, V. Croquette, M. Grigoriev, and F. Heslot. Single-molecule study of RuvAB-mediated Holliday-junction migration. *Proc Natl Acad Sci U S A*, 101(32):11611–6, 2004.

[18] R. Amit, O. Gileadi, and J. Stavans. Direct observation of RuvAB-catalyzed branch migration of single Holliday junctions. *Proc Natl Acad Sci U S A*, 101(32):11605–10, 2004.

[19] J. F. Leger, J. Robert, L. Bourdieu, D. Chatenay, and J. F. Marko. RecA binding to a single double-stranded DNA molecule: a possible role of DNA conformational fluctuations. *Proc Natl Acad Sci U S A*, 95(21):12295–9, 1998.

[20] R. Fulconis, A. Bancaud, J. F. Allemand, V. Croquette, M. Dutreix, and J. L. Viovy. Twisting and untwisting a single dna molecule covered by reca protein. *Biophysical Journal*, 87(4):2552–2563, 2004.

[21] T. van der Heijden, J. van Noort, H. van Leest, R. Kanaar, C. Wyman, N. Dekker, and C. Dekker. Torque-limited reca polymerization on dsdna (vol 33, pg 2099, 2005). *Nucleic Acids Research*, 33(8):2766–2766, 2005.

[22] B. Maier, D. Bensimon, and V. Croquette. Replication by a single DNA-polymerase of a stretched single strand DNA. *Proc. Natl. Acad. Sci. USA*, 97:12002–12007, 2000.

[23] Nancy R. Forde, David Izhaky, Glenna R. Woodcock, Gijs J. L. Wuite, and Carlos Bustamante. Using mechanical force to probe the mechanism of pausing and arrest during continuous elongation by Escherichia coli RNA polymerase. *PNAS*, 99(18):11682–13548, 2002.

[24] G.J.L. Wuite, S.B. Smith, M. Young, D. Keller, and C. Bustamante. Single-molecule studies of the effect of template tension on T7 DNA polymerase activity. *Nature*, 404:103–106, 2000.

[25] R. John Davenport, Gijs J.L. Wuite, Robert Landick, and Carlos Bustamante. Single-Molecule Study of Transcriptional Pausing and Arrest by E. coli RNA Polymerase. *Science*, 287(5462):2497–2500, 2000.

[26] Michelle D. Wang, Mark J. Schnitzer, Hong Yin, Robert Landick, Jeff Gelles, and Steven M. Block. Force and Velocity Measured for Single Molecules of RNA Polymerase. *Science*, 282(5390):902–907, 1998.

[27] K. C. Neuman, E. A. Abbondanzieri, R. Landick, J. Gelles, and S. M. Block. Ubiquitous transcriptional pausing is independent of rna polymerase backtracking. *Cell*, 115(4):437–447, 2003.

[28] E. A. Abbondanzieri, W. J. Greenleaf, J. W. Shaevitz, R. Landick, and S. M. Block. Direct observation of base-pair stepping by RNA polymerase. *Nature*, 438(7067):460–5, 2005.

[29] M. N. Dessinges, T. Lionnet, X. G. Xi, D. Bensimon, and V. Croquette. Single-molecule assay reveals strand switching and enhanced processivity of UvrD. *Proc Natl Acad Sci U S A*, 101(17):6439–44, 2004.

[30] S.B. Smith S. Grimes D.L. Anderson C. Bustamante D.E. Smith, S.J. Tans. The bacteriophage ϕ29 portal motor can package DNA against a large internal force. *Nature*, 413:748–752, 2001.

[31] Y. R. Chemla, K. Aathavan, J. Michaelis, S. Grimes, P. J. Jardine, D. L. Anderson, and C. Bustamante. Mechanism of force generation of a viral dna packaging motor. *Cell*, 122(5):683–692, 2005.

[32] Brent D. Brower-Toland, Corey L. Smith, Richard C. Yeh, John T. Lis, Craig L. Peterson, and Michelle D. Wang. Mechanical disruption of individual nucleosomes reveals a reversible multistage release of DNA. *PNAS*, 99(4):1960–1965, 2002.

[33] R. Seidel, J. van Noort, C. van der Scheer, J. G. P. Bloom, N. H. Dekker, C. F. Dutta, A. Blundell, T. Robinson, K. Firman, and C. Dekker. Real-time observation of dna translocation by the type i restriction modification enzyme ecor124i. *Nature Structural and Molecular Biology*, 11(9):838–843, 2004.

[34] R. Seidel, J. G. P. Bloom, J. van Noort, C. F. Dutta, N. H. Dekker, K. Firman, M. D. Szczelkun, and C. Dekker. Dynamics of initiation, termination and reinitiation of dna translocation by the motor protein ecor124i. *Embo Journal*, 24(23):4188–4197, 2005.

[35] L. K. Stanley, R. Seidel, C. van der Scheer, N. H. Dekker, M. D. Szczelkun, and C. Dekker. When a helicase is not a helicase: dsdna tracking by the motor protein ecor124l. *Embo Journal*, 25(10):2230–2239, 2006.

[36] T. T. Perkins, H. W. Li, R. V. Dalal, J. Gelles, and S. M. Block. Forward and reverse motion of single RecBCD molecules on DNA. *Biophys J*, 86(3):1640–8, 2004.

[37] N. H. Dekker, V. V. Rybenkov, M. Duguet, N. J. Crisona, N. R. Cozzarelli, D. Bensimon, and V. Croquette. The mechanism of type ia topoisomerases. *Proc Natl Acad Sci U S A*, 99(19):12126–31, 2002.

[38] G. Charvin, V. Croquette, and D. Bensimon. Single molecule study of dna unlinking by eukaryotic and prokaryotic type II topoisomerases. *PNAS*, 100(17):9820–9825, 2003.

[39] T.R. Strick, V. Croquette, and D. Bensimon. Single-molecule analysis of DNA uncoiling by a type II topoisomerase. *Nature*, 404:901–904, 2000.

[40] B. D. Brower-Toland, C. L. Smith, R. C. Yeh, J. T. Lis, C. L. Peterson, and M. D. Wang. Mechanical disruption of individual nucleosomes reveals a reversible multistage release of dna. *Proceedings of the National Academy of Sciences of the United States of America*, 99(4):1960–1965, 2002.

[41] A. Bancaud, N. C. E. Silva, M. Barbi, G. Wagner, J. F. Allemand, J. Mozziconacci, C. Lavelle, V. Croquette, J. M. Victor, A. Prunell, and J. L. Viovy. Structural plasticity of single chromatin fibers revealed by torsional manipulation. *Nature Structural and Molecular Biology*, 13(5):444–450, 2006.

[42] A. Ishijima, H. Kojima, T. Funatsu, M. Tokunaga, H. Higuchi, H. Tanaka, and T. Yanagida. Simultaneous observation of individual atpase and mechanical events by a single myosin molecule during interaction with actin. *Cell*, 92(2):161–171, 1998.

[43] Y. Harada, T. Funatsu, K. Murakami, Y. Nonoyama, A. Ishihama, and T. Yanagida. Single-molecule imaging of rna polymerase-dna interactions in real time. *Biophysical Journal*, 76(2):709–715, 1999.

[44] T. Hugel, N. B. Holland, A. Cattani, L. Moroder, M. Seitz, and H. E. Gaub. Single-molecule optomechanical cycle. *Science*, 296(5570):1103–1106, 2002.

[45] S. E. Halford, A. J. Welsh, and M. D. Szczelkun. Enzyme-mediated dna looping. *Annual Review of Biophysics and Biomolecular Structure*, 33:1–24, 2004.

[46] H. E. Choy and S. Adhya. Control of gal transcription through dna looping - inhibition of the initial transcribing complex. *Proceedings of the National Academy of Sciences of the United States of America*, 89(23):11264–11268, 1992.

[47] B. Sauer and N. Henderson. Site-specific dna recombination in mammalian-cells by the cre recombinase of bacteriophage-p1. *Proceedings of the National Academy of Sciences of the United States of America*, 85(14):5166–5170, 1988.

[48] L. Postow, C. D. Hardy, J. Arsuaga, and N. R. Cozzarelli. Topological domain structure of the escherichia coli chromosome. *Genes and Development*, 18(14):1766–1779, 2004.

[49] D. J. Sherratt, I. F. Lau, and F. X. Barre. Chromosome segregation. *Current Opinion in Microbiology*, 4(6):653–659, 2001.

[50] D. J. Sherratt. Bacterial chromosome dynamics. *Science*, 301(5634):780–785, 2003.

[51] J. Bath, L. J. Wu, J. Errington, and J. C. Wang. Role of bacillus subtilis spoiiie in dna transport across the mother cell-prespore division septum. *Science*, 290(5493):995–997, 2000.

[52] L. Aussel, F. X. Barre, M. Aroyo, A. Stasiak, A. Z. Stasiak, and D. Sherratt. Ftsk is a dna motor protein that activates chromosome dimer resolution by switching the catalytic state of the xerc and xerd recombinases. *Cell*, 108(2):195–205, 2002.

[53] C. Lesterlin C. Pages M. El Karoui C. Dennis M. Grigoriev J.-F. Allemand F.-X. Barre F. Cornet S. Bigot, O. A. Saleh. Kops: Dna motifs that control e. coli chromosome segregation by orienting the ftsk translocase. *EMBO. J.*, 24:3770–3780, 2005.

[54] C. Xu, J. Guild, W. W. Webb, and W. Denk. Determination of absolute two-photon excitation cross sections by in situ second-order autocorrelation. *Opt. Lett.*, 20:2372 – 2374, 1995.

[55] S. Wennmalm, L. Edman, and R. Rigler. Conformational fluctuations in single dna molecules. *Proceedings of the National Academy of Sciences of the United States of America*, 94(20):10641–10646, 1997.

[56] L. Edman and R. Rigler. Memory landscapes of single-enzyme molecules. *Proceedings of the National Academy of Sciences of the United States of America*, 97(15):8266–8271, 2000.

[57] L. Edman, U. Mets, and R. Rigler. Conformational transitions monitored for single molecules in solution. *Proceedings of the National Academy of Sciences of the United States of America*, 93(13):6710–6715, 1996.

[58] C. Gosse, A. Boutorine, I. Aujard, M. Chami, A. Kononov, E. Cogne-Laage, J. F. Allemand, J. Li, and L. Jullien. Micelles of lipid-oligonucleotide conjugates: Implications for membrane anchoring and base pairing. *Journal of Physical Chemistry B*, 108(20):6485–6497, 2004.

[59] D. Alcor, J. F. Allemand, E. Cogne-Laage, V. Croquette, F. Ferrage, L. Jullien, A. Kononov, and A. Lemarchand. Stochastic resonance to control diffusive motion in chemistry. *Journal of Physical Chemistry B*, 109(3):1318–1328, 2005.

[60] A.Ajdari F. Jülicher and J. Prost. Modeling molecular motors. *Rev.Mod.Phys.*, 69:1269, 1997.

[61] B. Maier, I. Chen, D. Dubnau, and M. P. Sheetz. Dna transport into bacillus subtilis requires proton motive force to generate large molecular forces. *Nature Structural and Molecular Biology*, 11(7):643–649, 2004.

[62] O. A. Saleh, C. Perals, F. X. Barre, and J. F. Allemand. Fast, dna-sequence independent translocation by ftsk in a single-molecule experiment. *Embo Journal*, 23(12):2430–2439, 2004.

[63] O. A. Saleh, S. Bigot, F. X. Barre, and J. F. Allemand. Analysis of dna supercoil induction by ftsk indicates translocation without groove-tracking. *Nature Structural and Molecular Biology*, 12(5):436–440, 2005.

[64] P. J. Pease, O. Levy, G. J. Cost, J. Gore, J. L. Ptacin, D. Sherratt, C. Bustamante, and N. R. Cozzarelli. Sequence-directed dna translocation by purified ftsk. *Science*, 307(5709):586–590, 2005.

[65] J. Bath, L. J. Wu, J. Errington, and J. C. Wang. Role of bacillus subtilis spoiiie in dna transport across the mother cell-prespore division septum. *Science*, 290(5493):995–997, 2000.

[66] M. Llosa, F. X. Gomis-Ruth, M. Coll, and F. de la Cruz. Bacterial conjugation: a two-step mechanism for dna transport. *Molecular Microbiology*, 45(1):1–8, 2002.

[67] A. Guasch, M. Lucas, G. Moncalian, M. Cabezas, R. Perez-Luque, F. X. Gomis-Ruth, F. de la Cruz, and M. Coll. Recognition and processing of the origin of transfer dna by conjugative relaxase trwc. *Nature Structural Biology*, 10(12):1002–1010, 2003.

[68] F. X. Gomis-Ruth, G. Moncalian, R. Perez-Luque, A. Gonzalez, E. Cabezon, F. de la Cruz, and M. Coll. The bacterial conjugation protein trwb resembles ring helicases and f-1-atpase. *Nature*, 409(6820):637–641, 2001.

[69] S. Mangenot, M. Hochrein, J. Radler, and L. Letellier. Real-time imaging of dna ejection from single phage particles. *Current Biology*, 15(5):430–435, 2005.

[70] J. Kindt, S. Tzlil, A. Ben-Shaul, and W. M. Gelbart. Dna packaging and ejection forces in bacteriophage. *Proceedings of the National Academy of Sciences of the United States of America*, 98(24):13671–13674, 2001.

[71] A. Evilevitch, L. Lavelle, C. M. Knobler, E. Raspaud, and W. M. Gelbart. Osmotic pressure inhibition of dna ejection from phage. *Proceedings of the National Academy of Sciences of the United States of America*, 100(16):9292–9295, 2003.

[72] R. Phillips P. K. Purohit, J. Kondev. *Proc. Natl. Acad. Sci. USA*, 100:3173Ű3178.

[73] A. A. Simpson, Y. Z. Tao, P. G. Leiman, M. O. Badasso, Y. N. He, P. J. Jardine, N. H. Olson, M. C. Morais, S. Grimes, D. L. Anderson, T. S. Baker, and M. G. Rossmann. Structure of the bacteriophage phi 29 dna packaging motor. *Nature*, 408(6813):745–750, 2000.

Caramels

Jean-Paul ABADIE

Ingrédients : N° 1

- 250 g. de crème liquide - 180 g. de sucre - 180 g. de glucose cristal - Arôme (orange ou zeste, vanille) N° 2

- 75 g. de beurre doux - ou demi-sel - 100 g. de chocolat blanc - 30 g. de chocolat noir - Noisettes ou noix (à souhait)

1) - Mettre tous les éléments N° 1 ensemble, cuire à 120ř en remuant avec un fouet.

2) - Ajouter le beurre, le chocolat et les noisettes (N° 2)

3) - Démouler dans un plat dont le fond a été garni d'un papier sulfurisé.

4) - Laisser reposer quelques heures.

5) - Découper en carré.

http://www.amphitryon-abadie.com/

Cinquième partie

Notice individuelle

Chapitre 1

Curriculum vitae et liste de publications

Jean-François Allemand
21/09/1969

J. F. **Allemand**
Laboratoire de Physique Statistique
ENS
24 rue Lhomond
75005 PARIS
FRANCE
Tel : 01 44 32 34 92
Email : allemand@lps.ens.fr

Formation :

- 1994-1997 : Doctorat de l'Université Pierre et Marie Curie : Micromanipulations de molécules d'ADN isolées (V. Croquette, ENS)
- 1989-1993 : Ancien élève de l'Ecole Normale Supérieure de Cachan : Stage DEA : Etalement de gouttes de polymères sur une pseudo-brosse de polymères (Liliane Léger, Collège de France) Maitrise :Excitons study in CdZnTe semiconductors nanostructures (Trinity College, Dublin)
- Agrégé de sciences physiques option physique

Situation professionnelle :

- 1989-1993 : Elève de l'Ecole Normale Supérieure de Cachan
- 1993-1994 : Service militaire : Ecole Militaire de Saint-Cyr Coëtquidan
- 1994-1998 : Agrégé préparateur à l'Ecole Normale Supérieure : département de physique.
- 1998- : Maître de conférences à l'Ecole Normale Supérieure : département de physique et de chimie.

Prix : Prix jeune chercheur de la SFP 1999

Responsabilités administratives et collectives :

- ACI jeune chercheur 2001-2004 : Contrôle mécanique de l'activité d'une molécule isolée (avec L. Jullien)
- Responsable principal ACI DRAB 2004-2007 : Etude d'un moteur permettant le déplacement de l'ADN, la protéine FtsK : mode d'assemblage, mécanisme de fonctionnement, conséquences sur la topologie de l'ADN pompé et pour la résolution des dimères de chromosomes dans la bactérie (avec F.X. Barre).
- Responsable partenaire ANR blanche 2005 : DNA traffic in bacteria: role and action mechanism of the ATP-dependent DNA translocase FtsK (2 partenaires, responsable F.X. Barre)
- Responsable partenaire ANR PCV 2006 : VIRNANOMOTOR (3 partenaires, responsable L. Letellier)
- Referee: PRL et EPJE
- Examinateur du concours d'entrée ENS : filière PC physique (1999-2002)

– Enseignement : Direction des études du département de chimie de l'ENS (2004-2005) et Sous direction du magistère interuniversitaire de chimie et des études du département de chimie de l'ENS (2002-2004)

Brevet : Apparatus for force and torsion measurements on biomolecules and applications, T.R. Strick , J.-F. **Allemand**, D. Bensimon, A. Bensimon and V.Croquette, US patent pending (1997).

Enseignement :

– Agrégation de physique options : physique (1994-1998)(2005-) (TPs, préparation à l'oral, tâches administratives) chimie (1998-2003) : Physico-chimie des polymères, Thermodynamique statistique (cours) procédés physico-chimiques (1998-2003) : Electromagnétisme et physique ondulatoire (cours, TDs)
– Magistère Interuniversitaire de Physique (1994-1998) : Hydrodynamique (TDs)
– Magistère Interuniversitaire de Chimie (1998-2005): Thermodynamique statistique, Thermodynamqie hors d'équilibre, Forces intermoléculaires (cours, TDs), responsable stages courts (3 semaines) et longs (6 mois), responsable de la formation
– Magistère Interuniversitaire de Biologie (2004-) Physique pour biologistes (cours)
– DEA de matière condensée (2001-2004) : Molécules uniques (cours)
– DEA Interface Physique Biologie (2004-) : Micromanipulations de molécules isolées (cours)
– Ecole Militaire Interarmées (1993) : Optique, Thermodynamique (DEUG) (cours TDs)

Encadrement de travaux de recherches : co-direction des thèses de E. Cognet-Laage soutenue en 2004 (a vec L. Jullien) , et de A. meglio (avec V. Croquette) en cours.

1.1 Liste de publications :

1.1.1 Journaux avec comités de lecture

Thématique : ADN

1. T. R. Strick, J.-F. **Allemand**, D. Bensimon, A. Bensimon and V. Croquette, The elasticity of a single supercoiled DNA molecule, Science, 271, 1835 (1996).
2. J.-F. **Allemand**, D. Bensimon, L. Jullien, A. Bensimon and V. Croquette ; pH dependent specific binding and combing of DNA, Biophys.J., 73, 2064 (1997).
3. Strick, T.R., **Allemand**, J.F., Bensimon, D., Croquette, V. The behavior of supercoiled DNA (1998) Biophys. J. 74, 2016-2028.
4. J.-F. **Allemand**, D. Bensimon, R. Lavery, V. Croquette. Stretched and overwound DNA form a Pauling-like structure with exposed bases. Proc. Nat. Acad. Sci. USA, 95, 14152-14157 (1998).
5. T. Strick, J.-F. **Allemand**, V. Croquette, D. Bensimon. Physical approaches to the study of DNA. J. Stat. Phys., 93 :647-672, (1998).
6. T.R. Strick, J.-F. **Allemand**, D. Bensimon, R. Lavery, V. Croquette, Phase coexistence in a single DNA molecule, Physica A, 263, 392 (1999).
7. J.-F. **Allemand**, T.R. Strick, V. Croquette and D. Bensimon, Twisting and stretching single DNA molecules, Prog. Biophys. Molec. Biol., (1999).
8. T.R. Strick, J.-F. **Allemand**, D. Bensimon and V. Croquette, Stress induced structural transitions in DNA and proteins, Ann. Rev. Biophys. Biomol. Struct., 29 (1999).
9. C. Bouchiat, M.D. Wang, S. M. Block, J.-F. **Allemand**, T. Strick, and V. Croquette , Estimating the persitence length of a worm-like chain molecule from force-extension measurements. Biophysical Journal, 76 :409-413, (1999).
10. R. Lavery, A. Lebrun, J.-F. **Allemand**, D. Bensimon, V. Croquette, Structure and mechanics of single biomolecules. Experiment and simulation, J. Phys. Condens. Matter 14 (2002) R383R414.
11. T.R. Strick, M.N. Dessinges, G. Charvin, N.H. Dekker, J-F **Allemand**, D. Bensimon, V. Croquette, Stretching of macromolecules and proteins , Rep. Prog. Phys. 65 (2002) R1-R45

12. A. Crut, D. Lasne, J.-F. **Allemand**, M. Dahan, and P. Desbiolles ; Transverse fluctuations of single DNA molecules attached at both extremities to a surface , PHYSICAL REVIEW E 67, 051910 (2003).

Interactions ADN-protéines et moteurs moléculaires

13. T. Strick, G. Charvin, N. Dekker, J-F. **Allemand**, D. Bensimon , V. Croquette, "Tracking enzymatic steps of DNA topoisomerases using single-molecule micromanipulation", C.R.A.S. Physique 3, (2002) 595-618
14. Lia, G., Bensimon, D., Croquette, V., **Allemand**, J-F, Dunlap, D., Lewis, D.E.A., Adhya, S., and Finzi, L. , Supercoiling and denaturation in Gal repressor heat unstable nucleoid protein (HU)-mediated DNA looping , PNAS, vol. 100, no. 20 11373-11377 (2003).
15. Jean-François **Allemand**, David Bensimon and Vincent Croquette; Stretching DNA and RNA to probe their interactions with proteins, Current Opinion in Structural Biology 2003, 13:266-274
16. A. Revyakin, J.-F. **Allemand**, V. Croquette, R. H. Ebright, and T. R. Strick, Single-Molecule DNA Nanomanipulation : Detection of Promoter-Unwinding Events, Methods in enzymology, 370, 577-598
17. Omar A Saleh, Corine Pérals, François-Xavier Barre, and Jean-François **Allemand**, Fast, DNA-sequence independent translocation by FtsK in a single-molecule experiment,The EMBO Journal (2004) 23, 2430-2439.
18. Renaud Fulconis, Aurélien Bancaud, Jean-Francois **Allemand**, Vincent Croquette, Marie Dutreix, and Jean-Louis Viovy, Twisting and Untwisting a Single DNA Molecule Covered by RecA Protein, Biophysical Journal Volume 87, 2552-2563 (2004).
19. G. Charvin, J.-F. **Allemand**, T. R. Strick, D. Bensimon and V. Croquette, Twisting DNA: single molecule studies,Contemporary Physics, September-October 2004, volume 45, number 5, pages 383 - 403
20. Saleh O.A., Bigot S., Barre F. -X. and J.-F. **Allemand**. Analysis of DNA supercoil induction by FtsK indicates translocation without groove-tracking. Nat Struct Mol Biol 2005: 12, 436-440.
21. O. A. Saleh, Jean-François **Allemand**, Vincent Croquette and David Bensimon, Single-Molecule-Manipulation Measurements of DNA Transport Proteins, ChemPhysChem 2005, 6, 813 - 818.
22. Sarah Bigot, Omar A. Saleh , Christian Lesterlin , Carine Pages , Meriem El Karoui , Cynthia Dennis , Mikhail Grigoriev , Jean-François **Allemand** , François-Xavier Barre and François Cornet, KOPS: DNA motifs

that control E. coli chromosome segregation by orienting the FtsK translocase, EMBO. J., 24, 3770-3780 (2005).

23. K. C. Neuman, O. A. Saleh , T. Lionnet, G. Lia, J-F **Allemand**, D. Bensimon and V. Croquette, Statistical determination of the step size of molecular motors, J. Phys.: Condens. Matter 17 (2005) S3811-S3820
24. J.-F. **Allemand**, S. Cocco, N. Douarche, and G. Lia, Loops in DNA: An overview of experimental and theoretical approaches,Eur. Phys. J. E 19, 293-302 (2006).
25. Bancaud A. , Silva N. C. E. , Barbi M. , Wagner G. , **Allemand** J. F. , Mozziconacci J. , Lavelle C., Croquette V. , Victor J. M., Prunell A. , Viovy, J. L., Structural plasticity of single chromatin fibers revealed by torsional manipulation, Nature Structural and Molecular Biology,Volume 13, 444-450 (2006).

Fluorescence et microscopie 2 photons :

26. E. Cogne, J-F **Allemand**, O. Ruel, J-B Baudin, V. Croquette, M. Blanchard-Desce, L. Jullien, "Diaroyl(methanato)boron difluoride as attractive fluorescent probes for applications relying on two-photon excitation ", Chem. Eur. J. 2004, 10, 1445 - 1455
27. C. Gosse, A. Boutourine, I. Aujard, M. Domi, A. Kononov, E. Cogne, J-F **Allemand**, J. LI, L. Jullien, Micelles of Lipid-Oligonucleotide Conjugates: Implications for Membrane Anchoring and Base Pairing, J. Phys. Chem. B 2004, 108, 6485-6497
28. S. Charier, O. Ruel, J-B Baudin, D. Alcor, J-F **Allemand** A. Meglio, L. Jullien , An Efficient Fluorescent Probe for Ratiometric pH Measurements in Aqueous Solutions, Angew. Chem. Int. Ed. Eng., 2004, 43, 4785-4788.
29. D. Alcor, JF **Allemand**, E. Cogné Laage, V. Croquette, F. Ferrage, L. Jullien, A. Kononov, A. Lemarchand, Stochastic Resonance to Control Diffusive Motion in Chemistry, J. Phys. Chem. B 2005, 109, 1318-1328
30. S. Charier, A. Meglio, D. Alcor, E. Cogné Laage, J-F **Allemand**, L. Jullien, A. Lemarchand, Reactant Concentrations from Fluorescence Correlation Spectroscopy with Tailored Fluorescent Probes. An Example of Local Calibration-Free pH Measurement., J. AM. CHEM. SOC. 2005, 127, 15491-15505
31. S. Charier, O. Ruel, J-B Baudin, D Alcor, J-F **Allemand**, A Meglio, L Jullien, B Valeur, Photophysics of a Series of Efficient Fluorescent pH

Probes for Dual-Emission-Wavelength Measurements in Aqueous Solutions, Chem. Eur. J. 2006, 12, 1097 - 1113

1.1.2 Comptes rendus de conférences

- Mesure de force sur des molécules biologiques, J.F. **Allemand**, T.R. Strick, A. Bensimon, D. Bensimon, A. Chiffaudel and V. Croquette in Quel Avenir pour la Physique ?, p.269, Proc. Conf. Grimentz, eds. B. Vittoz, A. Chatelain and T. Jalanti. (1997).
- Structures of supercoiled DNA and their biological implications, T.R. Strick, J.-F. **Allemand**, A. Bensimon, D. Bensimon and V. Croquette, in Dynamical Networks in Physics and Biology, p.299, Les Houches Workshop, Ed. D.Beysens and G.Forgacs, World Scientific (1998).
- Une nouvelle structure de la molécule d'ADN induite par une contrainte de torsion, J.-F. **Allemand**, T.R. Strick, S. Komilikis, D. Bensimon, R. Lavery and V. Croquette, "Des phénomènes critiques au Chaos", Colloque P.Bergé (1998).
- Twisting a single DNA molecule : experiments and models, T.R. Strick, J.-F. **Allemand**, D. Bensimon, V. Croquette, C. Bouchiat, M. Mézard and R. Lavery, in Topological concepts in low dimensional systems, Les Houches workshop, Ed.Conté, EDP Science (1999).
- "Twisting and stretching a DNA molecule leads to structural transitions" T.R. Strick, J.-F. **Allemand**, D. Bensimon, R. Lavery, and V. Croquette ; in Biological Physics Eds. H. Frauenfelder, G. Hummer and R. Garcia. AIP Conference Proceedings 487, p. 249-270, (1999)
- "Stretching of macromolecules and proteins", M-N. Dessinges, G. Charvin, N. Dekker, J-F. **Allemand**, D. Bensimon, and V. Croquette ; Protein Folding Cargèse Mai 2001.

1.1.3 Autres publications (vulgarisation, etc) :

- "L'ADN, Ressort Moléculaire", J.-F. **Allemand**, A. Bensimon, D. Bensimon, F. Caron, D. Chatenay, PH. Cluzel, V. Croquette, CH. Heller, R. Lavery, A. Lebrun, T.Strick et J.-L. Viovy, Pour La Science, 224, 76 (1996).
- "L'ADN, un polymère modèle", J.-F. **Allemand**, A. Bensimon, D. Bensimon, F. Caron, D. Chatenay, PH. Cluzel, V. Croquette, CH. Heller, R. Lavery, A. Lebrun, T.R. Strick et J.-L. Viovy, Images de la Physique, 111-118 (1997).

- "Le Jokari Moléculaire", J.-F. **Allemand**, D.Bensimon, V. Croquette, R. Lavery, B. Maier ,T. Strick, Biofutur, 190, 26 (1999).
- "The Manipulation of Single Biomolecules",T. Strick, J.-F. **Allemand**, V. Croquette, D. Bensimon, Physics Today, October 2001 Volume 54, Number 10.
- DNA mechanics and statistical mechanics, T.R. Strick, J.-F. **Allemand**, D. Bensimon and V. Croquette, Encyclopedia of Life Sciences.
- Controlled assembly of covalent and supramolecular chemical modules: from engineering of complex structures to high-performance chromatography, Alcor, D. and **Allemand**, J. F. and Aujard, I. and Baudin, J. B. and Benbrahim, C. and Charier, S. and Cogne-Laage, E. and Croquette, V. and Torres, A. E. and Ferrage, F. and Jullien, L. and Kononov, A. and Lemarchand, A. and Lemarchand, H. and Ruel, O., Russian Chemical Bulletin, 53, 7,1379-1384, 2004
- Tuning the effective molecular diffusion: a step toward control over oriented molecular motion, Alcor, D. and **Allemand**, J. F. and Aujard, I. and Barilero, T. and Baudin, J. B. and Benbrahim, C. and Bensimon, D. and Bourdoncle, A. and Charier, S. and Cogne-Laage, E. and Croquette, V. and Estevez-Torres, A. and Gagey, N. and Jullien, L. and Lemarchand, A. and Lemarchand, H. and Meglio, A. and Neveu, P. and Ruel, O., Actualite Chimique, 9-15,(2005)
- Biophysique à l'échelle de la molécule unique, J-F **Allemand**, Bulletin de la Société Française de Physique (2005).

1.2 Conférences invitées et seminaires depuis 2002

- Oxford Workshop on Site-specific Recombination, Genetic Transposition and DNA Dynamics, Oxford, England, 09/02
- Ecole Nanosciences, France, 03/04
- LMGM, Toulouse, France, 04/04
- Laboratoire CPMOH, Bordeaux, France, 05/04
- Laboratoire Physico-Chimie Curie, Paris, France, 05/04
- Edimbourg University, Chemistry department, Edimbourg, England, 11/04
- Laboratoire de Physique des Lasers, Villetaneuse, France, 11/04
- Physics 2005 - A Century after Einstein,Warwick, England, 04/05
- University of Santander, Santander, Spain, 05/05

- From Molecular Switches to Molecular Motors, Ascona, Switzerland, 09/05
- Les cinquièmes rencontres de Figeac, France, 10/05
- French-Indian Symposium on nanotechnologies, Goa, India, 01/06
- Ecole INSERM sur les moteurs moléculaires, Lalonde les Maures, France, 06/06

Résumé : Dans une première partie nous avons utilisé des techniques de micromanipulations de molécules d'ADN uniques avec des pinces magnétiques pour étudier la cinétique et thermodynamique de formation de boucles sur l'ADN par le répresseur GalR. Nous avons également étudié les propriétés de la translocase à ADN FtsK impliquée dans la ségrégation des chromosomes chez *E. coli*. Dans une seconde partie nous avons mis en place différentes expériences utilisant l'excitation biphotonique. Tout d'abord nous avons construit un dispositif pour mesurer les sections efficaces d'absorption à deux photons de molécules synthétisées au laboratoire. Nous avons ensuite mis en place la technique de corrélation de fluctuations de fluorescence pour mesurer des coefficients de diffusion et des constantes cinétiques.

Abstract : In the first part, we describe the use of the single DNA micromanipulation technique called magnetic tweezers to study the loop formation kinetics and thermodynamics in DNA caused by the GalR repressor. We also studied the properties of the DNA translocase FtsK involved in chromosome segregation in *E. coli*. In a second part we present experiments using two photons excitation. In a first set of experiments we did built an apparatus to perform two photons cross section absorption for molecules synthesized in the laboratory. Then we used fluorescence correlation spectroscopy to measure diffusion coefficents and kinetics constants.